MODELING PART DYNAMICS IN MACHINING PROCESSES CONSIDERING MATERIAL REMOVAL

A THESIS SUBMITTED TO
THE GRADUATE SCHOOL OF NATURAL AND APPLIED SCIENCES
OF
MIDDLE EAST TECHNICAL UNIVERSITY

BY

SİBEL ATLAR

IN PARTIAL FULFILLMENT OF THE REQUIREMENTS
FOR
THE DEGREE OF MASTER OF SCIENCE
IN
MECHANICAL ENGINEERING

DECEMBER 2007

Approval of the thesis:

MODELING PART DYNAMICS IN MACHINING PROCESSES CONSIDERING MATERIAL REMOVAL

submitted by **SİBEL ATLAR** in partial fulfillment of the requirements for the degree of **Master of Science in Mechanical Engineering Department, Middle East Technical University** by,

Prof. Dr. Canan Özgen _____
Dean, Graduate School of **Natural and Applied Sciences**

Prof. Dr. Kemal İder _____
Head of Department, **Mechanical Engineering**

Prof. Dr. H. Nevzat Özgüven _____
Supervisor, **Mechanical Engineering Dept., METU**

Assoc. Prof. Dr. Erhan Budak _____
Co-Supervisor, **Faculty of Engineering and Natural Sciences, SU**

Examining Committee Members:

Prof. Dr. Mehmet Çalışkan _____
Mechanical Engineering Dept., METU

Prof. Dr. H. Nevzat Özgüven _____
Mechanical Engineering Dept., METU

Assoc. Prof. Dr. Erhan Budak _____
Faculty of Engineering and Natural Sciences , SU

Asst. Prof. Dr. Yiğit Yazıcıoğlu _____
Mechanical Engineering Dept., METU

Prof. Dr. Yavuz Yaman _____
Aerospace Engineering Dept., METU

Date: 24/12/2007

I hereby declare that all information in this document has been obtained and presented in accordance with academic rules and ethical conduct. I also declare that, as required by these rules and conduct, I have fully cited and referenced all material and results that are not original to this work.

Name, Last Name: Sibel Atlar

Signature :

ABSTRACT

MODELING PART DYNAMICS IN MACHINING PROCESSES CONSIDERING MATERIAL REMOVAL

Atlar, Sibel

M.S., Department of Mechanical Engineering

Supervisor: Prof. Dr. H. Nevzat Özgüven

Co-Supervisor: Assoc. Prof. Dr. Erhan Budak

December 2007, 129 Pages

Self-excited chatter vibration in machining is one of the most important limitations on utilizing the increasing productivity of modern machine tools. In order to predict stable depth of cuts at high cutting speeds, the stability lobe diagram for a spindle-tool holder-tool combination must be developed. The frequency response function (FRF) of the system must be known for analytical prediction of the stability lobe diagrams. When the flexibility of the workpiece is important, the workpiece itself should be included in the system model by considering the variation of its dynamics at different stages of the machining process.

In this thesis, an exact structural modification method is used to find the frequency response functions of the workpiece to be machined at every stage of the machining process. In order to obtain the system matrices and the modal parameters of the original structure, a commercial finite element program MSC. Marc© is used. The frequency response functions of workpiece are calculated by

using the computer program developed in this thesis, and are compared with the ones found by MSC. Marc©. The stability lobe diagram of the system is obtained by combining the FRFs of the tool with those of the workpiece. The effects of the dynamic of the workpiece on the stability lobe diagrams are studied extensively by using the results of case studies presented in this thesis. In order to increase productivity, minimum chatter-free machining times are also calculated for different cases. For this purpose the effects of the different radial depth of cuts and different cutting strategies on the stability and the machining time are examined with various case studies.

Keywords: Chatter Vibrations, Chatter Stability, Structural Dynamics, Structural Modification.

ÖZ

TALAŞLI İMALATTA TALAŞ KALDIRMAYI DİKKATE ALAN PARÇA DİNAMİĞİ MODELLENMESİ

Atlar, Sibel
Yüksek Lisans, Makine Mühendisliği Bölümü
Tez Yöneticisi: Prof. Dr. H. Nevzat Özgüven
Ortak Tez Yöneticisi: Doç. Dr. Erhan Budak

Aralık 2007, 129 Sayfa

Gelişen takım tezgahlarının artan kapasitesini verimli kullanma yolunda en büyük engellerden birisi, metal kesme sürecinde ortaya çıkan ve "tırlama" adı verilen kendinden kaynaklı titreşimlerdir. Bir kesici takım için kararlı ve derin kesme sağlayacak en yüksek hızları hesaplayabilmek için iş mili - takım tutucu - takım kombinasyonunun kararlılık diyagramı elde edilmelidir. Kararlılık diyagramlarını analitik olarak elde etmek için ise sistemin frekans tepki fonksiyonunun bilinmesi gerekmektedir. İşlenen parçanın esnekliğinin önemli olduğu durumlarda, kesme sürecinin farklı aşamalarında parça dinamiği özelliklerinin değiştiği düşünülüp, iş parçası da sisteme dahil edilmelidir.

Bu tezde, iş parçasının işleme sürecinin her aşamasındaki frekans tepki fonksiyonlarını bulmak için yapısal değişiklik yöntemi kullanılmıştır. Esas yapının sistem matrisleri ile titreşim biçim parametrelerini elde edebilmek için sonlu elemanlar analiz programı MSC. Marc© kullanılmıştır. İş parçasının bu tez

çalışmasında geliştirilen program ile bulunan frekans tepki fonksiyonları, MSC. Marc© ile bulunan değerlerle karşılaştırılmıştır. Sistemin kararlılık diyagramları, iş parçasının ve kesici takımın frekans tepki fonksiyonlarının birleştirilmesiyle bulunmuştur. İş parçası dinamiğinin kararlılık diyagramlarına etkisi, bu tez çalışmasında yapılan örnek çalışmalarla kapsamlı şekilde incelenmiştir. Ayrıca üretim kapasitesini arttırmak için tırlamasız en kısa üretim zamanları değişik durumlar için hesaplanmıştır. Bu amaçla değişik radyal kesme derinlikleri ve kesme stratejilerinin kesme kararlılığı ve üretim zamanına etkileri çeşitli örnek çalışmalarla incelenmiştir.

Anahtar Kelimeler: Tırlama Titreşimleri, Tırlama Kararlılığı, Yapı Dinamiği, Yapısal Değişiklik.

To My Family

ACKNOWLEDGEMENTS

I would like to express my gratitude to my supervisor Prof. Dr. H. Nevzat Özgüven and co-supervisor Assoc. Prof. Dr. Erhan Budak for their guidance, criticism and insight throughout this work.

I would also like to thank my parents for their support and patience throughout my education. I am grateful to my friends for their suggestions and comments.

Lastly, I am grateful to my husband Yunus Baki Aral for his continuous help and encouragement.

TABLE OF CONTENTS

LIST OF TABLES

LIST OF FIGURES

LIST OF SYMBOLS

$\{\boldsymbol{x}\}$	Displacement vector
$\{\dot{\boldsymbol{x}}\}$	Velocity vector
$\{\ddot{\boldsymbol{x}}\}$	Acceleration vector
$\{\boldsymbol{F}\}$	Forcing vector
$\{\boldsymbol{R}\}$	Damping force vector
$\{\boldsymbol{\phi}\}$	Mass normalized eigenvector matrix of the system
$[\boldsymbol{M}]$	Mass matrix
$[\boldsymbol{K}]$	Stiffness matrix
$[\boldsymbol{H}]$	Damping (hysteretic) matrix
$[\boldsymbol{C}]$	Damping (viscous) matrix
$[I]$	Identity(unit) matrix
$[\Delta\boldsymbol{M}]$	Modification mass matrix
$[\Delta\boldsymbol{K}]$	Modification stiffness matrix
$[\Delta\boldsymbol{H}]$	Modification damping (hysteretic) matrix
$[\boldsymbol{\beta}]$, $[\boldsymbol{\alpha}]$	Receptance matrix of original system
$[\boldsymbol{\alpha}]$, $[\boldsymbol{\gamma}]$	Receptance matrix of modified system
$[\boldsymbol{D}]$	Dynamic stiffness matrix
F_t	Cutting force in the tangential direction
F_r	Cutting force in the radial direction
K_t	Cutting force coefficient in the tangential direction
K_r	Cutting force coefficient in the radial direction
$G(\omega)$	Total transfer function of the system
K_f	Cutting force coefficient in the feed direction
N	Number of teeth(flutes) of the cutter

V_f	Feed rate
T	Period
a	axial depth of cut
a	Directional coefficients
f_t	Feed per tooth
h	Modulated chip thickness
i	Unit imaginary number
k	An integer corresponding to the number of vibration waves within a tooth period
l_w	Cutting length at one pass(step)
nop	Number of pass(step)
n_t	Rotational frequency of the cutter (in rpm)
t_m	Machining time
x_c, x_w	Dynamic displacements of the cutter and workpiece in the x direction
y_c, y_w	Dynamic displacements of the cutter and workpiece in the y direction
α	Average directional coefficients
γ	Loss factor
ε	Phase difference between the inner and outer modulations
ω	Excitation frequency
ω_c	Chatter frequency
ω_r	r^{th} eigenfrequency of the system
ϕ_j	Angular immersion of tooth (j)
ϕ_P	Pitch angle of the cutter
ϕ	Angular position of the cutter
Ω	Rotational speed of the tool in rad/sec
Λ	Eigenvalue of the system

CHAPTER 1

INTRODUCTION

1.1 General

Self-excited vibration which is called "*chatter*" is one of the most common problems in machining. Chatter vibrations results in

- poor surface finish,
- dimensional inaccuracy in machined parts,
- reduced tool life,
- limitation on material removal rate,
- necessity for additional finishing processes,
- damage to the tool, part and machine.

Therefore, chatter results in poor quality, reduced productivity and increased cost.

The machine-tool chatter vibrations can be classified as regeneration [1] and mode coupling [2] based on their underlying physical mechanism. Mode coupling occurs whenever the relative vibration between the tool and the workpiece exists simultaneously in at least two directions in the plane of the cut. Regenerative chatter occurs due to variation in the chip thickness during the machining processes. Because of the structural vibrations, an oscillatory surface is left by the cutter in the initial pass. In the next pass, the vibrating cutter removes the wavy surface left from the previous wavy surface. As a result of these two waves a variable, or modulated, chip thickness is obtained as shown in Figure 1.1. The periodically varying chip thickness would result in oscillatory cutting forces and leads to growing the vibrations.

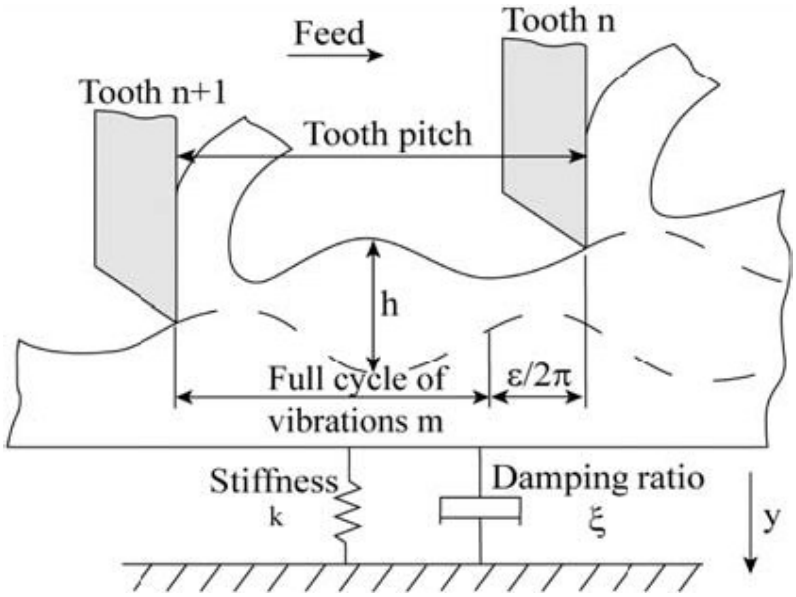

Figure 1.1 Regenerative chatter model with one degree of freedom

Many studies have been performed on chatter to predict chatter-free cutting conditions. Stability lobe diagrams as shown in Figure 1.2 have been generated which contain chatter-free depth of cuts and cutting speeds to maximize the material removal rate in a stable region. The stability lobe diagrams are based on the frequency response functions (FRFs) of the system. Since chatter is a result of the relative movement between the machine/tool and the workpiece, the dynamics of the workpiece (especially for thin-walled slender structures) play a very important role on the generation of stability lobe diagrams. Furthermore, during a cutting process, the dynamics of the workpiece changes continuously due to material removal. As a result, in order to predict more realistic stability lobe diagrams, the dynamics the workpiece must be updated for every stages of the process.

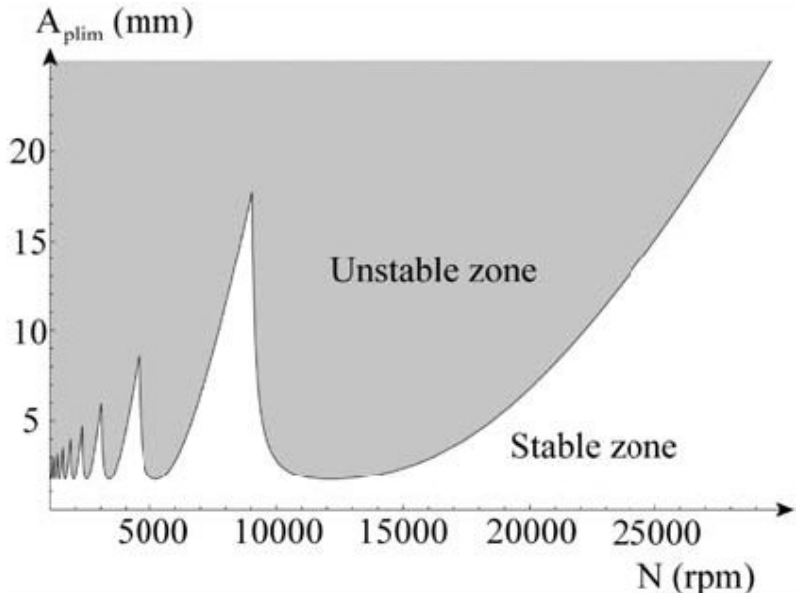

Figure 1.2 Characteristic plot of stability lobes

Performing experiments or finite element analysis of the workpiece at every stage of machining to obtain FRFs of the workpiece is impractical and time-consuming. However, the FRFs of the workpiece can be obtained from the response data of the original structure and modification matrices by using the structural modification methods. An analytical model of the original structure or its measured response is usually used in the structural modification methods. The modal model or the FRFs of the original workpiece can be estimated from the experiment in order to obtain the FRFs of the modified workpiece. Furthermore, the analytical model of the original structure formed in a finite element program may be used for predicting the FRFs of the original structure in the structural modification methods.

1.2 Literature Survey

Several studies have been done on chatter vibrations until now. Taylor [3] stressed the importance of chatter and difficulty in its suppression exactly one century ago

(1907). However, until 1950s no analytical method or solution was developed on chatter problems. First Tobias [1, 4] and Fischwick [1] established the basis of the regenerative chatter theory. They found the first analytical formulation of the dynamic cutting force variation as a function of variation of chip thickness and feed velocity. Then, Tlusty and Polacek [5] generated a chatter model for orthogonal cutting which is based on time invariant process dynamics. A feedback model explaining chatter as a closed loop interaction between the structural dynamics and the cutting process was presented by Merrit [6]. In turning, the orientation of the cutting forces and chip thickness are not a functions of time, however in milling the cutting forces, chip thickness and the direction of the excitation vary with time and have an intermittent nature due to rotating cutter. Tlusty and Koenigsberger [2] adapted their orthogonal cutting chatter stability model to milling process considering an average direction and average number of teeth in cut to find stability lobes. Opitz et al. [7, 8] generated an improved lumped model in the average force direction. Tlusty et al. [9-11] presented a method of generating stability lobes using time domain simulations of the chatter vibrations in milling. Sridhar et al. [12, 13] derived a detailed dynamic force formulation in milling. Minis and Yanushevsky [14, 15] used Floquet's Theorem and Fourier series for milling stability formulation. Then, using the Nyquist criterion they solved the problem numerically. Altıntaş and Budak [16] presented a new method for the analytical prediction of stability limits in milling. In their formulation, the time varying dynamic cutting force coefficients are approximated by their Fourier series components. Their analytical method was verified with numerical and experimental results and presented for the generation of the stability lobe diagrams [17].

In order to form the chatter models, the dynamic response of the machine tool structure is required. Tool point FRFs are usually measured using impact testing and modal analysis [18]. Considering great variety of machine tool configurations, tool holder and cutting tool geometries, to make a new test for every combination can be quite time consuming and impractical. Schmitz [19, 20] used receptance coupling method to predict the dynamics of tool holder-end mill assembly using

beam component modes. It is suggested that the dynamics of the spindle-holder subassembly can be obtained experimentally by performing an impact test at the holder tip for once. Then, the measured FRF can be coupled with the dynamics of the tool which is obtained analytically. In a recent study, Ertürk et al. [21, 22] presented an analytical approach to predict the tool point FRF by modeling the whole system (spindle, tool holder and tool). They also used the model developed to analyze the effects of bearing supports and spindle-holder and tool-holder interfaces on the FRF [23], and demonstrated the use of the model in fast and practical generation of the stability diagrams [24].

As mentioned earlier, if the workpiece to be machined is dynamically flexible, to obtain the stability limits accurately the workpiece dynamics must be included in the analysis. However, the dynamics of the workpiece continuously vary during machining due to the mass removal. Thus, the variation of the dynamics of the workpiece must be considered in the generation of the stability lobes. At this point, it becomes very important to use an efficient structural modification method in order to find the frequency response functions of the modified (machined) structures at intermediate steps of the machining process. This is one of the main objectives of this study.

The first reanalysis techniques were originally developed for the reduction of the computational time for the dynamic analysis of large structures. Many different reanalysis techniques are available in literature. Component mode synthesis was first presented by Hurty in 1965 [25]. After that several methods using the component mode synthesis technique have been presented. In these model reduction methods, the aim is to reduce computational time in the analysis of large structures by selecting most dominant modes [26-29].

For reanalysis purposes, dual modal space structural modification and local eigenvalue modification techniques were developed. Local eigenvalue modification (LEVM) was presented by Weissenburger [30] in 1968. Synder et al. [31, 32] extended LEVM to include damping. O'Callahan and Chou [33] used the

three dimensional generalized beam element in conjunction with LEVM procedure and presented a method to obtain more realistic structural modifications. Luk and Mitchell [34-36] developed the dual modal space structural modification method. The dual modal space structural modification method and transfer matrix method were combined by Elliott and Mitchell [37, 38] in order to make more accurate beam modifications.

As mentioned above, the structural modification methods can be divided in two categories: theoretical or experimental methods. In order to obtain a validated modal model of the structure which is modified, vibration tests can be performed and it can be used for structural modification calculations. However, the main drawback of the experimental methods is difficulties in getting the rotational degrees of freedoms from experimental data. Another restriction is that the accuracy of the modal model affects the accuracy of the reanalysis results. High dependence of experimentally determined modal models to model truncation has been shown by Braun and Ram [39] and by Elliott and Mitchell [40]. Not taking some particular modes of the original system which affects the other modes can cause errors in the modified model. In the reanalysis problems, to use FRFs of the original structure directly without using modal parameters eliminates the modal truncation problem. The problems of the FRF coupling method using experimentally obtained FRFs have been discussed by Ewins [41]. Chou et al. [42] have presented an expansion method to overcome the problems about the difficulties in measuring vibration response of rotational degrees of freedoms.

Özgüven has developed a structural modification method using FRFs of the original structure and system matrices of the modifying structure [43-45]. Özgüven first introduced the matrix inversion method to obtain the receptances of a damped system from its undamped counterparts [43]. Then, he presented a new method to calculate FRFs of non-proportionally damped structures using undamped modal data without matrix inversion [44]. Both of these methods can be applied to the structural modification problems as explained in reference 45 in which the method is also extended to structural modifications with adding additional degrees of

freedom. Main advantage of these methods is that inversion of a single matrix with the order of the size of the modifying structure (which is in most cases much less than the total dof of the system) is required. The recursive solution algorithm suggested by Özgüven [44] avoids matrix inversion, which does not only reduce the computational time, but also avoids the problems in inverting ill-conditioned matrices.

1.3 Objective

In this thesis, it is aimed to find the FRFs of the workpiece at intermediate stages of the machining process by adding the removed mass step by step to the final shape of the part until the initial workpiece dimensions are obtained. Özgüven's Structural Modification Method [43] is used to find the FRFs at intermediate stages, and then the FRFs of the workpiece are combined with tool point FRFs before generating the stability lobe diagram. The ultimate goal is to find the stability diagrams by considering the workpiece dynamics at every stage of the machining so that chatter can be avoided during the whole process. Thus it is aimed:

- to obtain the FRFs of the machined part (workpiece) efficiently by using an analytical method, instead of making finite element analysis or experiments to find FRFs at every stage
- to study in detail the effects of the changing dynamics of the workpiece on stability diagrams
- to obtain more realistic stability diagrams when thin-walled and slender parts are machined.

1.4 Scope of the Study

The outline of the thesis is as follows:

In Chapter 2, chatter theory and prediction of stability diagrams are reviewed briefly. Then the theory of the structural modification methods used, namely, Matrix Inversion Method [43] and Özgüven's Recursive Formulation [44] are given.

Chapter 3 outlines the computer program written using the structural modification methods, and gives the verification of the program by comparing the results obtained in this study with those obtained with a finite element program, MSC. Marc©.

In Chapter 4, the changing dynamics of the workpiece and its effect on the stability diagrams are analyzed in detail with case studies. The results of the case studies presented are discussed.

In Chapter 5, conclusions and suggestions for future work are given.

CHAPTER 2

THEORY

2.1 Chatter Theory and Stability Diagrams

Chatter is the result of the dynamic interactions between the machine tool and the workpiece. Chatter vibrations result in poor surface finish and reduced tool life. Tlusty et al. [5] and Tobias [4] identified the most powerful source of self-excitation which is associated with the structural dynamics of the machine tool and the feedback between the subsequent cuts on the same cutting surface resulting in regeneration of waviness on the cutting surfaces, and thus modulation in the chip thickness [46]. Under certain conditions the amplitude of vibrations grows and the cutting system becomes unstable. Although chatter is always associated with vibrations, in fact it is fundamentally due to instability in the cutting system. For a certain cutting speed there is a limiting depth of cut above which the system becomes unstable, and chatter develops. The chatter stability limit in orthogonal cutting is given as [2],

$$\boldsymbol{b}_{\lim} = \frac{-1}{2.\boldsymbol{K}_f.\mathrm{Re}[\boldsymbol{G}(\boldsymbol{\omega})]} \tag{2.1}$$

where $\boldsymbol{K}_f$ is the cutting force coefficient in the feed direction which is measured or calibrated through testing [47], $\mathrm{Re}[\boldsymbol{G}(\boldsymbol{\omega})]$ is the real part of the resultant FRF in the chip thickness direction. $\boldsymbol{G}(\boldsymbol{\omega})$ is the total transfer function of the system which can be determined by summing tool and workpiece transfer functions, i.e., $[\boldsymbol{G}(\boldsymbol{\omega})] = [\boldsymbol{G}_{cutter}(\boldsymbol{\omega})] + [\boldsymbol{G}_{workpiece}(\boldsymbol{\omega})]$.

The chip thickness variation, which is responsible for chatter vibrations, is a result of the dynamic displacements of the tool and the workpiece during cutting. Since the same cutting force acts on the cutter and the workpiece, but in the opposite directions, the total displacement (distance) can be found by multiplying the their respective transfer functions by the cutting force. By summing the transfer functions of the cutter and the workpiece, and by multiplying this total transfer function with the cutting force, the total chip thickness variation can be obtained. Therefore, the total transfer function of the system can be taken the summation of the cutter and the workpiece transfer functions.

2.1.1 Stability of Milling Process

2.1.1.1 Dynamic Chip Thickness and Milling Forces

The milling cutter and work piece are considered to have two orthogonal modal directions as shown in Figure 2.1. Milling forces excite both cutter and workpiece causing vibrations which are imprinted on the cutting surface. Each vibrating cutting tooth removes the wavy surface left from the previous tooth resulting in modulated chip thickness which can be expressed as follows [48]:

$$h_j(\phi) = \left[\Delta x.\sin\phi_j + \Delta y.\cos\phi_j\right] \tag{2.2}$$

where $\phi_j = (j-1).\phi_p + \phi$ is the angular immersion of tooth (j) for a cutter with constant pitch angle $\phi_p = 2.\pi / N$ and N teeth. $\phi = \Omega.t$ is the angular position of the cutter measured with respect to the first tooth, Ω (rad/sec) being the rotational speed of the tool.

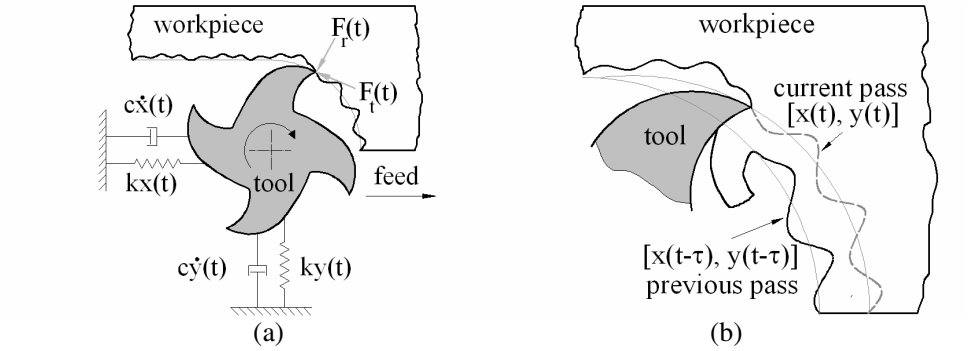

Figure 2.1 (a) Cross sectional view of an end mill showing regeneration and dynamic forces, and (b) a closer look up to the dynamic chip thickness.

The static part of the chip thickness is neglected in the stability analysis. The dynamic displacements are defined as follows:

$$\begin{aligned} \Delta x &= (x_c - x_c^o) - (x_w - x_w^o), \\ \Delta y &= (y_c - y_c^o) - (y_w - y_w^o) \end{aligned} \tag{2.3}$$

where (x_c, y_c) and (x_w, y_w) are the dynamic displacements of the cutter and the work piece in the x and y directions, respectively. The superscript (o) denotes the dynamic responses in the previous tooth period which are imprinted on the cut surface. The dynamic cutting forces on tooth (j) in the tangential and the radial directions can be expressed as follows:

$$F_{t_j} = K_t . a . h_j(\phi) \quad ; \quad F_{r_j} = K_r . F_{t_j}(\phi) \tag{2.4}$$

where a is the axial depth of cut, and K_t and K_r are the cutting force coefficients which are experimentally identified. After substituting h_j from equation (2.2) into (2.4), and summing up the forces on each tooth ($F = \Sigma F_j$), the dynamic milling forces can be resolved in x and y directions as follows:

$$\begin{Bmatrix} F_x \\ F_y \end{Bmatrix} = \frac{1}{2} . a . K_t . \begin{bmatrix} a_{xx} & a_{xy} \\ a_{yx} & a_{yy} \end{bmatrix} \begin{Bmatrix} \Delta x \\ \Delta y \end{Bmatrix} \tag{2.5}$$

where a values are the directional coefficients [16, 17] due to the rotation of the tool which makes equation (2.5) time-varying :

$$\{F(t)\} = \frac{1}{2}.a.K_t.[A(t)]\{\Delta(t)\} \tag{2.6}$$

$[A(t)]$ is periodic at the tooth passing frequency $\omega = \Omega.N$ and with the corresponding period of $T = 2.\pi/\omega$. In general, the Fourier series expansion of the periodic term is used for the solution of the periodic systems [50]. The solution can be obtained numerically by truncating the resulting infinite determinant. However, in chatter stability analysis the inclusion of the higher harmonics in the solution may not be required as the response at the chatter limit is usually dominated by a single chatter frequency. Starting from this idea, Budak and Altintas [16, 17, 49] have shown that the higher harmonics do not affect the accuracy of the predictions, and it is sufficient to include only the average term in the Fourier series expansion of $[A(t)]$:

$$[A_0] = \frac{1}{T}\int_0^T [A(t)]dt \tag{2.7}$$

As all the terms in $[A(t)]$ are valid within the cutting zone between start and exit immersion angles (ϕ_{st}, ϕ_{ex}), equation (2.7) reduces to the following form in the angular domain:

$$[A_0] = \frac{1}{\phi_p}\int_{\phi_{st}}^{\phi_{ex}} [A(\phi)]d\phi = \frac{N}{2.\pi}\begin{bmatrix} \alpha_{xx} & \alpha_{xy} \\ \alpha_{yx} & \alpha_{yy} \end{bmatrix} \tag{2.8}$$

where the integrated, or average, directional coefficients are given as:

$$\alpha_{xx}=\frac{1}{2}\left[\cos 2\phi-2K_r\phi+K_r\sin 2\phi\right]_{\phi_{st}}^{\phi_{ex}} \;;\; \alpha_{xy}=\frac{1}{2}\left[-\sin 2\phi-2\phi+K_r\cos 2\phi\right]_{\phi_{st}}^{\phi_{ex}}$$
$$\alpha_{yx}=\frac{1}{2}\left[-\sin 2\phi+2\phi+K_r\cos 2\phi\right]_{\phi_{st}}^{\phi_{ex}} \;;\; \alpha_{yy}=\frac{1}{2}\left[-\cos 2\phi-2K_r\phi-K_r\sin 2\phi\right]_{\phi_{st}}^{\phi_{ex}} \quad (2.9)$$

Then, equation (2.6) reduces to the following form:

$$\{\boldsymbol{F}(t)\}=\frac{1}{2}.a.\boldsymbol{K}_t[A_0]\{\Delta(t)\} \quad (2.10)$$

2.1.1.2 Chatter Stability Limit

The dynamic displacement vector, $\{\Delta(t)\}$, in equation (2.10) can be determined using the dynamic properties of the structures, frequency response functions, and the dynamic forces. By substituting the response and the delay terms in equation (2.10), the following expression is obtained [16, 17]:

$$\{\boldsymbol{F}\}e^{i\omega_c t}=\frac{1}{2}.a.\boldsymbol{K}_t.(1-e^{-i\omega_c T})[A_0][\boldsymbol{G}(i\omega_c)]\{\boldsymbol{F}\}e^{i\omega_c t} \quad (2.11)$$

Here, $\{\boldsymbol{F}\}$ represents the amplitude of the dynamic milling force $\{\boldsymbol{F}(t)\}$, and the transfer function matrix is given as

$$[\boldsymbol{G}(i\omega_c)]=[\boldsymbol{G}_{cutter}(i\omega_c)]+[\boldsymbol{G}_{workpiece}(i\omega_c)]$$
$$[\boldsymbol{G}_p]=\begin{bmatrix}\boldsymbol{G}_{p_{xx}} & \boldsymbol{G}_{p_{xy}}\\ \boldsymbol{G}_{p_{yx}} & \boldsymbol{G}_{p_{yy}}\end{bmatrix} \qquad (p=c,w) \quad (2.12)$$

Equation (2.11) has a non-trivial solution only if its determinant is zero,

$$\det[[\boldsymbol{I}]+\Lambda[\boldsymbol{G}_0(i\boldsymbol{\omega}_c)]]=0 \tag{2.13}$$

where $[\boldsymbol{I}]$ is the unit matrix, and the oriented transfer function matrix is defined as:

$$[\boldsymbol{G}_0]=[\boldsymbol{A}_0][\boldsymbol{G}] \tag{2.14}$$

and the eigenvalue (Λ) in equation (2.13) is given as:

$$\Lambda=-\frac{\boldsymbol{N}}{4\boldsymbol{\pi}}\boldsymbol{K}_t\boldsymbol{a}(1-\boldsymbol{e}^{-i\boldsymbol{\omega}_c\boldsymbol{T}}) \tag{2.15}$$

Λ can easily be computed from equation (2.13) numerically. However, an analytical solution is possible if the cross transfer functions, $\boldsymbol{G}_{xy}$ and $\boldsymbol{G}_{yx}$, are neglected:

$$\Lambda=-\frac{1}{2\boldsymbol{a}_0}\left(\boldsymbol{a}_1\pm\sqrt{\boldsymbol{a}_1^2-4\boldsymbol{a}_0}\right) \tag{2.16}$$

where

$$\begin{aligned}\boldsymbol{a}_0&=\boldsymbol{G}_{xx}(i\boldsymbol{\omega}_c)\boldsymbol{G}_{yy}(i\boldsymbol{\omega}_c)(\boldsymbol{\alpha}_{xx}\boldsymbol{\alpha}_{yy}-\boldsymbol{\alpha}_{xy}\boldsymbol{\alpha}_{yx})\\ \boldsymbol{a}_1&=\boldsymbol{\alpha}_{xx}\boldsymbol{G}_{xx}(i\boldsymbol{\omega}_c)+\boldsymbol{\alpha}_{yy}\boldsymbol{G}_{yy}(i\boldsymbol{\omega}_c)\end{aligned} \tag{2.17}$$

Since the transfer functions are complex, Λ will also be complex. However, the axial depth of cut, $\boldsymbol{a}$, is a real number. Therefore, when $\Lambda=\Lambda_{\boldsymbol{R}}+\boldsymbol{i}\Lambda_{\boldsymbol{I}}$ and $\boldsymbol{e}^{-i\boldsymbol{\omega}_c\boldsymbol{T}}=\cos\boldsymbol{\omega}_c\boldsymbol{T}-\boldsymbol{i}.\sin\boldsymbol{\omega}_c\boldsymbol{T}$ are substituted in Eq. (2.15), the complex part of the equation has to vanish yielding

$$\boldsymbol{\kappa}=\frac{\Lambda_{\boldsymbol{I}}}{\Lambda_{\boldsymbol{R}}}=\frac{\sin\boldsymbol{\omega}_c\boldsymbol{T}}{1-\cos\boldsymbol{\omega}_c\boldsymbol{T}} \tag{2.18}$$

Equation (2.18) can be solved to obtain a relation between the chatter frequency and the spindle speed [16, 17]:

$$\omega_c T = \varepsilon + 2.k.\pi \quad , \quad \varepsilon = \pi - 2.\psi \quad , \quad \psi = \tan^{-1}\kappa \quad , \quad n = \frac{60}{N.T} \tag{2.19}$$

where ε is the phase difference between the inner and outer modulations, k is an integer corresponding to the number of vibration waves within a tooth period, and n is the spindle speed (rpm). After the imaginary part in equation (2.15) is vanished, the following is obtained for the stability limit [16, 17]:

$$a_{\lim} = -\frac{2.\pi.\Lambda_R}{N.K_t}\left(1+\kappa^2\right) \tag{2.20}$$

Therefore, for a given cutting geometry, cutting force coefficients, tool and workpiece transfer functions, and a chatter frequency ω_c, Λ_I and Λ_R can be determined from equation (2.16), and can be used in equations (2.19) and (2.20) to determine the corresponding spindle speed and the stability limit. When this procedure is repeated for a range of chatter frequencies and number of vibration waves, k, the stability lobe diagram for a milling system is obtained.

2.2 Structural Modifications without Additional Degrees of Freedom

2.2.1 Matrix Inversion Method

The matrix inversion method presented by Özgüven [43] originally developed to calculate the FRFs of the damped structures from undamped modal data, and then

later applied to structural modification problems [45]. In this section, the generalized form of the formulation for structural modifications is explained.

Consider a system with n degrees of freedom which can be written as

$$[M]\{\ddot{x}\}+i[H]\{x\}+[K]\{x\}=\{F\} \tag{2.21}$$

where $[M]$ is mass matrix,

$[H]$ is structural damping matrix

$[K]$ is stiffness matrix

$\{F\}$ is a generalized force vector

$\{x\}$ is the vector of generalized coordinates.

For a harmonic excitation force $\{F\}$ at frequency ω, the response $\{x\}$ can be found as

$$\{x\}=\left[[K]-\omega^2[M]+i[H]\right]^{-1}\{F\} \tag{2.22}$$

Then the receptance matrix $[\alpha]$ can be written as

$$[\alpha]=\left[[K]-\omega^2[M]+i[H]\right]^{-1} \tag{2.23}$$

In a similar manner, the receptance matrix of the modified system can be written as

$$[\gamma]=\left[[K]+[\Delta K]-\omega^2[[M]+[\Delta M]]+i[[H]+[\Delta H]]\right]^{-1} \tag{2.24}$$

where $[\Delta K]$, $[\Delta M]$ and $[\Delta H]$ are stiffness, mass and damping modification matrices, respectively. Inverting both sides of equations (2.23) and (2.24) and one can obtain

$$[\gamma]^{-1} = [\alpha]^{-1} + [D] \tag{2.25}$$

where $[D]$ denotes the dynamic structural modification matrix and is expressed as

$$[D] = [\Delta K] - \omega^2[\Delta M] + i[\Delta H] \tag{2.26}$$

Pre-multiplying all terms of equation (2.25) by $[\alpha]$ and post-multiplying them by $[\gamma]$ gives

$$[\alpha] = [\gamma] + [\alpha][D][\gamma] \tag{2.27}$$

$[\gamma]$ can be obtained as

$$[\gamma] = [[I] + [\alpha][D]]^{-1}[\alpha] \tag{2.28}$$

When the structural modification is local

$$[D] = \begin{bmatrix} [D_{11}] & [0] \\ [0] & [0] \end{bmatrix} \tag{2.29}$$

then equation (2.28) can be written in partitioned form, so that the receptance submatrices of the modified system can be obtained [43] as

$$[\gamma_{11}] = [[I] + [\alpha_{11}][D_{11}]]^{-1}[\alpha_{11}] \tag{2.30}$$

$$[\gamma_{12}]^T = [\gamma_{21}] = [\alpha_{21}][[I] - [D_{11}][\gamma_{11}]] \tag{2.31}$$

$$[\gamma_{22}] = [\alpha_{22}] - [\alpha_{21}][D_{11}][\gamma_{12}] \tag{2.32}$$

Subscripts 1 and 2 correspond to modified and unmodified regions of the structure, respectively. As can be seen from the equations, to find the receptance matrix of a modified system it is sufficient to the take the inverse of a single matrix which has an order equal to the number of coordinates involved in the structural modifications. So if the modification is made on a small number of coordinates, the computational time will be reduced considerably.

2.2.2 Özgüven's Recursive Formulation

This method, like the matrix inversion method, was developed to calculate the receptances of non-proportionally damped structures from the undamped counterparts [44]. The algorithm developed can easily be used for structural modification problems without adding additional degrees of freedom to the system [45].

Consider the system with n degrees of freedom which can be expressed as

$$[\boldsymbol{M}]\{\ddot{\boldsymbol{x}}\}+\boldsymbol{i}[\boldsymbol{H}]\{\boldsymbol{x}\}+[\boldsymbol{K}]\{\boldsymbol{x}\}=\{\boldsymbol{F}\} \tag{2.33}$$

In a similar manner, the system equation of the modified system can be written as

$$[[\boldsymbol{M}]+[\Delta\boldsymbol{M}]]\{\ddot{\boldsymbol{x}}\}+\boldsymbol{i}[[\boldsymbol{H}]+[\Delta\boldsymbol{H}]]\{\boldsymbol{x}\}+[[\boldsymbol{K}]+[\Delta\boldsymbol{K}]]\{\boldsymbol{x}\}=\{\boldsymbol{F}\} \tag{2.34}$$

where $[\Delta\boldsymbol{K}]$, $[\Delta\boldsymbol{M}]$ and $[\Delta\boldsymbol{H}]$ are respectively stiffness, mass and damping modification matrices. The terms with modification matrices in equation (2.34) can be taken to the other side of the equation and can be regarded as a set of external forces to the original structure (which can be written in terms of dynamic stiffness values and the displacement of the system). Then the equation of motion can be written as

$$[M]\{\ddot{x}\}+i[H]\{x\}+[K]\{x\}=\{F\}+\{D\} \tag{2.35}$$

where $\{D\}$ is a vector representing dynamic stiffness forces defined as

$$\{D\}=-[\Delta M]\{\ddot{x}\}-i[\Delta H]\{x\}-[\Delta K]\{x\} \tag{2.36}$$

For a harmonic excitation force $\{F\}$ at frequency ω, equation (2.35) takes the form

$$\left[[K]-\omega^2[M]+i[H]\right]\{x\}=\{F\}+\{D\} \tag{2.37}$$

where

$$\{D\}=-\left[[\Delta K]-\omega^2[\Delta M]+[\Delta H]\right]\{x\} \tag{2.38}$$

Equation (2.35) permits one to consider the modified system as an unmodified system with two sets of external forces one of which is defined in terms of the unknown dynamic displacements $\{x\}$ of the modified system. The receptances of the unmodified system described by equation (2.35) can easily be found by modal superposition.

If a typical coordinate *s* is considered, the dynamic stiffness force on this coordinate can be written as

$$D_s=-\sum_{k=1}^{n} d_{sk}x_k \tag{2.39}$$

where

$$d_{sk}=k_{sk}-\omega^2 m_{sk}+ih_{sk} \tag{2.40}$$

Then, the response of the modified system, $\{\boldsymbol{x}\}$, to a harmonic external force, $\{\boldsymbol{F}\}$, can be found by considering the unmodified system with two sets of harmonic forces as implied by equation (2.35). From the definition of receptance, the dynamic displacement of the p^{th} coordinate can be written as

$$\boldsymbol{x}_p = \sum_{s=1}^{n} \boldsymbol{\beta}_{ps} \left(\boldsymbol{F}_s + \boldsymbol{D}_s \right) \tag{2.41}$$

$$\boldsymbol{x}_p = \sum_{s=1}^{n} \boldsymbol{\beta}_{ps} \boldsymbol{F}_s - \sum_{s=1}^{n} \boldsymbol{\beta}_{ps} \sum_{k=1}^{n} \boldsymbol{d}_{sk} \boldsymbol{x}_k \tag{2.42}$$

Both $\boldsymbol{x}_p$ and $\boldsymbol{x}_k$ are the displacements in the modified system. Then the receptance $\boldsymbol{\alpha}_{pj}$ of the modified system can be obtained from equation (2.42) by dividing all terms by $\boldsymbol{F}_j$ and setting all external forces, except $\boldsymbol{F}_j$, to zero:

$$\boldsymbol{\alpha}_{pj} = \boldsymbol{\beta}_{pj} - \sum_{s=1}^{n} \boldsymbol{\beta}_{ps} \sum_{k=1}^{n} \boldsymbol{d}_{sk} \left(\boldsymbol{x}_k / \boldsymbol{F}_j \right) \tag{2.43}$$

Since the receptance $\boldsymbol{\alpha}_{pj}$ is defined as the displacement of the p^{th} coordinate when there is a unit external force at the j^{th} coordinate while all the other external forces are zero, the term $\boldsymbol{x}_k / \boldsymbol{F}_j$ in equation (2.43) can be identified as $\boldsymbol{\alpha}_{kj}$ and equation (2.43) can be written as

$$\boldsymbol{\alpha}_{pj} = \boldsymbol{\beta}_{pj} - \sum_{s=1}^{n} \boldsymbol{\beta}_{ps} \sum_{k=1}^{n} \boldsymbol{d}_{sk} \boldsymbol{\alpha}_{kj} \tag{2.44}$$

which is valid for any p and j (p = 1, 2, ..., n; j = 1, 2, ..., n). If only a single element of the dynamic stiffness matrix, say $\boldsymbol{d}_{sk}$, is considered while the rest of the modification elements are taken to be zero, equation (2.44) takes the form of

$$\boldsymbol{\alpha}_{pj} = \boldsymbol{\beta}_{pj} - \boldsymbol{\beta}_{ps} \boldsymbol{d}_{sk} \boldsymbol{\alpha}_{kj} \qquad (p = 1, 2, \ldots, n; j = 1, 2, \ldots, n) \tag{2.45}$$

from which α_{kj} can be obtained (by taking $p = k$) as

$$\alpha_{kj} = \beta_{kj} / (1 + \beta_{ks} d_{sk}) \qquad (j = 1, 2, \ldots, n) \qquad (2.46)$$

Once the α_{kj} ($j = 1, 2, \ldots, n$) are calculated from equation (2.46), the remaining receptance values α_{pj} ($p = 1, 2, \ldots, k-1, k+1, \ldots, n$; $j = 1, 2, \ldots, n$) are found from the calculated values of α_{kj} ($j = 1, 2, \ldots, n$) by using equation (2.45).

The above formulation gives the receptance of the system composed of the unmodified system and a single modification element d_{sk}. If the calculated receptances are treated as β values in equations (2.45) and (2.46), a new set of receptances can be calculated by considering another modification element of the original dynamic stiffness matrix $[D]$. If this procedure is repeated for all elements of $[D]$, the final receptance matrix $[\alpha]$ gives the receptances of the modified system.

A considerable reduction in the computational effort can be achieved if the modification is local,

$$[D] = \begin{bmatrix} [D_{11}] & [0] \\ [0] & [0] \end{bmatrix} \qquad (2.47)$$

Then, α_{kj} ($j = 1, 2, \ldots, n$) can be found from equation (2.46), and equation (2.45) may be used to find α_{pj} for only m values of p, where m is the order of the submatrix $[D_{11}]$. Therefore, the final values of α_{pj} ($p = 1, 2, \ldots, m$; $j = 1, 2, \ldots, n$) which include the effect of all the m^2 modification element values can be calculated without computing the receptances corresponding to only unmodified coordinates (i.e., without calculating $[\alpha_{22}]$). Thus the number of recomputations of

each receptance will be reduced from n^2 to m^2, since the number of modification elements will be just m^2.

Calculating of the receptances corresponding to unmodified coordinates, then can be achieved by using equation (2.44)

$$\alpha_{pj} = \beta_{pj} - \sum_{s=1}^{m} \beta_{ps} \sum_{k=1}^{m} d_{sk} \alpha_{kj} \tag{2.48}$$

for p = m+1, . . ., n; $j = p$, . . ., n.

A further improvement in the formulation is made by considering one column of the dynamic stiffness matrix at a time. When, say, the k^{th} column of the dynamic stiffness matrix $[\boldsymbol{D}_{11}]$ is considered, from equation (2.44) one can write

$$\alpha_{pj} = \beta_{pj} - \left(\sum_{s=1}^{m} \beta_{ps} d_{sk} \right) \alpha_{kj} \tag{2.49}$$

or $p = k$,

$$\alpha_{kj} = \beta_{kj} \Big/ \left(1 + \sum_{s=1}^{m} \beta_{ks} d_{sk} \right) \qquad (\ j = 1, 2, \ldots, n\ ) \tag{2.50}$$

After calculating the α_{kj} (j = 1, 2, ..., n), which include the effect of the k^{th} column of the dynamic stiffness matrix, the remaining elements of $[\alpha_{11}]$ and $[\alpha_{12}]$ can be found from equation (2.49) for j = 1, 2, ..., n , and p = 1, 2, . ., k-1, k+1, . ., m. After repeating this procedure m times (k = 1, 2, ..., m), the final values of the upper m x n portion of $\lfloor \alpha \rfloor$ will be obtained. The remaining elements of the receptances matrix can be obtained from equation (2.48).

CHAPTER 3

COMPUTER PROGRAM AND VERIFICATION

3.1 Overview of the Computer Program

The computer program is developed in Visual C++ 6.0© and Matlab©. The program is based on the Matrix Inversion Method [43]. The program uses the output file of MSC. Marc Mentat© which has ".out" extension. The program reads and stores the eigenvectors, eigenfrequencies and the system matrices of each element from this file. A text file is formed which includes the nodes of the modified elements. If there are nodes restricted in motion, their numbers must be removed and renumbering must be performed. The user must define the total number of degrees of freedom (dofs) of the system, the number of dofs of the modifying matrices, the number of the modes extracted from FE model and the starting frequency, ending frequency and frequency step values of required FRF calculation. The program firstly calculates the receptance of the unmodified structure using modal parameters by modal summation formulation which is given as

$$\alpha_{ij}(\omega) = \sum_{r=1}^{N} \frac{\phi_{ir}\phi_{jr}}{\omega_r^2 - \omega^2 + i\gamma\omega_r^2} \tag{3.1}$$

where $\alpha_{ij}(\omega)$, ϕ, ω_r and γ are the receptance matrix, mass normalized eigenvector , r^{th} eigenfrequency of the system, and loss factor respectively.

Then using Matrix Inversion Method [43] the receptance of the modified structure is calculated at required frequency range and at all nodes; but only the FRFs at the required nodes (locations) are stored.

3.2 Extraction of the Program Input Data from Finite Element Program

As previously mentioned, in order to find the changing dynamics of the workpiece in a machining process by using structural modification methods, the FRFs of the original structure and the modification matrices (mass, stiffness and damping matrices) are needed. For this purpose, first, the workpiece with its final shape and the removed mass are modeled by using the finite element analysis (FEA) program, MSC. Marc©. Then, the modal parameters and system matrices of the workpiece are obtained through modal analysis. The reason for choosing MSC. Marc© program is to give the system matrices in its output file without any extra command or program. Only the choice of element matrices button in the "Output File" tab is enough in order to obtain element system matrices in the pre/post processor, MSC. Mentat©. The format of the output file of MSC. Marc© is available in Appendix A. In order to read the eigenfrequencies and eigenvectors from the file and to write them in a matrix/vector form, a program was also written in Visual C++ 6.0©. The structural modification program was written in Matlab© due to its predefined functions.

In order to obtain modification matrices, modeling the removed mass which is added to the original workpiece, is not sufficient in the calculations. In both beam and plate models of the workpiece in the FEA program, the workpiece is modified by changing its thickness. Because the stiffness of the beam and plate in bending is related with area moment of inertia, change in thickness does not result in a

linearly proportional change in the stiffness of the workpiece. The area moment of inertia changes with the third power of the thickness in the structures with rectangular cross section. In order to find modification stiffness matrix, the removed volume is modeled with both initial and final thicknesses. Then, by taking the difference of the stiffness matrices of two models, the modification stiffness matrix is obtained. For the modification mass matrix, such a process is not required since the variation in the thickness of the workpiece affects the area term in the mass matrix. Therefore, the mass matrix changes linearly with changing thickness of the workpiece, and the modification mass matrix can be determined by modeling the removed mass in the FEA program directly.

3.3 Verification

In this section, it is aimed to verify the computer program developed. For this purpose, the results obtained with the computer program are compared with those found by using a finite element model of the workpiece. A beam and plate models are used for the workpiece in verifying the program. The FRFs of the modified workpiece are calculated by using both the computer program developed and the finite element program and then the results obtained are compared.

3.3.1 Beam Model

The beam model used for the workpiece is shown in Figure 3.1 where the respective sizes are given follows:

Length: 100 mm
Width: 50 mm

Thickness: 5 mm

The boundary conditions of the beam are taken as fixed-free. The material of the beam is steel with Young's modulus of 200GPa, Poisson's ratio of 0.3 and the density of 7800 kg/m^3. The damping models of MSC. Marc© used in the beam model are given in equation (3.2).

$$[C] = a.[M] + \frac{2.b}{\omega}.[K] \tag{3.2}$$

where a and b are the damping coefficients,

$[C], [M], [K]$ are the damping, mass and stiffness matrices,

ω is the excitation frequency.

The damping coefficients a and b are taken as 0.03 and 0.02, respectively, in the beam models used in the case studies given in this thesis.

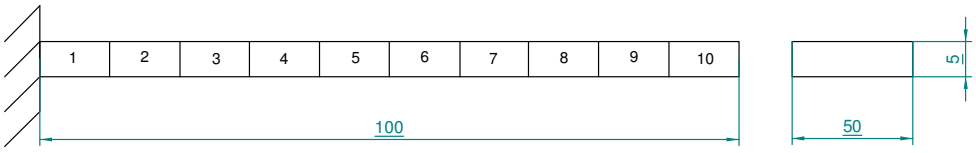

Figure 3.1 Beam model

The workpiece is modeled in MSC. Marc Mentat© with beam elements (Element type 5) as shown in Figure 3.2. Each node of the beam element has 3 degrees of freedom (displacement in x axis, displacement in y axis and rotation in z axis) and the total degree of freedom of the model is 30 with 10 elements.

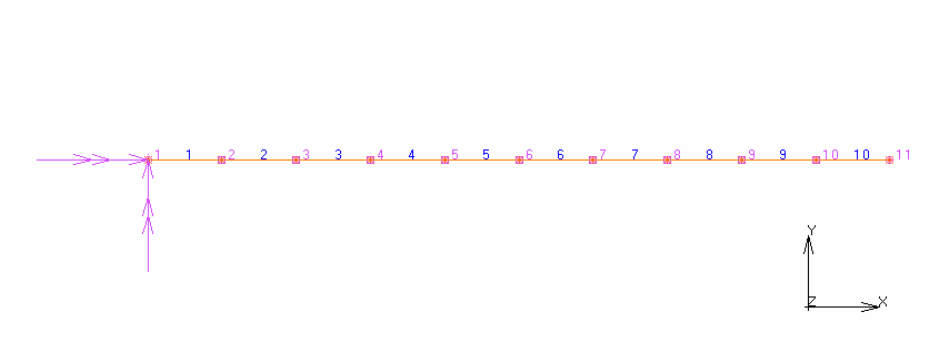

Figure 3.2 Beam model in MSC. Marc Mentat©

3.3.1.1 Modification

An additional mass with a thickness of 10mm is added to the 10th and the 6th element as shown in Figure 3.3. The material is the same as that of the original structure. The FRFs of the modified structure is calculated by MSC. Marc© and also by the program developed using the structural modification (SM) method. As seen in Figure 3.4, the FRF curves found by MSC. Marc© and the SM method match very well so that they seem as only one curve.

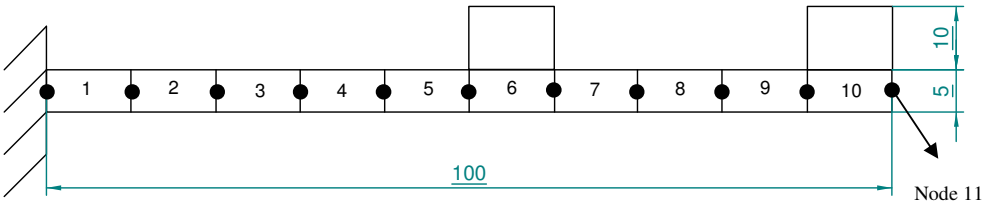

Figure 3.3 Modified beam model

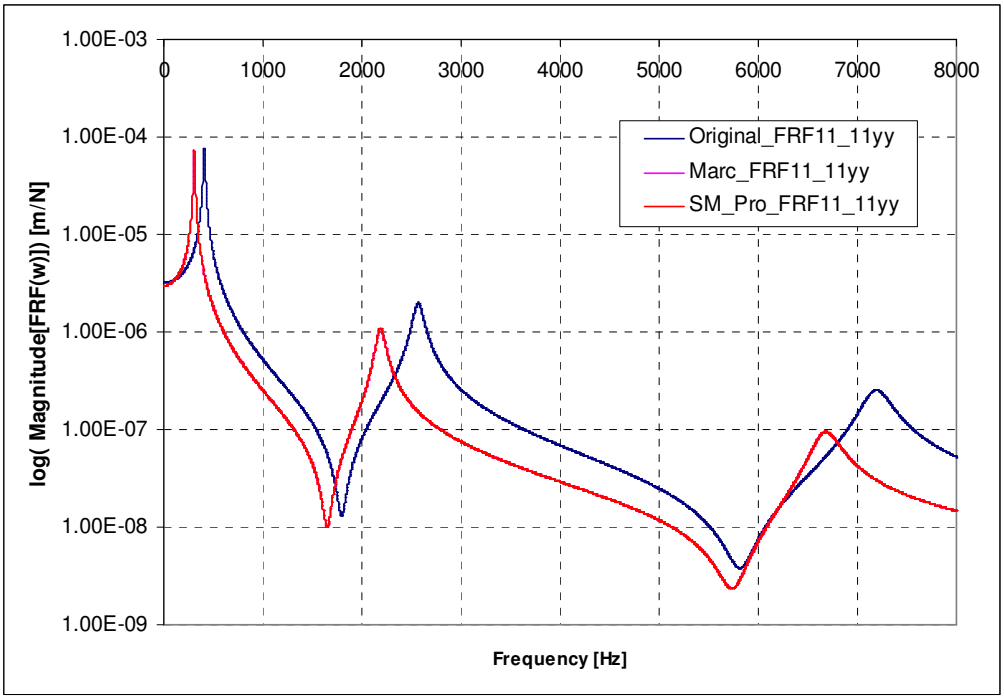

Figure 3.4 FRFs of the original and modified model calculated by MSC. Marc© and the SM method

3.3.2 Plate Model

The plate model is shown in Figure 3.5 where the respective sizes are given follows:

Length: 150 mm
Width: 100 mm
Thickness: 10 mm

The boundary conditions of the plate are taken as fixed-free. The material of the plate is steel with Young's modulus of 200 GPa, Poisson's ratio of 0.3 and the

density 7800 kg/m^3. As mentioned in Section 3.3.1, the damping coefficients ***a*** and ***b*** are taken as 0.03 and 0.02, respectively.

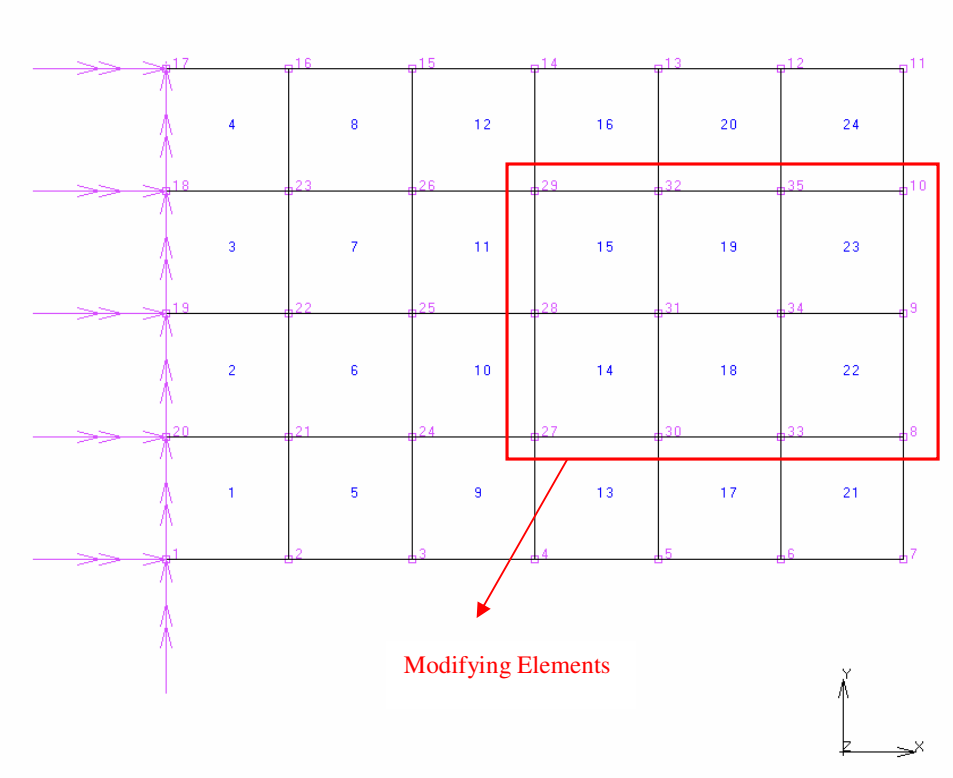

Figure 3.5 Plate Model

The workpiece is modeled in MSC. Marc Mentat© with shell elements (Element type 139) as shown in Figure 3.5. Each node of the beam element has 6 degrees of freedom (displacement in x axis, displacement in y axis, displacement in z axis, rotation in x axis, rotation in y axis and rotation in z axis) and the total degree of freedom of the model is 180 (The motion of 5 nodes are restricted in all directions) with 24 elements.

3.3.2.1 Modification

Additional masses with a thickness of 10mm is added to the 14th, 15th, 18th, 19th, 22nd and 23rd element as shown in Figure 3.5. The material is the same as that of the original structure. The FRFs of the modified structure are calculated by MSC. Marc© and also by the program developed using the structural modification (SM) method. As seen in Figure 3.6, the FRF curves found by MSC. Marc© and the SM method match very well so that they seem as only one curve.

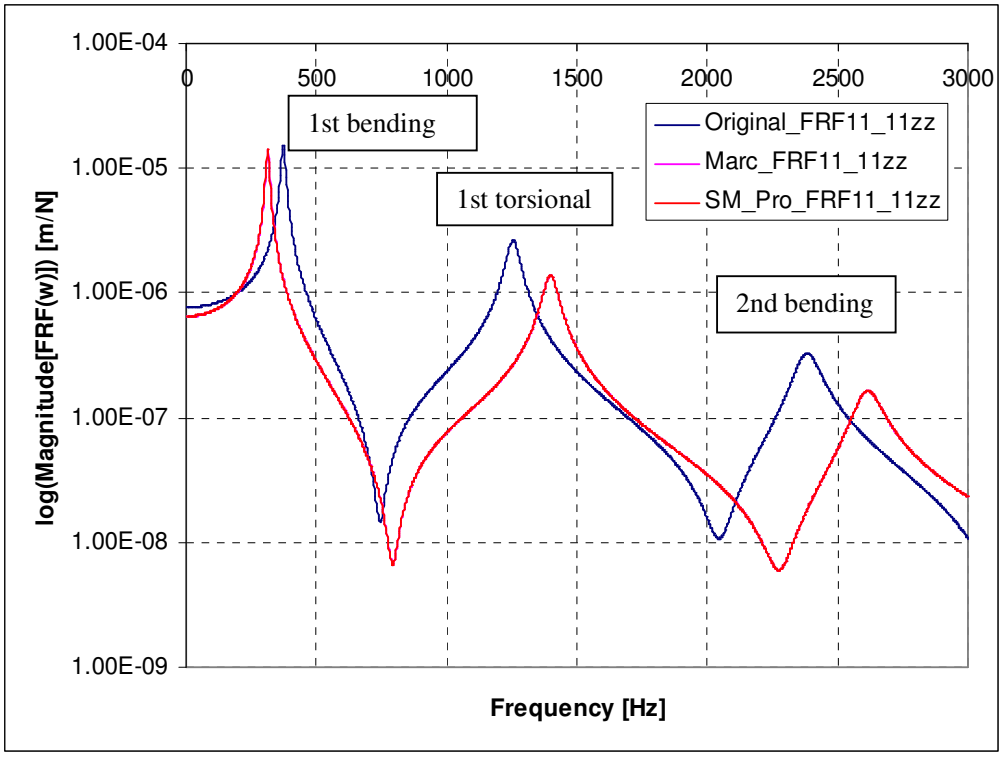

Figure 3.6 FRFs of the original and modified model calculated by MSC. Marc© and the SM method

The identical results obtained in both models verify the program developed. This was an expected result, as the method used in structural modification is an exact one. Therefore the program gives the same results with MSC. Marc©.

As shown in Figure 3.6, with this modification the first natural frequency of the workpiece decreases as the second and the third ones increase. Since increasing the workpiece thickness at the free end affects the stiffness of the workpiece less in the first mode shape, the first natural frequency of the workpiece reduces due to mass effect of the modification. Because of the mode shapes of the 2nd (1st torsional) and the 3rd (2nd bending) natural frequencies, the thickness increase at this location causes increased workpiece stiffness, and thus increased natural frequencies.

CHAPTER 4

EFFECT OF THE FLEXIBILITY OF THE WORKPIECE ON STABILITY DIAGRAMS

4.1 Effects of Workpiece Flexibility

In machining processes, the geometry, and thus the dynamics of the workpiece change continuously. During cutting, mass, stiffness and damping of the workpiece vary as a result of the removed mass. If the flexibility of the workpiece becomes comparable with tool-tool holder-spindle system at any stage of the machining process, the effect of work dynamics on the process dynamics and stability must be taken into account. For such cases, the stability diagrams should be formed by using the system FRF which is the addition of the tool point and the workpiece FRFs.

As mentioned in Chapter 2, chatter stability limit is inversely proportional to the real part of the FRFs of the system. In the machining of a flexible workpiece, the part flexibility is further increased resulting in significant reduction in stable depth of cuts. Thus, if the effect of the workpiece flexibility is not included in the stability analysis, chatter can occur at unexpected speeds and depths resulting in problems during production.

In this chapter, the effect of workpiece dynamics for an already flexible part or for a part whose flexibility is increased during the machining, on machining stability is studied in detail with case studies. Since chatter is a common problem in milling

operations where flexible parts such as thin walled components are machined using slender cutting tools, the applications are focused on milling processes. The workpiece is modeled both as a beam and as a plate in a finite element program, MSC. Marc Mentat©. Assuming a cutting strategy which defines the workpiece's geometry variation pattern, the workpiece is meshed, and by using an inverse process, the removed material is virtually added to the geometry of the workpiece continuously until the original part geometry is obtained. At every machining step, the FRFs of the workpiece is found by the structural modification method [43] using the FRF of the main body and the removed section properties. These FRFs are summed with the FRFs of the tool-holder-spindle assembly calculated by an analytical modeling approach [21-24], and used in the analytical stability diagram generation [16, 17].

4.2 Case Studies

4.2.1 Beam Model of the Workpiece

In order to obtain FRFs at different stages and locations of the workpiece during machining, as a first attempt the workpiece is modeled as a beam in FE program, MSC. Marc Mentat©.

The beam model is shown in Figure 4.1 where the respective sizes are given follows:

Length : 100 mm
Width : 50 mm
Thickness : 15 mm

The material of the beam is steel with Young's modulus of 200GPa, Poisson's ratio of 0.3 and the density of 7800 kg/m^3. As mentioned in Section 3.3.1 the damping coefficients $\boldsymbol{a}$ and $\boldsymbol{b}$ are taken as 0.03 and 0.02 respectively. The boundary conditions of the beam are taken as fixed-free. This model resembles a part clamped on the machine tool table such as a turbine or compressor blade.

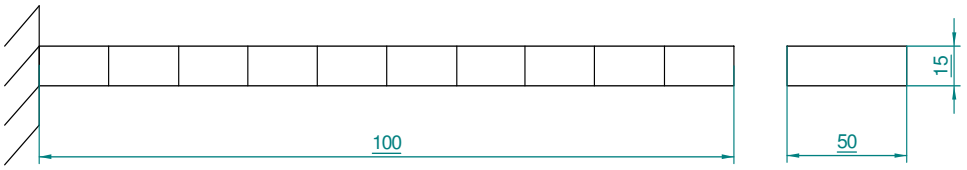

Figure 4.1 Beam model

The workpiece is modeled in MSC. Marc Mentat© with beam elements (Element type 5) as shown in Figure 4.2. Each node of the beam element has 3 degrees of freedom (displacement in x axis, displacement in y axis and rotation in z axis) and the total degree of freedom of the model is 30 with 10 elements.

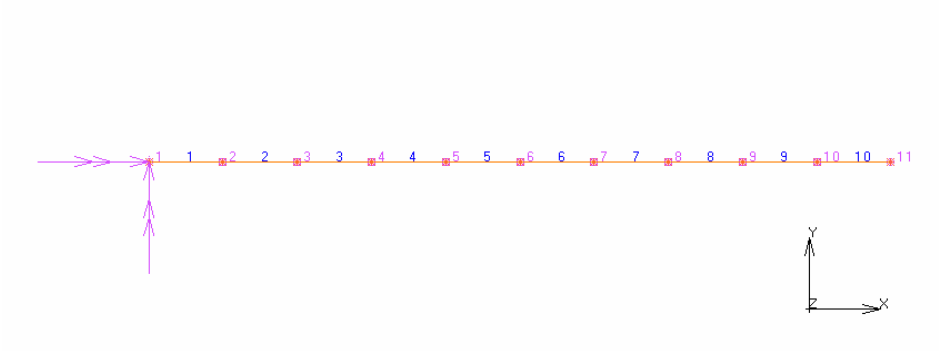

Figure 4.2 Beam model in MSC. Marc Mentat©

4.2.1.1 Tool-Holder-Spindle Model

As mentioned in Section 4.1, a spindle-holder-tool combination is selected, and its tool point FRF is used to predict the stability diagrams. The material used for the elements of the assembly is steel with Young's modulus of 200GPa, Poisson's ratio of 0.3 and mass density of 7800 kg/m^3. The material loss factor is assumed to be 0.003.

The geometry of the tool is shown in Figure 4.3 where the sizes are given as follows:

Segments length(mm) : 0.10 0.01
Outer diamaters(mm) : 25 28
Outer diameters of segments inside the tool holder(mm) : 28
Inner diameters of segments inside the tool holder(mm) : 0

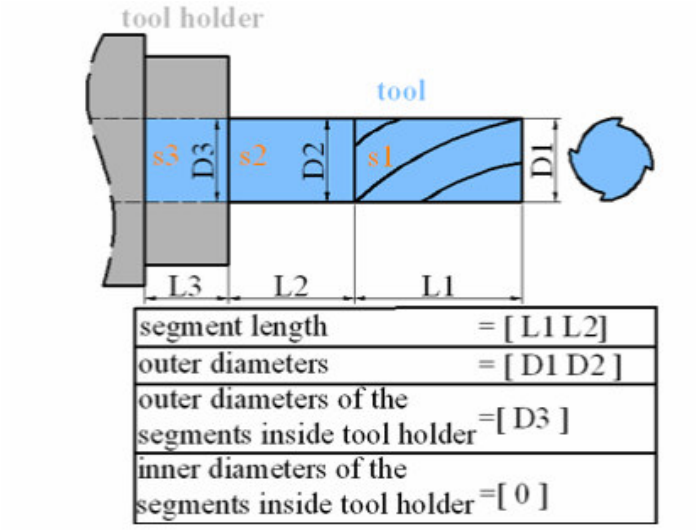

Figure 4.3 Tool geometry

The geometry of the tool holder is shown in Figure 4.4 where the sizes are given as follows:

Segments length(mm) : 30 24 28

Outer diamaters(mm) : 64 55 61

Inner diameters(mm) : 28 28 28

Outer diameters of segments inside the tool holder(mm) : 54 48 40 32

Inner diameters of segments inside the tool holder(mm) : 16 16 16 16

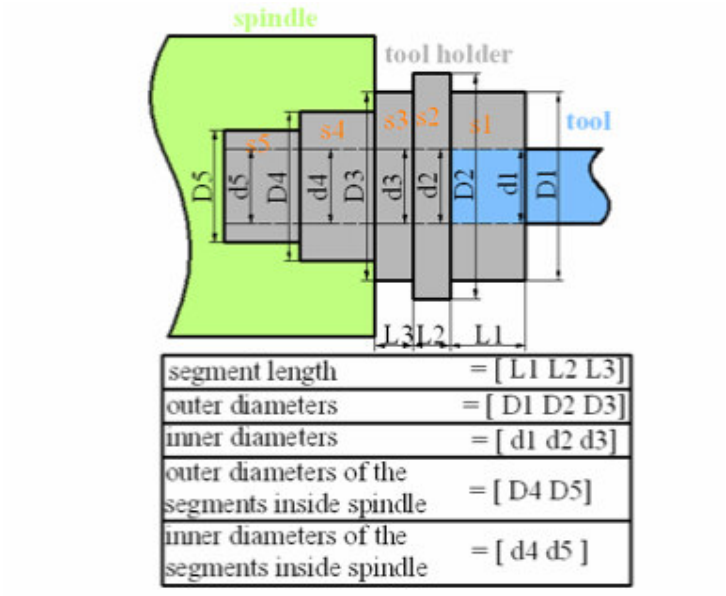

Figure 4.4 Tool holder geometry

The geometry of the spindle is shown in Figure 4.5 where the sizes are given as follows:

Segments length(mm) : 16 30 30 30 8 140 86 55 20 30 70

Outer diamaters(mm) : 66 66 66 66 66 76 70 62 54 54 54

Inner diameters(mm) : 54 48 40 32 24 24 24 24 24 24 24

Segments having bearings : 1 3 8 9

Translational stiffness [N/m] : 60e7 60e7 2.5e6 2.5e6

Translational damping [N.s/m] : 800 800 200 200

Rotational stiffness [N/m] : 0 0 0 0

Rotational damping [N.s/m] : 0 0 0 0

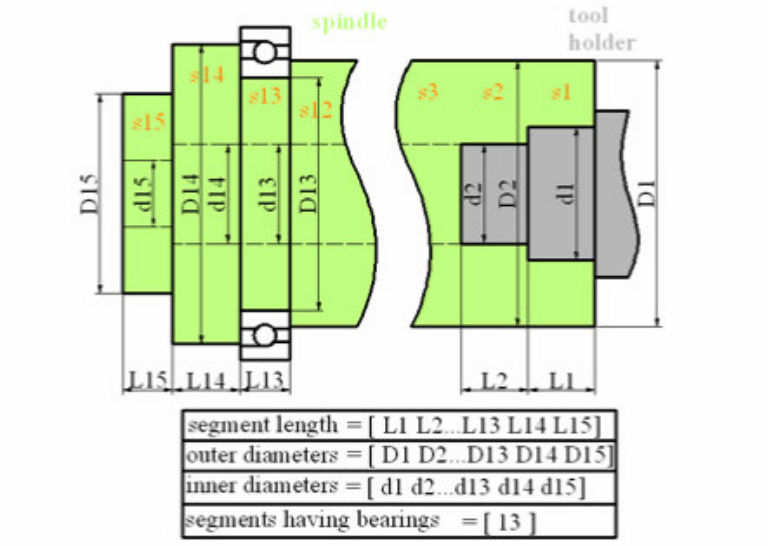

Figure 4.5 Spindle geometry

In order to find the tool point FRF of this system, an analytical modeling approach developed by Ertürk, et. al [21-24] is used.

4.2.1.2 Machining Process and FRFs of the Workpiece

The workpiece is assumed to be machined in three main cutting cycles. These are

- ***Roughing cut*** : Thickness of the workpiece is reduced from 15 mm to 10 mm (radial depth of cut = 5 mm) completely.

- ***Semifinishing cut*** : Thickness of the workpiece is reduced from 10 mm to 5 mm(radial depth of cut = 5 mm) completely.

- ***Finishing cut*** : Thickness of the workpiece is reduced from 5 mm to 3 mm(radial depth of cut = 2 mm) completely.

The tangential and radial cutting force coefficients, K_t and K_r, used in order to determine the stability limits are taken as 626 MPa and 0.1597 respectively. As an initial assumption, the axial depth of cut is taken as 10 mm so that the workpiece is machined in 10 steps per cut (pass). In order to name the machining steps a coding convention is used. For example, B15 stands for 5.step of the first cut (roughing cut). In order to see the variation of the dynamics of the beam clearly, the FRFs of the beam at the same location, but in different cuts are compared. By comparing the FRFs of the workpiece in different cuts at the same location, the effect of the thickness change of the workpiece on the FRFs of the system, and the stability diagrams is studied. By comparing the FRFs of the workpiece at different locations (at the end, the middle and the tip of the workpiece), the effect of the location change during machining on the stability limits is also examined with the case studies.

4.2.1.3 FRFs of the Workpiece and Stability Diagrams at the First Step of the Cut

The geometry of the workpiece at the 1st step of cutting in the roughing, semifinishing and finishing passes are shown in Figure 4.6. In order to see the effect of the thickness change of the workpiece, the FRFs of the beam B11, B21

and B31 are drawn in Figure 4.7. The FRFs of the beam combined with the FRFs of the tool are given in Figure 4.8, to observe the effect of the FRFs of the workpiece on combined system FRFs.

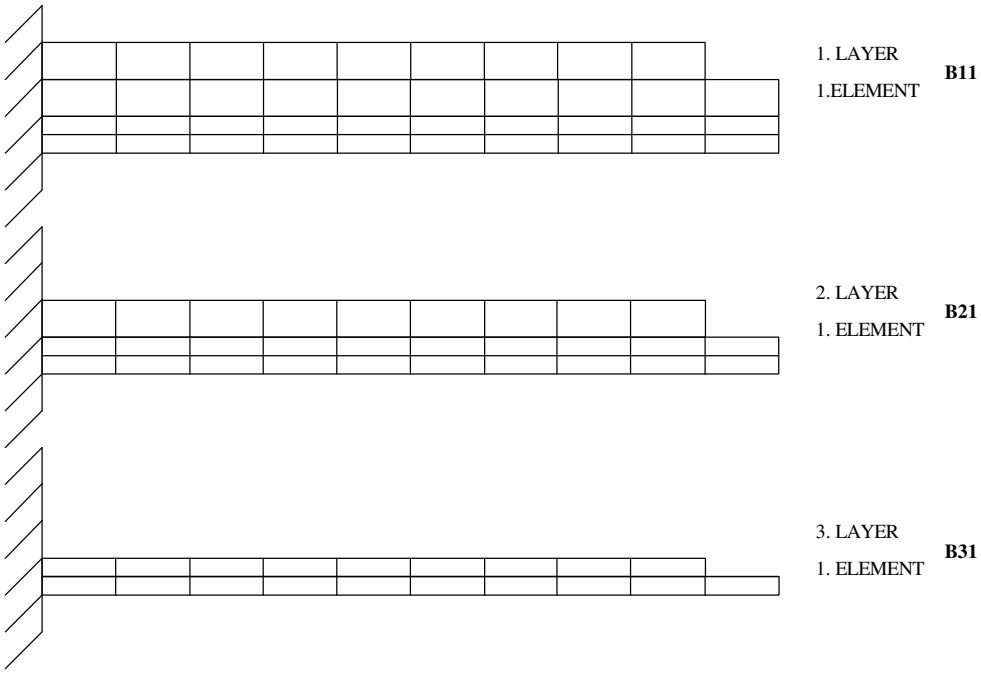

Figure 4.6 Beam models at the end of first step of 1st, 2nd and 3rd cuts

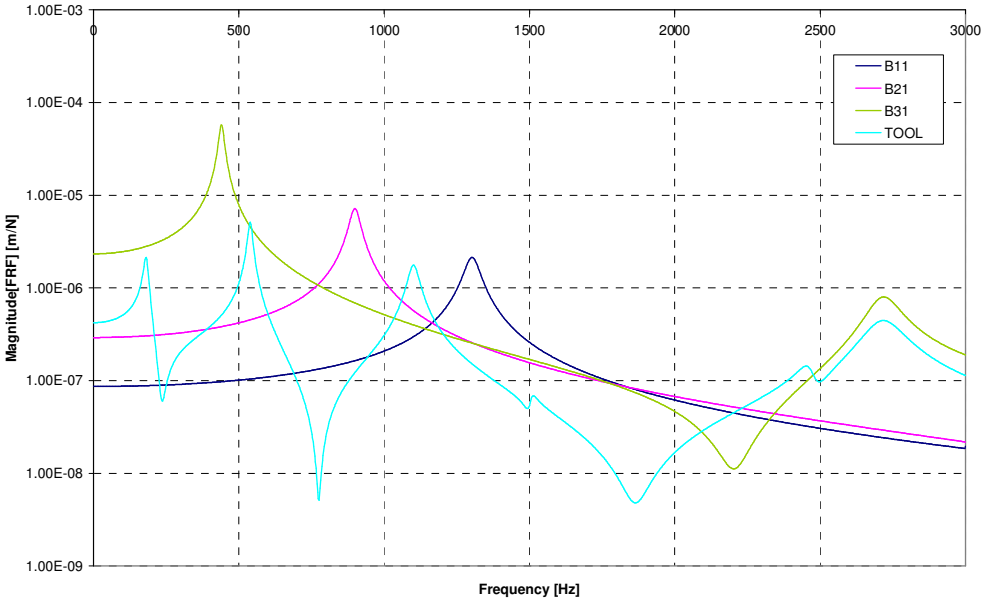

Figure 4.7 FRFs of the workpiece at the end of first step of 1st, 2nd and 3rd cuts

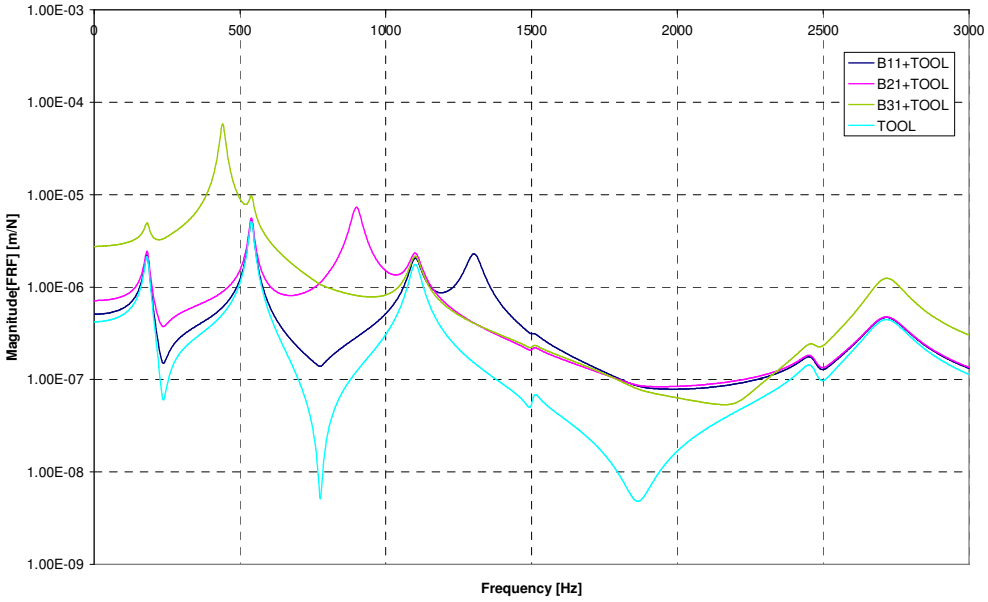

Figure 4.8 Combined FRFs of the workpiece and tool at the end of first step of 1st, 2nd and 3rd cuts

As seen from Figure 4.7 and 4.8, the magnitude of the FRFs of the workpiece increases as the workpiece becomes thinner as expected. While at the beginning of the process the flexibility of the tool is higher than that of the workpiece, at the end of the process the FRFs of the workpiece become dominant. The natural frequencies of the workpiece reduce while the thickness of the workpiece decreases as shown in Figure 4.7. This is expected since as the workpiece becomes more flexible its stiffness reduces resulting in lower natural frequencies.

The stability lobe diagrams including the changing dynamics of the workpiece at the end of the first step of the 1st, 2nd and 3rd cuts are shown in Figure 4.9.

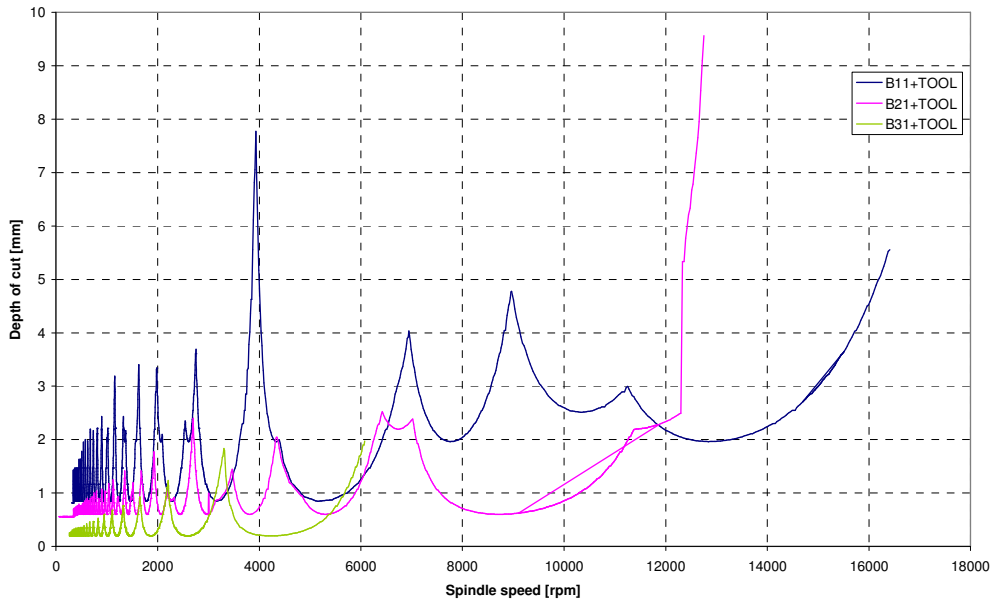

Figure 4.9 Stability lobe diagram including the FRFs of the workpiece at the end of first step of 1st, 2nd and 3rd cuts

Due to trimming problem of the program used in generating the stability lobe diagrams, in some of the stability graphs extra curves can be seen, they should not be taken into consideration.

In the stability diagrams, the stability curves may not finish at the same spindle speed for different cases. The reason is the fact that the location of the first lobe, and the other lobes, depend on the system natural frequencies. Thus, for different cases, the first lobes correspond to different spindle speeds.

As shown in Figure 4.9, the stability limit curve becomes lower and lower, as the thickness of the workpiece is reduced and becomes more flexible as expected. The absolute stability limit which is the minimum value of the stable depths, becomes lower, as the workpiece's thickness is reduced. The same behaviour can be observed in the peak stability values. The peak amplitudes of the stability limit curve decreases due to increased FRF amplitudes. The modifications done on the workpiece also affects the relative peak amplitudes of the FRFs for different modes of the structure. The amount of change in the FRF peak amplitudes as a result of the mass removal can be different for different modes of the structure. Then, the stability lobes corresponding to different modes can move up or down and left and right resulting in various forms of intersections among them. As a result, in addition to the reduced absolute and peak stability limits, some stability pockets may disappear as the workpiece becomes thinner. The spindle speeds corresponding to the peaks of the stability curve usually move to lower speeds with increasing flexibility of the workpiece. In conclusion, the variation of the workpiece dynamics results in a significant decrease in stable axial depths and speeds if the workpiece is much more flexible than the tool, and the workpiece dynamics should be included in the system FRFs used in stability calculations.

4.2.1.4 FRFs of the Workpiece and Stability Diagrams at the Fifth Step of the Cut

The geometry of the workpiece at the 5^{th} step of cutting in the roughing, semifinishing and finishing passes are shown in Figure 4.10. In order to see the

effect of the thickness change of the workpiece, the FRFs of the beam B15, B25 and B35 are drawn in Figure 4.11. The FRFs of the beam combined with the FRFs of the tool are given in Figure 4.12 to see the variation in the combined system FRFs with changing of the workpiece's thickness.

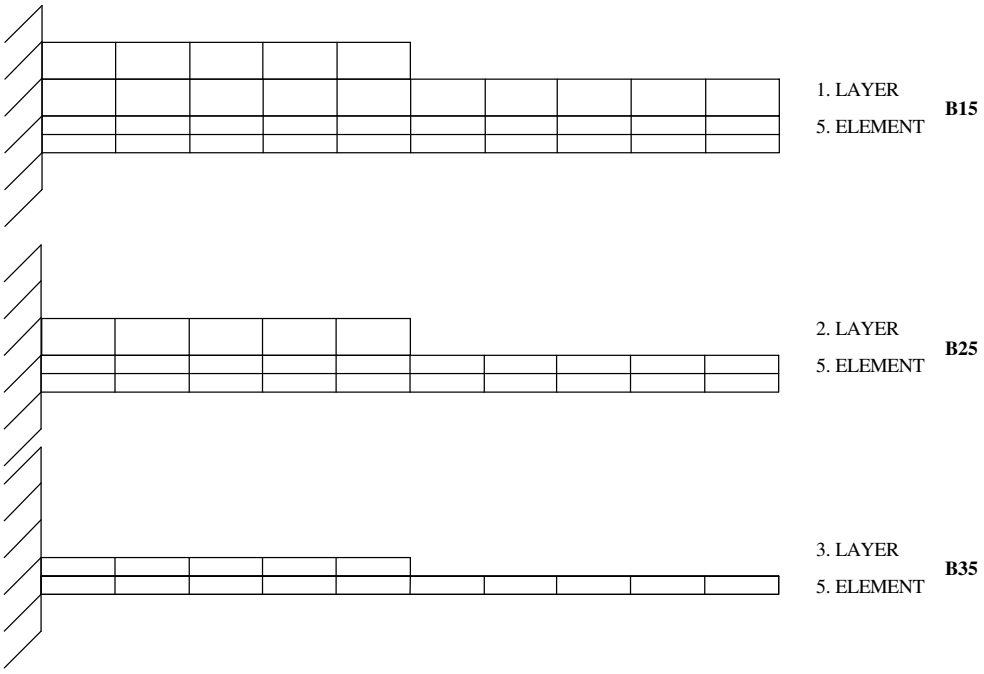

Figure 4.10 Beam models at the end of fifth step of 1st, 2nd and 3rd cuts

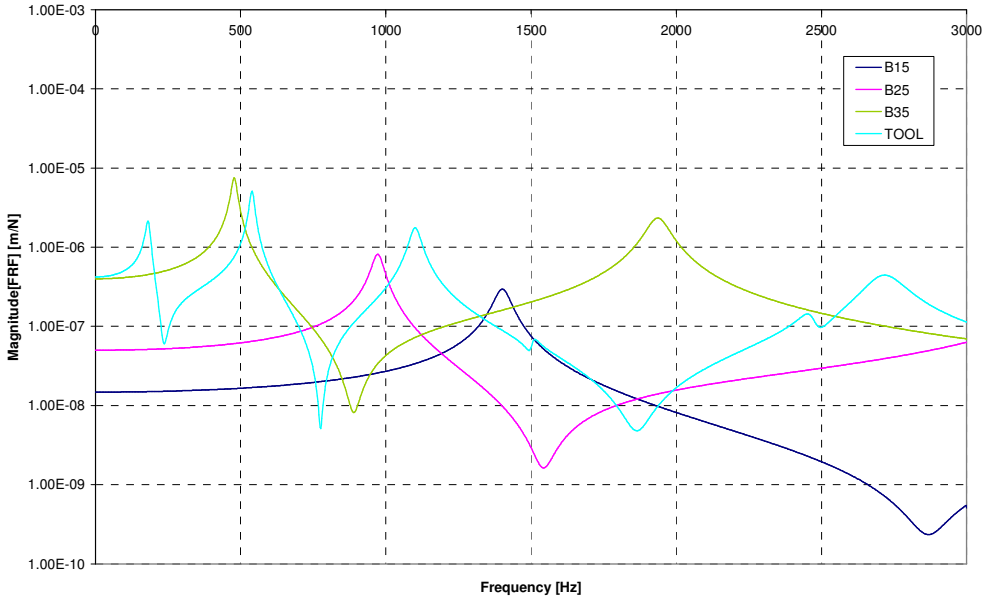

Figure 4.11 FRFs of the workpiece at the end of fifth step of 1st, 2nd and 3rd cuts

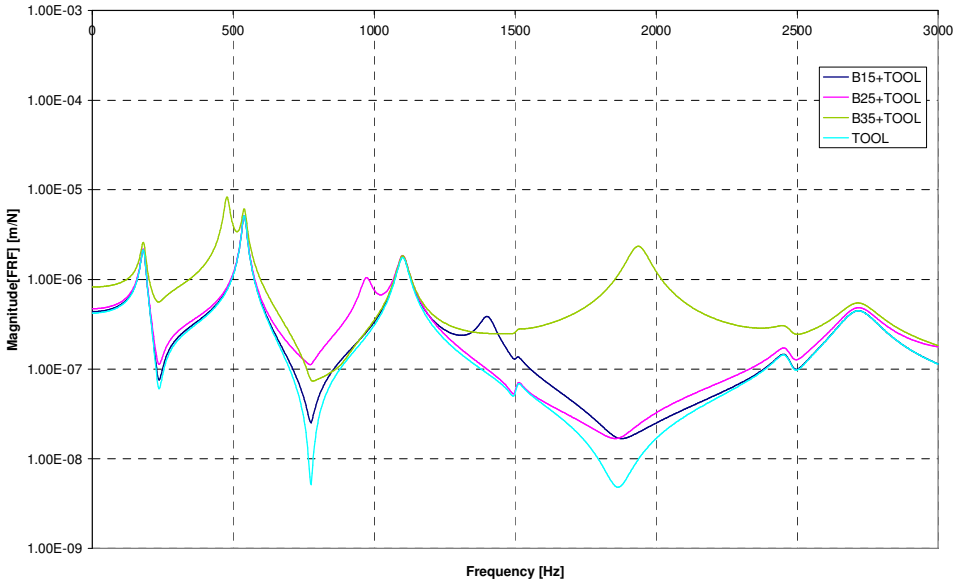

Figure 4.12 Combined FRFs of the workpiece and tool at the end of fifth step of 1st, 2nd and 3rd cuts

As shown in Figure 4.11, the peak FRFs of the workpiece are less than the peak FRFs at the bottom (at the 1st location) of the workpiece in all cutting cycles due to the boundary conditions of the structure. As the tool moves from the free to the fixed end of the workpiece, the workpiece becomes stiffer, and thus flexibility of the workpiece reduces where the tool FRF is more important for stability.

The stability lobe diagrams including the changing dynamics of the workpiece at the end of the fifth step of 1st, 2nd and 3rd cuts are shown in Figure 4.13.

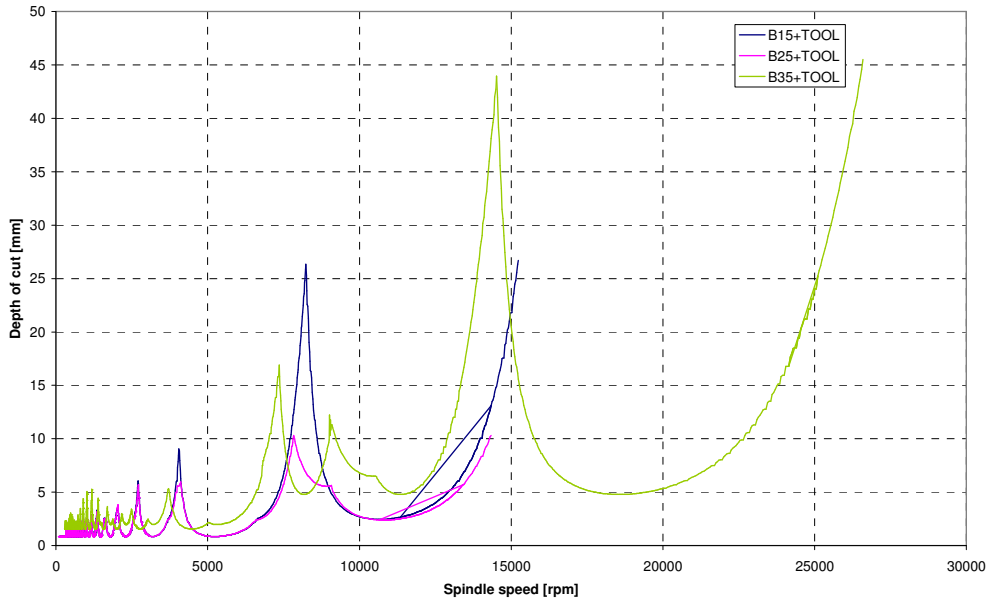

Figure 4.13 Stability lobe diagrams including the FRFs of the workpiece at the end of fifth step of 1st, 2nd and 3rd cuts

As can be seen from Figure 4.13 because the FRFs of the workpiece at the first and second cut are lower than the FRFs of the tool, the flexibility of the tool becomes dominant and the stability curves at these stages seem similar. Only some peaks of the stability curves take lower depths of cut values as the workpiece becomes thinner. At the third cut, however, the workpiece becomes as flexible as the tool.

The stability curve at the third cut becomes higher than the curve of the first and second stage at some regions of the diagram in Figure 4.13, while it is expected to become lower. The reason is that the material removed from the workpiece at the third stage is less than those of the other stages. This means that the radial depth of cut at the third cutting cycle (2 mm) is less than those at other two cuts (5 mm).

Stability diagrams can be generated in terms of axial depth of cut for a given depth of cut and also in terms of radial depth of cut for a given axial depth of cut [48]. The stable axial depth of cut is usually inversely proportional with stable radial depth of cut. In other words, for a chatter-free cutting taking smaller radial depth of cut can result in higher stable axial depth of cut. This is the reason for having higher absolute stable axial depths in third cutting cycle than those in other two cycles.

4.2.1.5 FRFs of the Workpiece and Stability Diagrams at the Ninth Step of the Cut

The geometry of the workpiece at the 9^{th} step of cutting in the roughing, semifinishing and finishing passes are shown in Figure 4.14. In order to see the effect of the thickness change of the workpiece at this location, the FRFs of the beam B19, B29 and B39 are given in Figure 4.15. The FRFs of the beam combined with the FRFs of the tool are given in Figure 4.16 to see the variation in the combined system FRFs with changing of the workpiece's thickness.

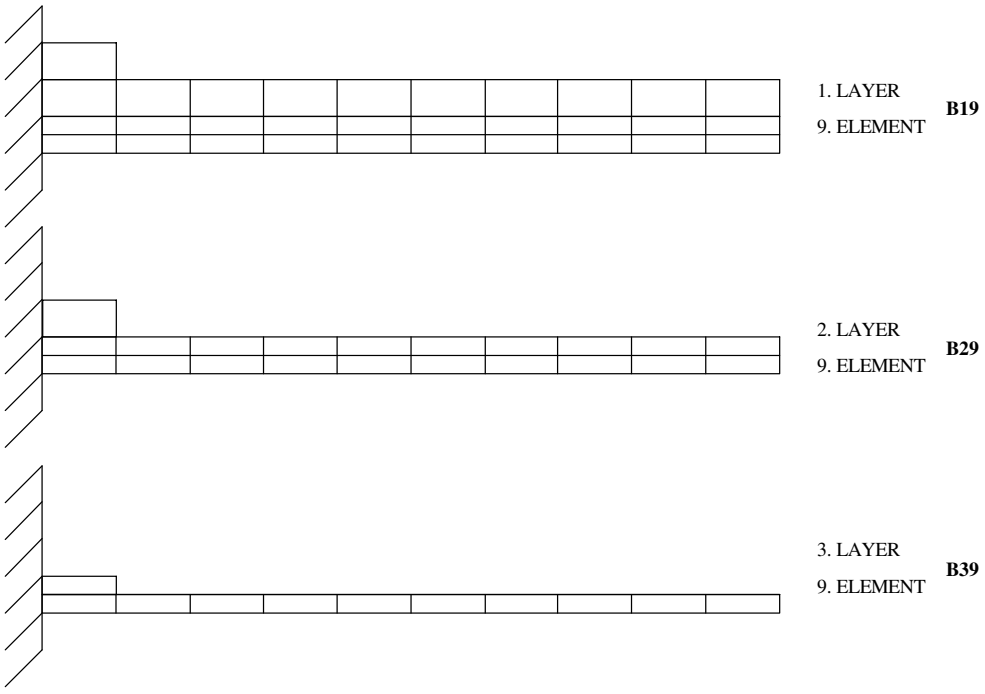

Figure 4.14 Beam models at the end of ninth step of 1st, 2nd and 3rd cuts

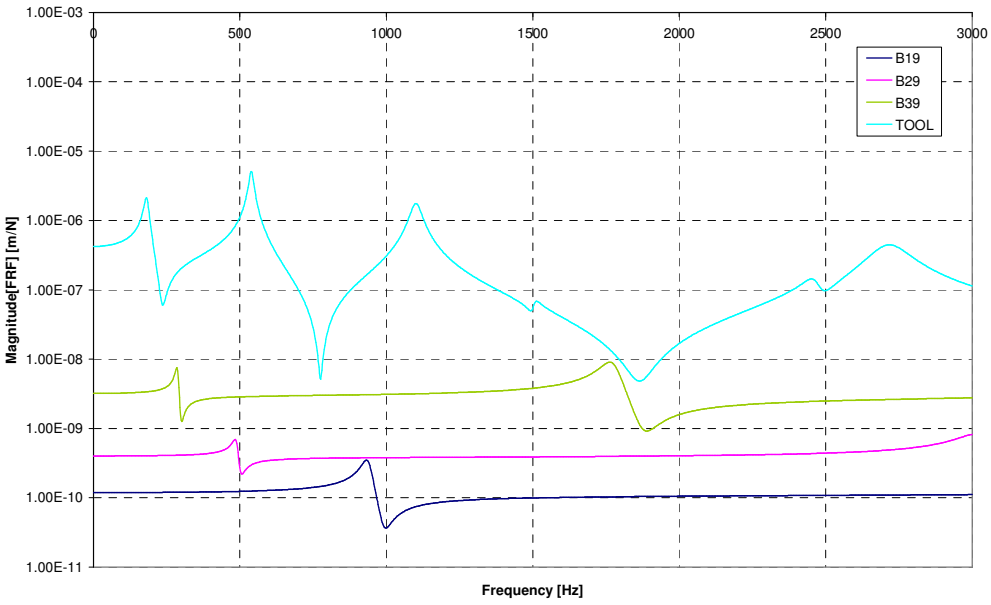

Figure 4.15 FRFs of the workpiece at the end of ninth step of 1st, 2nd and 3rd cuts

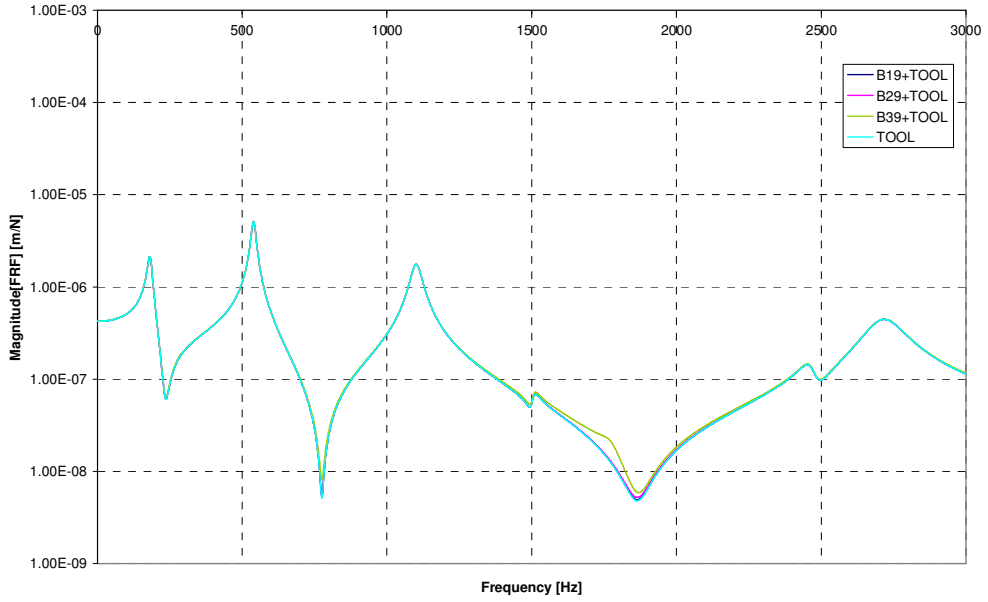

Figure 4.16 Combined FRFs of the workpiece and tool at the end of ninth step of 1^{st}, 2^{nd} and 3^{rd} cuts

The FRFs of the workpiece near to the fixed end have the lowest values compared to the other locations, as the stiffness of the workpiece is the largest in this region. Since the FRFs of the workpiece are very low compared to those of the tool, total FRFs of the system and the tool are nearly the same as seen in Figure 4.16. In such a case, only the FRF of the tool can be used to predict the stability diagrams accurately.

The stability lobe diagrams including the changing dynamics of the workpiece at the end of the ninth step of the 1^{st}, 2^{nd} and 3^{rd} cuts are shown in Figure 4.17. Since the stability diagrams of B19 and B29 are the same, they seem as one curve in Figure 4.17.

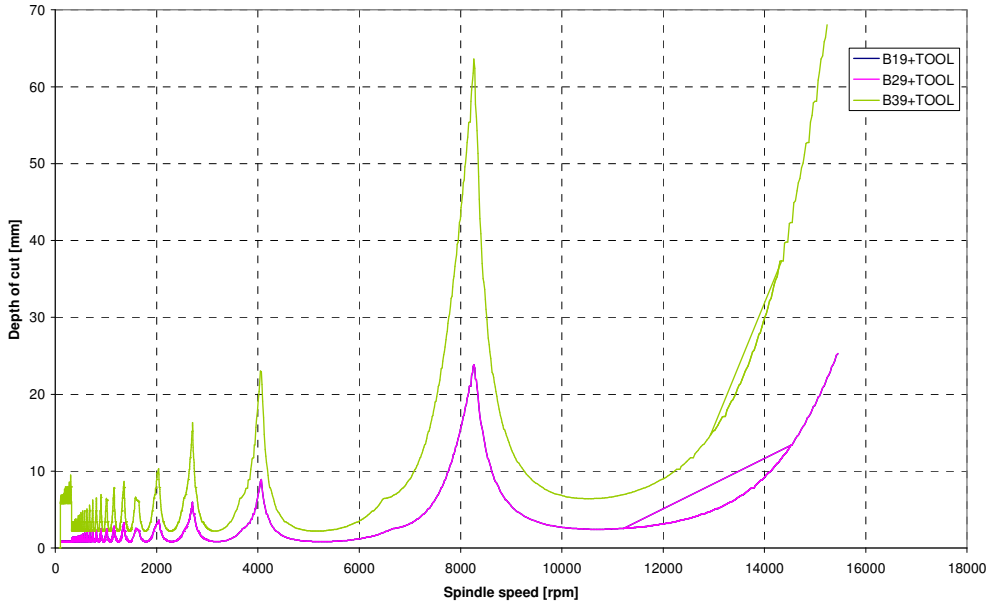

Figure 4.17 Stability lobe diagrams including the FRFs of the workpiece at the end of ninth step of 1st, 2nd and 3rd cuts

The FRFs of the system is the same at all the cuts since the system dynamics is mainly governed by the tool FRF at this location. Therefore, the stability curves are the same for all cuts at this location except the finishing cut where the radial depth of cut is different than the previous two cuts. From the results presented in this section, it can be concluded that the variation of the workpiece dynamics does not affect the stability limits when the tool is much more flexible than the workpiece in which case the workpiece dynamics can be neglected.

4.2.1.6 Variation of the Workpiece Dynamics

In this section, the variation of the workpiece dynamics as a result of the mass removal is analyzed in terms of peak FRF values and natural frequencies. Every step in the machining cycle is numbered as used to present the variations. The

changes in the 1st and 2nd natural frequencies of the workpiece are given in Figure 4.18. In addition, the variations in the peak FRF amplitudes of the workpiece for the first two natural frequencies are shown in Figure 4.19.

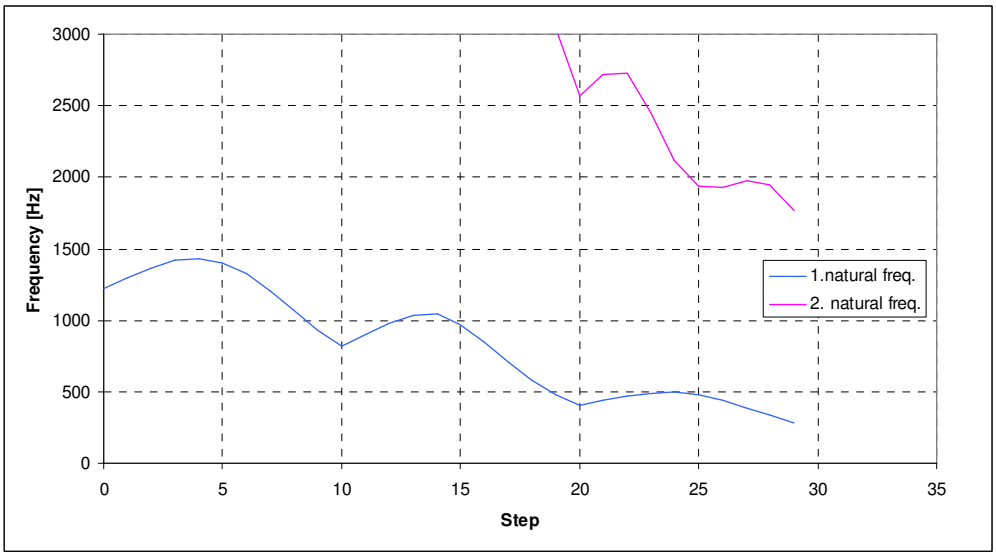

Figure 4.18 Variation in the 1st and 2nd natural frequencies of the workpiece during machining

At every cut, the variation in the natural frequencies of the workpiece shows a similar trend. The natural frequency of the workpiece increases until the workpiece is machined from the free end to the middle of the workpiece. Then, the frequency decreases while machining from the middle to the head of the workpiece. This behaviour can be explained by considering the respective stiffnesses of the part at the free and fixed ends. The material removed from the free end does not affect the stiffness of the beam as it is mainly determined by the workpiece thickness at the fixed end. Thus, the removed mass from the free end results in increased natural frequencies. The situation is the opposite for the fixed end where the removed material results in significant loss of stiffness. However, since the motion is quite limited at this location the removed mass does not affect the inertial forces. Thus, the mass removal from the fixed end results in reduced natural frequencies.

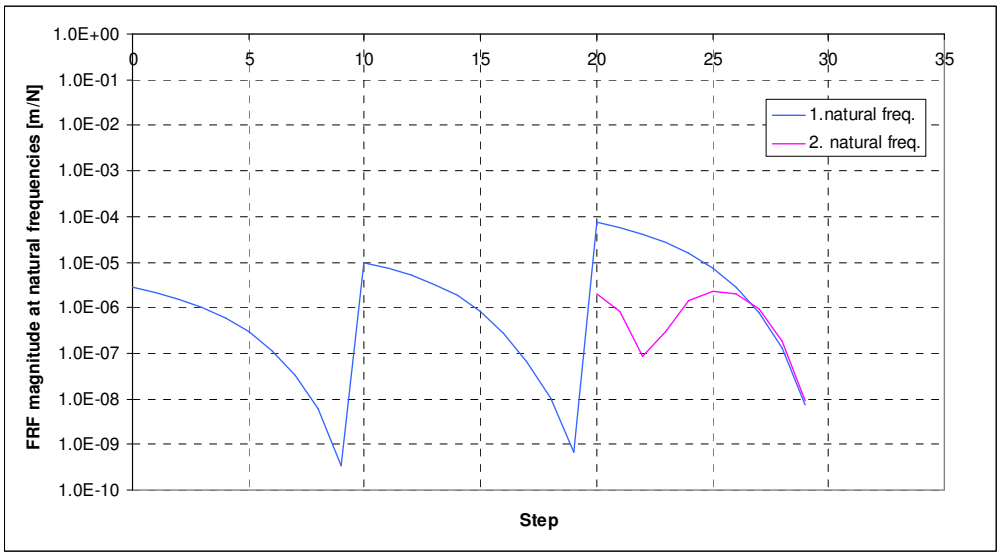

Figure 4.19 Variation of the peak FRF amplitudes of the workpiece at the 1st and 2nd natural modes

Change in the magnitude of the FRFs of the workpiece shows an expected behaviour as mentioned in Section 4.2.1.4 The FRF values of the workpiece decrease as the location is varied from the free end to the fixed end of the workpiece.

4.2.1.7 Variation of the Stable Spindle Speeds and Depth of Cuts

In this section, the effect of the variation of the part dynamics as a result of the mass removal on stability is analyzed in terms of stable depth of cut values and corresponding spindle speeds. The variation in maximum stable depth of cut and spindle speeds for the 1st and 2nd lobes of the stability diagram are given in Figure 4.20 and 4.21 for different machining steps.

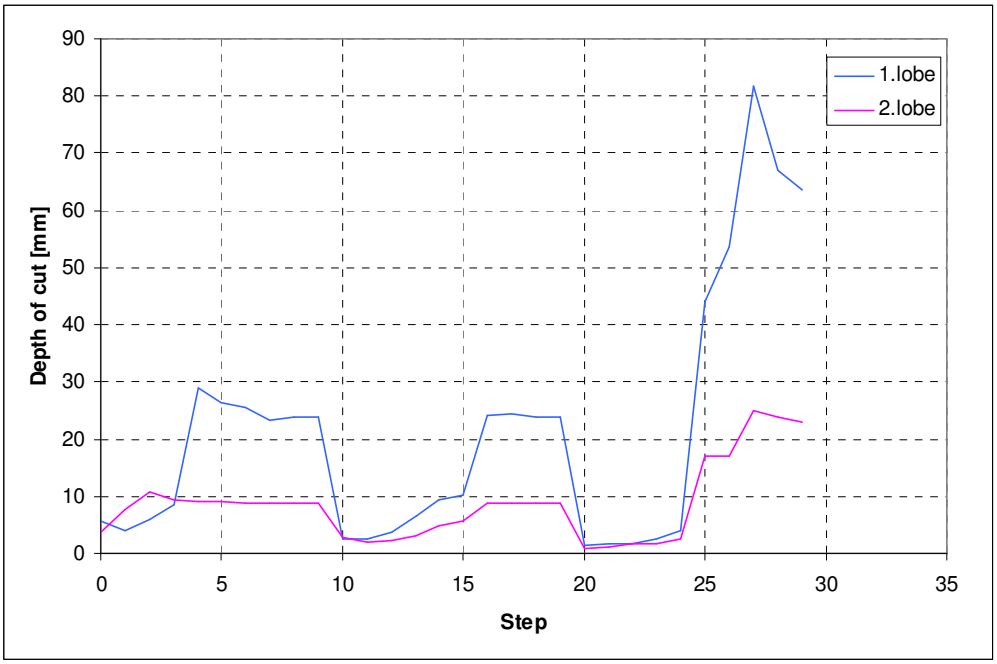

Figure 4.20 Variation of the stable depth of cuts for the 1st and 2nd stability lobes during machining of the workpiece

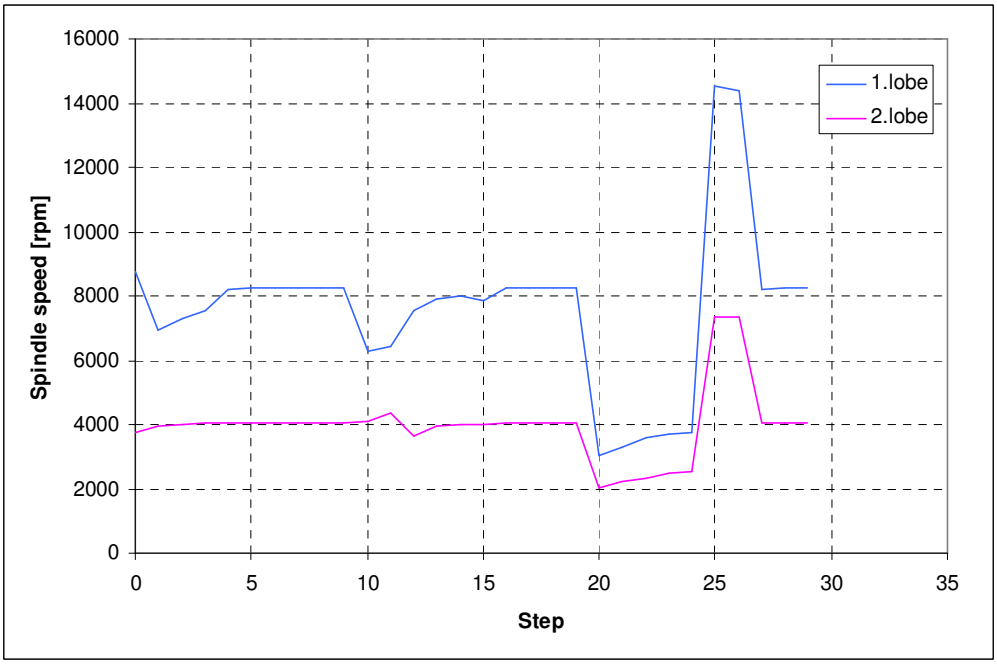

Figure 4.21 Variation of the spindle speeds corresponding to the 1st and 2nd lobes during machining of the workpiece

The variation patterns for the stable spindle speeds and depth of cuts in the first and the second lobes can be explained by examining the FRF variations during machining as presented in the previous sections. For instance, in the roughing cut from 1st step to 4th step, since the FRFs of the workpiece are higher than the FRFs of the tool at these locations, the workpiece dynamics become dominant in the overall FRFs of the system. However, the amplitude of the workpiece's FRFs reduces due to the movement of the locations where the FRFs calculated from free end to the middle of the workpiece, and the stable depth of cuts in the 1st and 2nd lobes take higher values. After the 4th step, the FRFs of the tool become more flexible than the workpiece and the variation in the stable depth of cuts and speeds nearly remains constant. The same trend can be observed in the semifinishing cut as well. In the finishing cut, the workpiece becomes very flexible and the increase in the stable depth of cuts continues until the 7th step, as the workpiece FRFs are still dominant according to those of the tool. After this step, the FRFs of the tool start to dominate stability and due to the flexibility of tool the stable depth of cuts decreases.

If the stable depth of cuts at the same locations but different cutting cycles are compared from the roughing cut to the finishing cut, stable depths become smaller between 1st - 4th step locations due to increase in the flexibility of the workpiece. In the roughing and the semifinishing cut the stable depth of cuts take nearly same values at between 5th and 9th step locations, since only the tool dynamics affect the stability. In the finishing cut until the 7th step, the workpiece dynamics dominate the stability curve and stable axial depth of cuts get higher values than the other two cuts. From 7th step to the fixed end, the tool start to affect the stability and the stable depth values reduce.

The spindle speeds corresponding to stable depth of cuts nearly remain constant at the roughing and the semifinishing cut; only at the 1st and 2nd steps of these cuts a decrease is observed. These locations are the most effective regions of the FRFs of the workpiece on stability and the flexibility of the workpiece causes these falls in Figure 4.21. In the finishing cut the decrease in the spindle speeds of the lobes corresponds to the machining from the 1st step to 4th step. Since the workpiece becomes significantly flexible at these steps of the machining, the decrease is observed in a wider region of the machining process than other two cuts. Also another observation from the Figure 4.20 and 4.21 is that the machining steps in which the stable depth of cuts show a fall in value are the common with the steps in which the spindle speeds decrease.

In conclusion, the variations in chatter-free depth of cuts and spindle speeds are consistent with the variation in the workpiece dynamics, and the influence of the workpiece flexibility on the chatter stability can be observed easily when the workpiece is as flexible as the tool.

4.2.1.8 Minimum Chatter-Free Machining Time

As mentioned before, chatter is one of the most important limitations on the productivity and the part quality. Performing stability analysis to predict chatter-free depth of cuts at the high spindle speeds becomes very important to increase the stable mass removal rate. This will lead to minimized machining time increasing the productivity. In this study, two methods are used in order to determine the possible minimum chatter-free machining time of the workpiece.

In the first method, one common maximum chatter-free depth of cut and the corresponding spindle speed values are identified for every cut, and used for the whole cut. In order to find the common maximum depth of cut value, all the

stability diagrams are drawn on one graph for the considered cut such as roughing. Firstly, at the first lobe, a common peak point is determined on the graph as shown in Figure 4.22. After finding this point from the data exactly, 80 percent of the depth of cut value at this point can be taken as the maximum chatter-free depth of cut. If this value is lower than the common peak point at the 2nd lobe, the same procedure is repeated for this lobe. Using the depth of cut and corresponding spindle speed values, the machining time is calculated. The maximum stable depth of cut and spindle speed combination in the stability lobes give the minimum time.

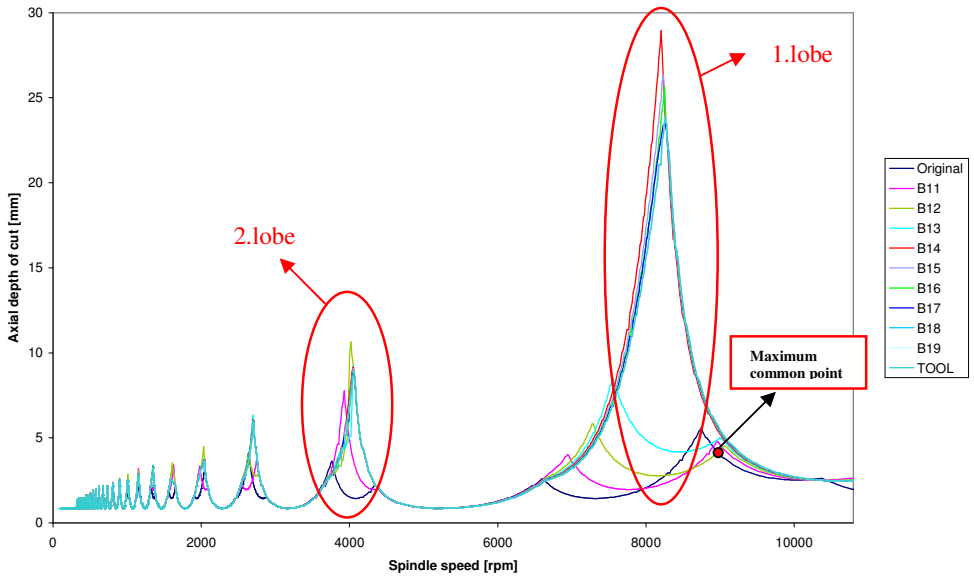

Figure 4.22 Graphical representation of the first method used for machining conditions for minimum machining time

In the second method, for every step of a cut, the possible maximum depth of cut and the corresponding spindle speed are identified, and used for that specific pass. After finding the maximum stable depth of cut and corresponding spindle speed of every step of a cut as shown in Figure 4.23, total time of the corresponding cut is determined by summing the machining time of all steps of a cut.

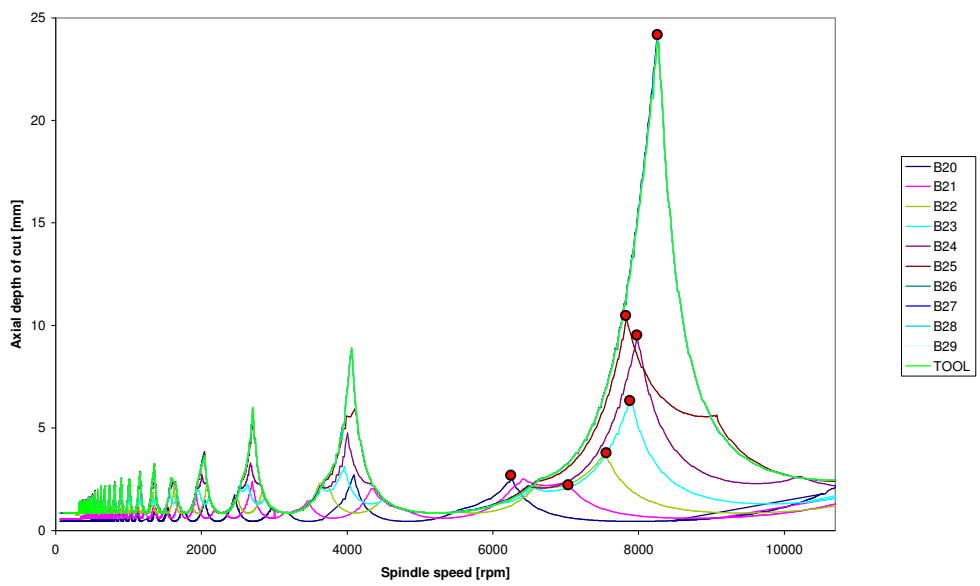

Figure 4.23 Graphical representation of the second method for machining conditions for minimum machining time

Machining time in a milling process is given as,

$$t_m = nop.\frac{l_w}{V_f} \tag{4.1}$$

where t_m is machining time,

nop is number of pass(step),

l_w is cutting length at one pass(step) and

V_f is feed rate.

V_f can be found as

$$V_f = N.f_t.n_t \tag{4.2}$$

where N is the number of teeth(flutes) of the cutter,

f_t is feed per tooth (in mm/rev per tooth)

n_t is rotational frequency of the cutter(in rpm).

In machining time calculations, f_t is taken as 0.15 for roughing cut and 0.10 for semi-finishing and finishing cuts. These values are used for all cases as the effect of the feed on the stability is minimal. N is taken as 4 assuming a 4 fluted milling cutter, and l_w is 50 mm in the beam model. ***nop*** is determined by dividing the length of the workpiece (100 mm in the beam model) to the maximum axial depth of cut and n_t is taken maximum spindle speed corresponding maximum axial depth of cut.

For example, if the semi-finishing cut of the workpiece given in Section 4.2.1 is considered, the graph of the stability diagrams at every step of the semi-finishing cut is determined as shown in Figure 4.24. By the help of this graph, the maximum common chatter-free depth of cut and the corresponding speed are determined. In the first lobe, the depth of cut and the spindle speed are in the ranges of 1.60-1.64 mm and 6400-6450, respectively. Because this point is at the intersection of the stability curve of B20 and B22, more exact values of the intersection point is found by using the data points used in the stability diagram. In this case, the depth of cut at the intersection is found as 1.62 mm at 6420 rpm. Then taking 80 percent of the depth of cut value as a safety factor, the stable depth of cut is obtained as 1.29 mm. In order to find the spindle speed which is at the middle of this intersection lobe exactly, the intersection speeds of this lobe must be determined. For this purpose, all intersection speeds which have the determined maximum common stable depth of cut value (1.29 mm in this case) on the each stability curve of a corresponding cut are found as shown in Figure 4.25. The maximum of the lower spindle speeds of the stability curves and the minimum of the higher spindle speeds of the stability curves are selected in order to find the middle of the inner intersection lobe. In this case, they are found as 6286 and 6540 rpm. Taking the average of these speeds, optimum (middle) spindle speed is calculated as 6413 rpm as shown

in Figure 4.26. At the end, optimum depth of cut and spindle speed are determined as 1.29 mm and 6413 rpm.

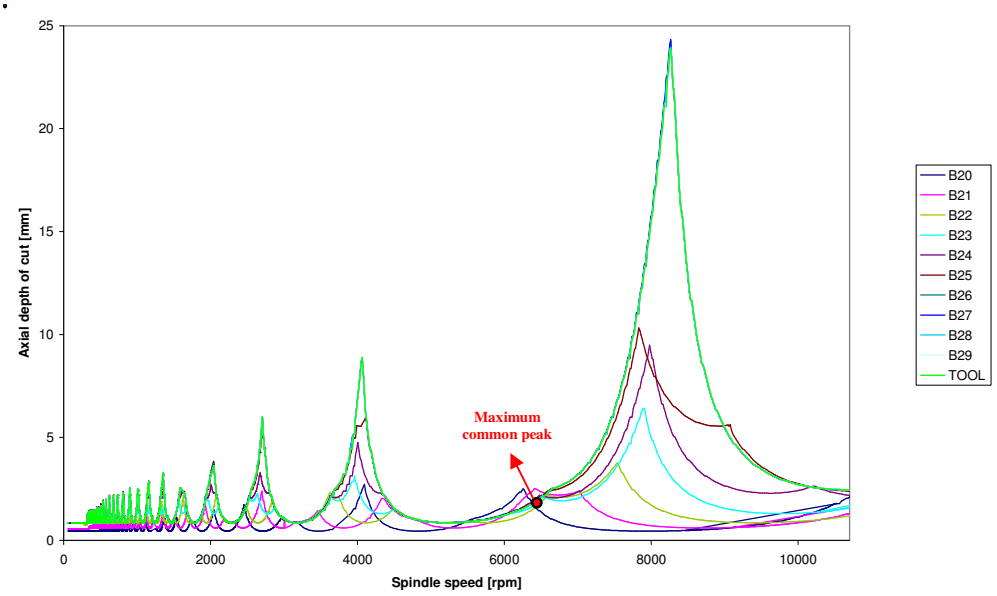

Figure 4.24 Stability diagrams at every step of the semi-finishing cut

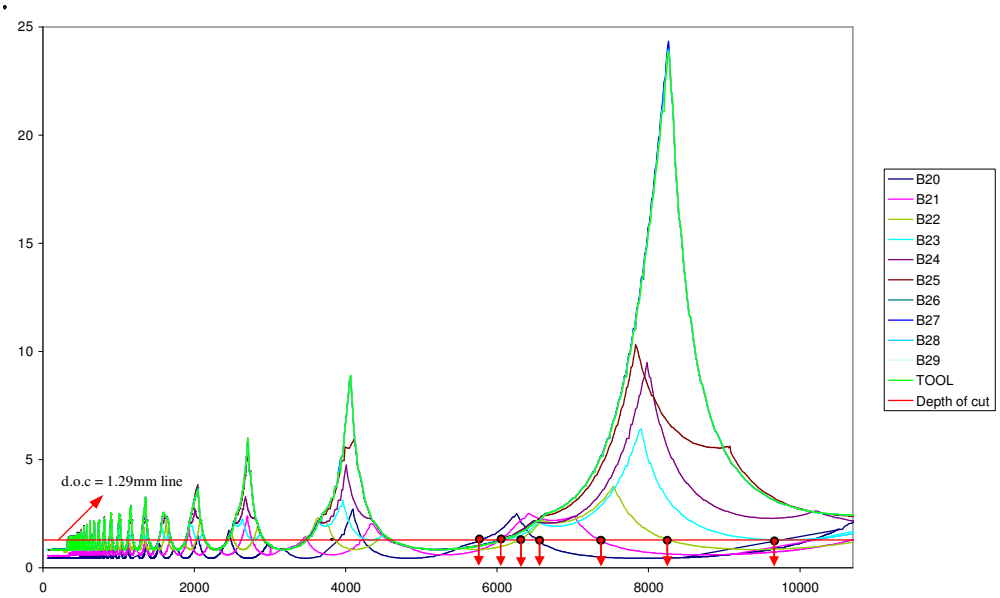

Figure 4.25 Spindle speeds values of the stability curves at the first lobe at the depth of cut = 1.29 mm

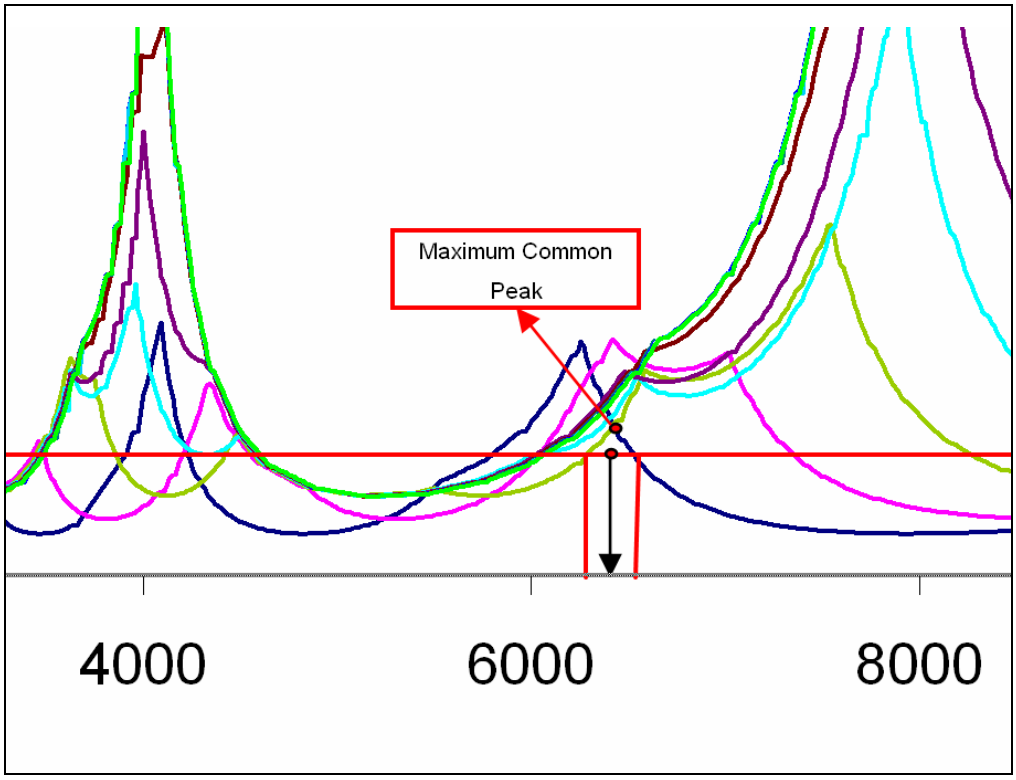

Figure 4.26 Average spindle speed of inner intersection lobe at the depth of cut of 1.29 mm

After the optimum depth of cut and spindle speed values are determined, ***nop*** can be found as

$$\boldsymbol{nop} = \boldsymbol{roundup}\left(\frac{\boldsymbol{L}}{\text{maximum axial depth of cut}}\right) = \boldsymbol{roundup}\left(\frac{100}{1.29}\right) = 78 \qquad (4.3)$$

By taking $\boldsymbol{N}$, the number of the teeth of the cutter as 4, $\boldsymbol{f_t}$ the feed per tooth as 0.1 and using the optimal spindle speed 6413 rpm, feed rate can be calculated as

$$\boldsymbol{V_f} = \boldsymbol{N}.\boldsymbol{f_t}.\boldsymbol{n_t} = 4\boldsymbol{x}0.1\boldsymbol{x}6413 = 2565.2 \text{ mm/min} \qquad (4.4)$$

Then the machining time of the semi-finishing cut by using one common depth of cut and spindle speed is found as

$$t_m = nop.\frac{l_w}{V_f} = 78.\frac{50}{2565.2} = 1.52\,\text{min} \tag{4.5}$$

By applying the same procedure to determine one common depth of cut and spindle speed at every cut, the machining time values are found as shown in Table 4.1.

Table 4.1 Machining time calculation parameters at every cut

	Spindle speed(rpm)	Depth of cut(mm)	nop	Feed per tooth	Time(min)
Roughing cut	8940	3.32	31	0.15	0.29
Semi-finishing cut	6413	1.29	78	0.1	1.52
Finishing cut	3143	0.53	189	0.1	7.52
				Total time	9.33

If maximum chatter-free depth of cut and spindle speed are found for every step(pass) in one cut using the second method, the results are found as shown in Table 4.2-4.4. B10, B20 and B30 correspond to the first machining steps of the roughing, semifinishing and finishing cuts. Here “0”(zero) means that the FRFs of unmachined workpiece at every cut is used in order to determine stability limit curve.

Table 4.2 Machining time calculation parameters at the roughing cut

Roughing cut	Spindle speed(rpm)	Depth of cut(mm)	nop	Feed per tooth	Time(min)
B10	8753	4.45	3	0.15	0.03
B11	8978	3.82	4	0.15	0.03
B12	9068	3.63	3	0.15	0.03
B13	7568	6.77	2	0.15	0.02

B14-B19	8213	16.10	4	0.15	0.04
				Total time	0.15

Table 4.3 Machining time calculation parameters at the semi-finishing cut

Semi-finishing cut	Spindle speed(rpm)	Depth of cut(mm)	nop	Feed per tooth	Time(min)
B20	6240	2.01	5	0.1	0.10
B21	6675	2.02	5	0.1	0.09
B22	7508	3.00	4	0.1	0.07
B23	7868	5.13	2	0.1	0.03
B24	7965	7.59	2	0.1	0.03
B25	7830	8.25	2	0.1	0.03
B26-B29	8220	16.71	3	0.1	0.05
				Total time	0.40

Table 4.4 Machining time calculation parameters at the finishing cut

Finishing cut	Spindle speed(rpm)	Depth of cut(mm)	nop	Feed per tooth	Time(min)
B30	3047	0.90	12	0.1	0.49
B31	3255	0.88	12	0.1	0.46
B32	3465	1.37	8	0.1	0.29
B33	3683	1.85	6	0.1	0.20
B34	3743	2.87	4	0.1	0.13
B35	7290	11.83	1	0.1	0.02
B36	7275	11.99	1	0.1	0.02
B37-B39	8190	44.53	1	0.1	0.02
				Total time	1.63

Full machining time can be found in the second method as,

$$\text{Full machining time} = 0.15 + 0.40 + 1.63 = \boldsymbol{2.18\ min = 130.8\ s} \quad (4.6)$$

As shown in Table 4.1, full machining time is found as 9.33 minutes (559.8 s) if the first method is used. As a result, taking maximum depth of cut and spindle speed at every step of the process reduced the machining time to one forth of the time compared to the case where one common depth of cut and spindle speed are used for every cutting cycle. Using the stability lobe diagrams found by combining

the FRFs of the tool and the workpiece, the maximum chatter-free values can be calculated at the intermediate stages of the process, and the machining time can be shortened significantly.

4.2.1.9 Effect of the Different Radial Depths of Cuts on the Stable Machining Time

In this section the effect of the radial depth of cut on the stability is discussed and the results of the previous section are compared with the new machining process which has the different radial depths at the roughing, semifinishing and finishing cuts.

The same beam and tool-holder-spindle models in Section 4.2.1 are used in this machining process.

4.2.1.9.1 Machining with Different Radial Depth of Cut

The machining with different radial depth of cut than the previous section is studied in this section. Again the machining consists of three main cuts:

- ***Roughing cut*** : Thickness of the workpiece is reduced from 15 mm to 8 mm (radial depth of cut = 7 mm) completely.

- ***Semi-finishing cut*** : Thickness of the workpiece is reduced from 8 mm to 4 mm(radial depth of cut = 4 mm) completely.

- ***Finishing cut*** : Thickness of the workpiece is reduced from 4 mm to 3 mm(radial depth of cut = 1 mm) completely.

Again the axial depth of cut is taken as 10 mm as an initial assumption so that the workpiece is machined in 10 steps per cut (pass). The FRFs of the workpiece at the first step of the machining at the previous section and at this section are compared according to the roughing, semifinishing and finishing cuts. In the figures the graphs with "n" subscript which stands for "new machining" represent the FRFs of the workpiece at the machining explained in this section.

The FRFs of the workpiece at the previous and the new machining of the 1st steps of the roughing, semifinishing and finishing cuts are given in Figure 4.27, 4.28 and 4.29 respectively.

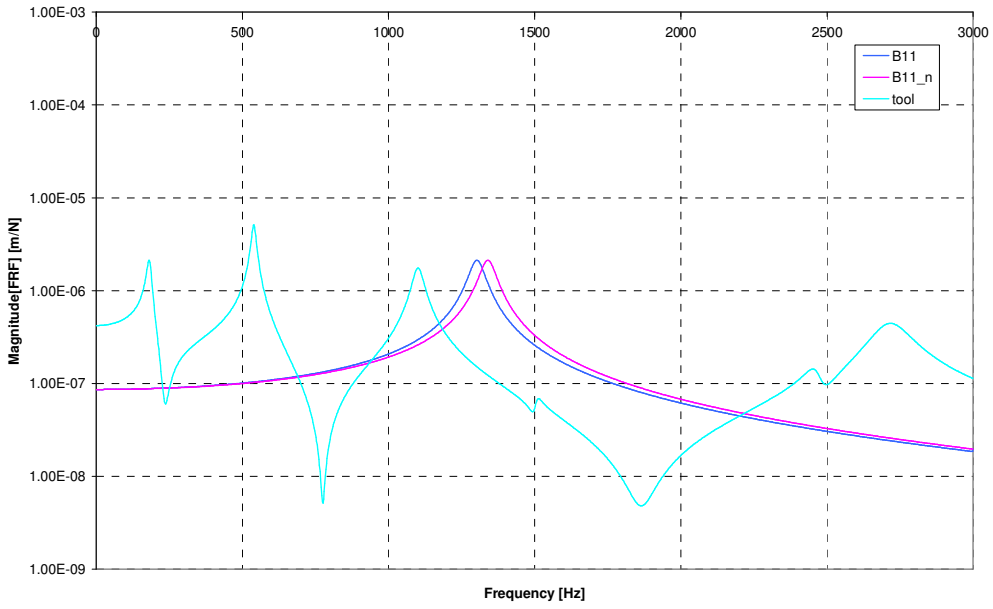

Figure 4.27 The FRFs of the workpiece at the first step of the roughing cut of the previous and new machining process

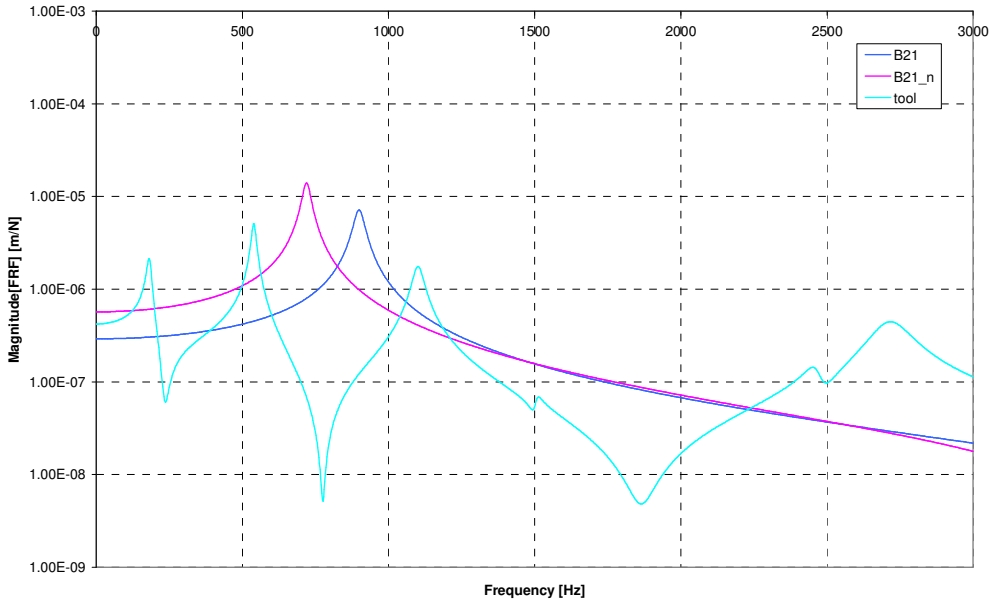

Figure 4.28 The FRFs of the workpiece at the first step of the semifinishing cut of the previous and new machining process

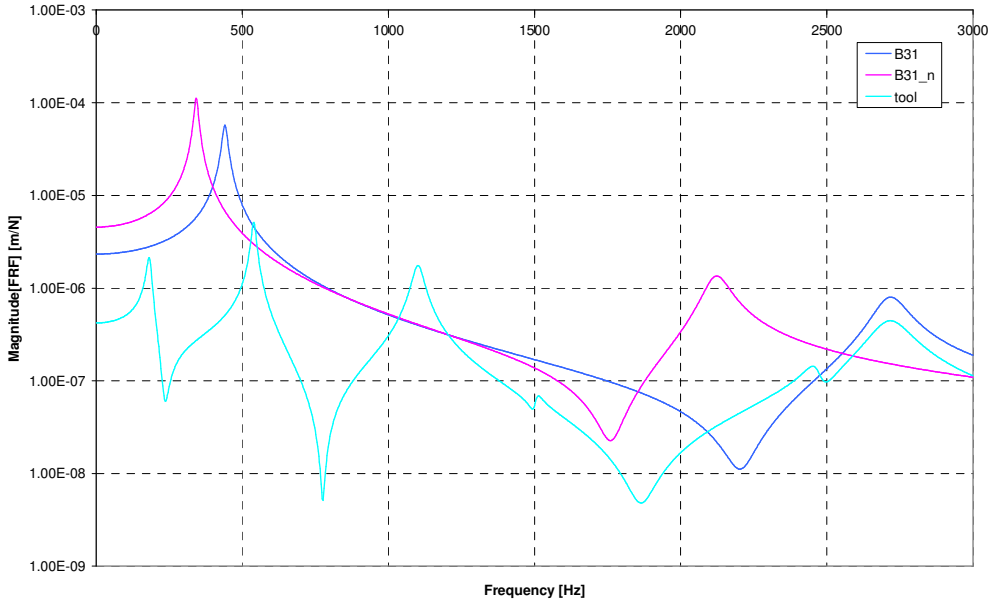

Figure 4.29 The FRFs of the workpiece at the first step of the finishing cut of the previous and new machining process

As shown in Figure 4.28 and 4.29, The FRFs of the workpiece at the semifinishing and finishing cuts of the new machining are higher than those of the previous machining. Only at the roughing cut the FRFs of the workpiece are at the same level in both machining. The reason is that the thickness of the unmachined region of the beam is the same at the roughing cut, whereas this thickness is lower at the new machining than the previous one at the other two cuts.

The stability diagrams including the FRFs of the workpiece at the first steps of the roughing, semifinishing, finishing cut at the previous and new machining are given in Figure 4.30, 4.31 and 4.32, respectively.

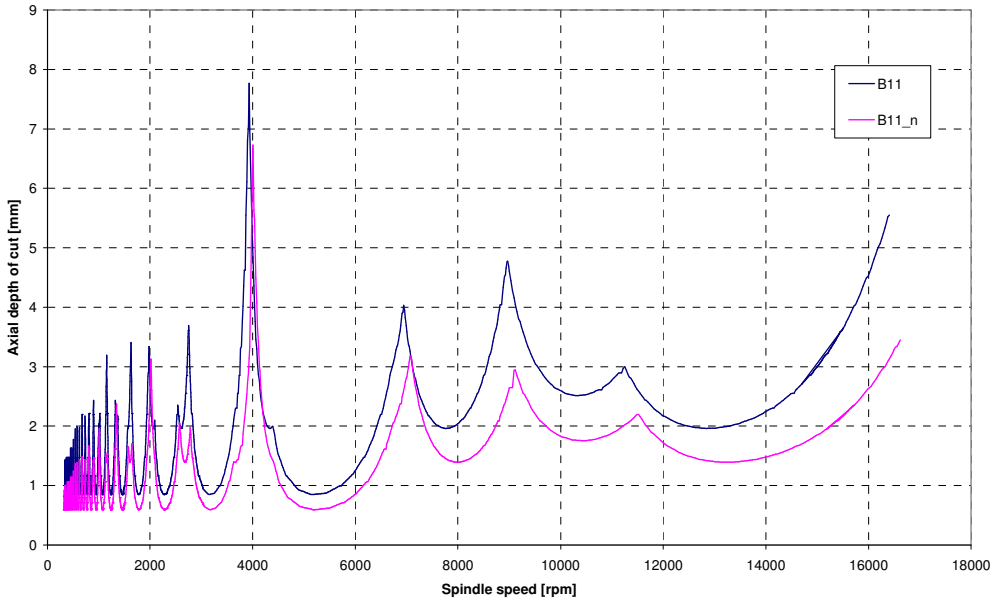

Figure 4.30 The stability diagram including the FRFs of the workpiece at the first step of the roughing cut of the previous and new machining process

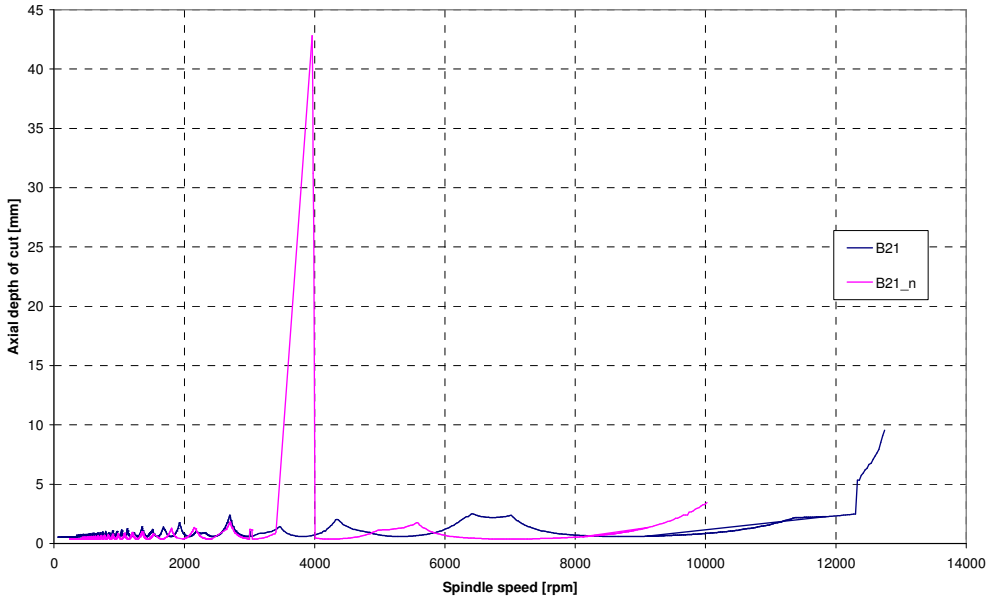

Figure 4.31 The stability diagram including the FRFs of the workpiece at the first step of the semifinishing cut of the previous and new machining process

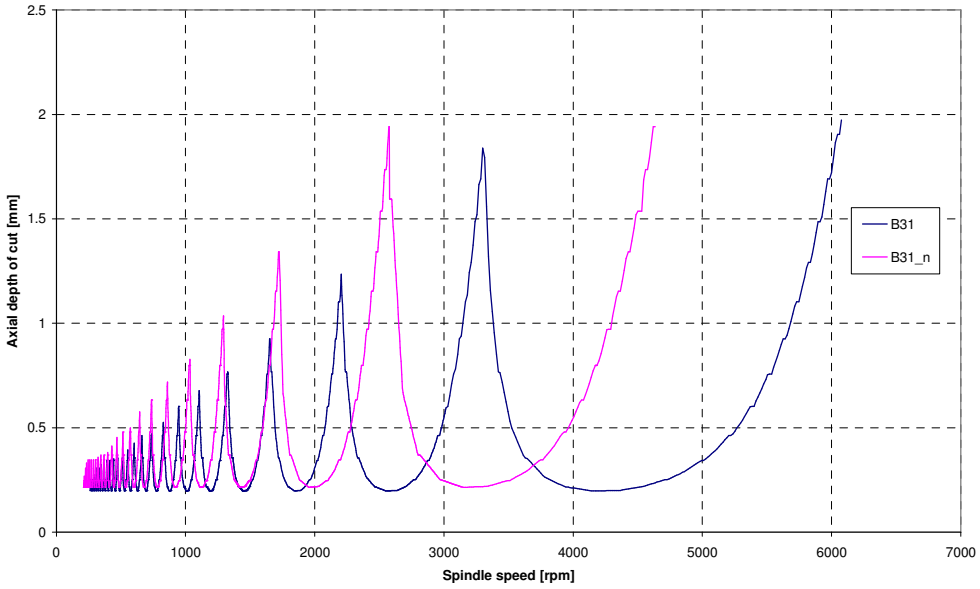

Figure 4.32 The stability diagram including the FRFs of the workpiece at the first step of the finishing cut of the previous and new machining process

From these results, it can be concluded that the stability values of the high speeds in the semifinishing reduce at the new machining since the workpiece is more flexible at the new machining due to thinner unmachined thickness of the workpiece. In the semifinishing cut, the peak stability of the new machining is higher because of smaller radial depth of cut value. In the roughing cut the absolute and peak stability also get lower at the new machining due to the larger radial depth of cut.

4.2.1.9.2 Minimum Chatter-Free Machining Time

In this section the chatter-free machining time of the new process is calculated using the two methods mentioned in Section 4.2.1.8.

The machining time found using the first method is given in Table 4.5.

Table 4.5 Machining time calculation parameters at every cut using first method

	Spindle speed(rpm)	Depth of cut(mm)	nop	Feed per tooth	Time(min)
Roughing cut	9135	1.92	53	0.15	0.48
Semi-finishing cut	5138	0.79	126	0.1	3.07
Finishing cut	2465	1.03	98	0.1	4.97
				Total time	8.52

The machining times of the roughing, semifinishing and the finishing cut found by using the second method are given in Table 4.6, 4.7 and 4.8, respectively.

Table 4.6 Machining time calculation parameters at the roughing cut

Roughing cut	Spindle speed(rpm)	Depth of cut(mm)	nop	Feed per tooth	Time(min)
B10	8768	3.11	4	0.15	0.04

B11	9158	2.35	5	0.15	0.05
B12	9293	2.09	5	0.15	0.04
B13	8168	16.74	1	0.15	0.01
B14-B19	8228	13.55	5	0.15	0.05
				Total time	0.19

Table 4.7 Machining time calculation parameters at the semifinishing cut

Semi-finishing cut	Spindle speed(rpm)	Depth of cut(mm)	nop	Feed per tooth	Time(min)
B20	4695	1.11	10	0.1	0.27
B21	5528	1.41	8	0.1	0.18
B22	6023	2.01	5	0.1	0.10
B23	6023	2.52	4	0.1	0.08
B24	6638	2.42	5	0.1	0.09
B25	20600	26.60	1	0.1	0.01
B26-B29	8228	24.47	2	0.1	0.03
				Total time	0.76

Table 4.8 Machining time calculation parameters at the finishing cut

Finishing cut	Spindle speed(rpm)	Depth of cut(mm)	nop	Feed per tooth	Time(min)
B30	2444	1.04	10	0.1	0.51
B31	2553	1.36	8	0.1	0.39
B32	2651	2.15	5	0.1	0.24
B33	2723	3.42	3	0.1	0.14
B34	2720	5.28	2	0.1	0.09
B35	4508	6.10	2	0.1	0.06
B36	12945	62.84	1	0.1	0.01
B37	13260	74.56	1	0.1	0.01
B38	8228	150.34	1	0.1	0.02
B39	8198	110.58	1	0.1	0.02
				Total time	1.49

Full machining time can be found in the second method as,

$$\text{Full machining time} = 0.19 + 0.76 + 1.49 = \boldsymbol{2.44\ min = 146.4\ s} \quad (4.7)$$

The machining times found in the previous section where the radial depth of cuts are 5 mm, 5 mm, 2 mm in the roughing, semifinishing and finishing cuts

respectively are compared with those found in this section where the radial depth of cuts are 7 mm, 4 mm, 1 mm in the roughing, semifinishing and finishing cuts respectively. The machining times determined by using the first method at the two machining processes are given in Table 4.9.

Table 4.9 Machining time calculation parameters at every cut of the previous and new machining using first method

	Previous Machining			**New Machining**		
	Spindle speed(rpm)	**Depth of cut(mm)**	**Time (min)**	**Spindle speed(rpm)**	**Depth of cut(mm)**	**Time (min)**
Roughing cut	8940	3.32	0.29	9135	1.92	0.48
Semi-finishing cut	6413	1.29	1.52	5138	0.79	3.07
Finishing cut	3143	0.53	7.52	2465	1.03	4.97
		Total time(min)	9.33		**Total time(min)**	8.52

In the roughing cut, it can be seen that the new machining takes longer time than the previous machining. Since the radial depth of the cut in the new machining (7 mm) is larger than that in the previous machining (5 mm), the stable axial depth of cut is lower in the new machining according to the previous one. As a result, the machining takes long with the new machining strategy.

In the semifinishing cut, again the machining time is longer in the new process. The reason for that is the difference in the flexibility of the workpiece in the semifinishing cuts of the two machining processes as shown in Figure 4.28. The thickness of the workpiece at the beginning of the semifinishing cut in the new machining is 8 mm as this value is 10 mm in the previous machining. Thus the stable axial depth of cut value is smaller in the new machining due to the workpiece flexibility and the machining takes longer.

In the finishing cut, the effect of the radial depth of cuts is observed on the machining time again. The new machining with smaller radial depth of cut (1 mm) takes shorter time than the previous machining with radial depth of cut of 2 mm.

The machining times determined by using the second method at the two machining processes are given in Table 4.10, 4.11 and 4.12.

Table 4.10 Machining time calculation parameters in the roughing cut of the previous and new machining using second method

	Previous Machining			**New Machining**		
Roughing cut	**Spindle speed(rpm)**	**Depth of cut(mm)**	**Time (min)**	**Spindle speed(rpm)**	**Depth of cut(mm)**	**Time (min)**
B10	8753	4.45	0.03	8768	3.11	0.04
B11	8978	3.82	0.03	9158	2.35	0.05
B12	9068	3.63	0.03	9293	2.09	0.04
B13	7568	6.77	0.02	8168	16.74	0.01
B14-B19	8213	16.10	0.04	8228	13.55	0.05
		Total time	0.15		**Total time**	0.19

Table 4.11 Machining time calculation parameters in the semifinishing cut of the previous and new machining using second method

	Previous Machining			**New Machining**		
Semifinishing cut	**Spindle speed(rpm)**	**Depth of cut(mm)**	**Time (min)**	**Spindle speed(rpm)**	**Depth of cut(mm)**	**Time (min)**
B20	6240	2.01	0.10	4695	1.11	0.27
B21	6675	2.02	0.09	5528	1.41	0.18
B22	7508	3.00	0.07	6023	2.01	0.10
B23	7868	5.13	0.03	6023	2.52	0.08
B24	7965	7.59	0.03	6638	2.42	0.09
B25	7830	8.25	0.03	20600	26.60	0.01
B26-B29	8220	16.71	0.05	8228	24.47	0.03
		Total time	0.40		**Total time**	0.76

Table 4.12 Machining time calculation parameters in the finishing cut of the previous and new machining using second method

	Previous Machining				New Machining		
Finishing cut	**Spindle speed (rpm)**	**Depth of cut(mm)**	**Time (min)**	**Finishing cut**	**Spindle speed (rpm)**	**Depth of cut(mm)**	**Time (min)**
B30	3047	0.90	0.49	**B30**	2444	1.04	0.51
B31	3255	0.88	0.46	**B31**	2553	1.36	0.39
B32	3465	1.37	0.29	**B32**	2651	2.15	0.24
B33	3683	1.85	0.20	**B33**	2723	3.42	0.14
B34	3743	2.87	0.13	**B34**	2720	5.28	0.09
B35	7290	11.83	0.02	**B35**	4508	6.10	0.06
B36	7275	11.99	0.02	**B36**	12945	62.84	0.01
B37-B39	8190	44.53	0.02	**B37**	13260	74.56	0.01
				B38	8228	150.34	0.02
				B39	8198	110.58	0.02
		Total time	1.63			**Total time**	1.49
		Full machining time	2.18			**Full machining time**	2.44

The trend observed in the machining times of the previous and new machining when the first method is used can be observed in the machining times determined when the second method is used. The machining times are generally reduced in the second method. In the roughing cut, the new machining takes longer time as shown in Table 4.10 due to the larger radial depth of cut as mentioned before. In the semifinishing cut, due to more flexible workpiece in the new machining, more time spends in the new process. As in the first method, in the finishing cut the machining time of the new process is shorter than the time of the previous process because of the smaller radial depth in the new machining. In the total machining time, the previous machining takes shorter with a small difference. From these results it can be said that the machining time can be minimized by using the effects of the radial depth of cut and the workpiece flexibility. Also taking higher radial depth in the roughing cut has small effect on the machining time due to the same starting thickness of the workpiece and this property can be used to shorten the machining time by higher mass removal in the roughing cut.

4.2.1.10 Effect of the Different Cutting Strategies on the Stable Machining Time

In this section the effect of the cutting patterns on the stability is discussed and the results of the two machining with previous cutting strategy are compared with those of the machining with new cutting strategy.

In Section 4.2.1.8 and 4.2.1.9, the thickness of the workpiece is reduced through the length of the workpiece uniformly. For instance, at the end of the roughing cut with a radial depth of cut of 5 mm the workpiece's thickness is reduced from 15 mm to 10 mm everywhere. This cutting pattern can be called as "layer removal".

In the new cutting strategy the workpiece's thickness is reduced to its final thickness at the same location. For instance at the first step the thickness of the free end of the workpiece is reduced from 15 mm to 10 mm. At the second step, the thickness of the same location is reduced from 10 mm to 5 mm and at the third step this thickness is reduced to 3 mm at the same location as shown in Figure 4.33. Thus the thickness of the end of the workpiece takes the final value of the machining. After that step, the same process is done at the next location of the workpiece. At the end of the whole process, the workpiece has a thickness of 3 mm everywhere. This cutting pattern can be called as "step removal".

The same beam and tool-holder-spindle models in Section 4.2.1 are used in this machining process.

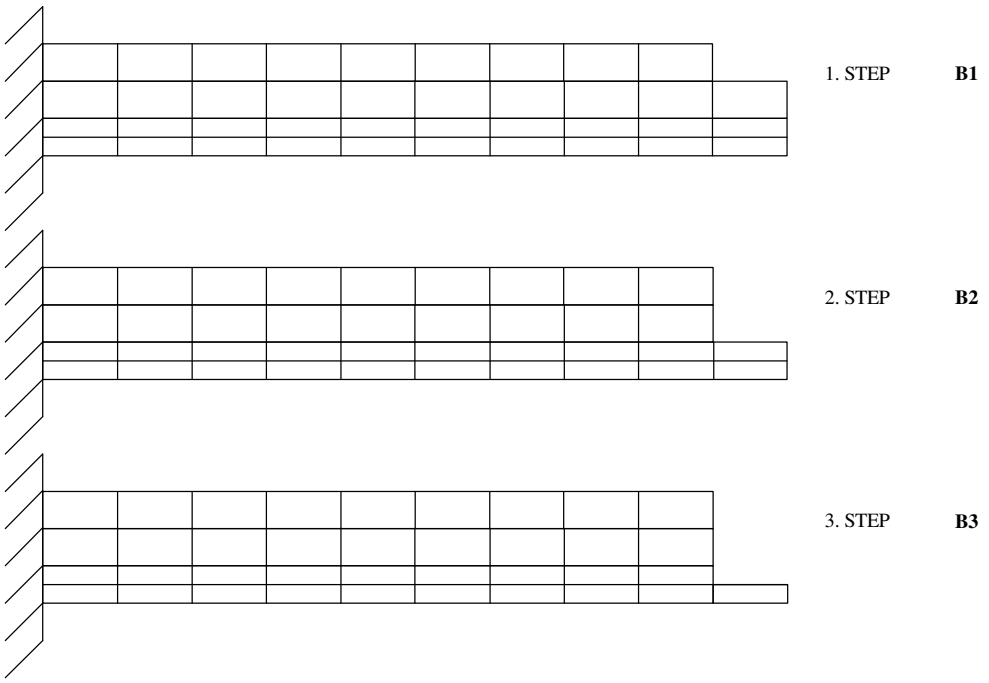

Figure 4.33 Beam models at the end of 1st, 2nd and 3rd steps in the "step removal" cutting

4.2.1.10.1 Machining with Step Removal

The step removal machining is studied in this section. Again in the roughing, semifinishing and finishing steps the radial depths are 5 mm, 5 mm and 2 mm respectively.

Again the axial depth of cut is taken as 10 mm as an initial assumption. The FRFs of the workpiece at the first, second, third steps of the "step removal" and those at the first steps of the "layer removal" in the roughing, semifinishing, finishing cuts are compared. In the figures the graphs with "s" subscript stand for "step removal" machining, the graphs with "l" subscript stand for "layer removal" machining.

The FRFs of the workpiece at the 1st step of the roughing cut of the layer removal and at the first step of the step removal are given in Figure 4.34.

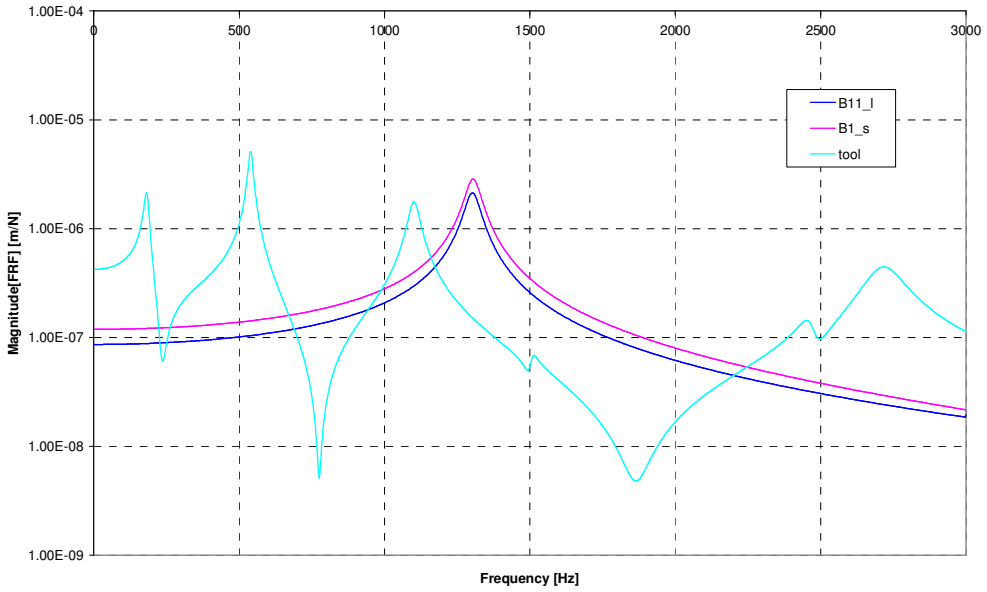

Figure 4.34 The FRFs of the workpiece at the 1st step of the roughing cut of the layer removal and at the 1st step of the step removal

The FRFs of the workpiece at the first step of the step removal are higher than those at the first step of the roughing cut of the layer removal since the locations where the FRFs of the workpiece calculated are different at two methods. Due to the different machining strategies, the FRFs of the workpiece at the 1st step of the step removal are calculated at the free end of the workpiece (at the 10th node of the beam model) as the FRFs of the workpiece at the first step of the roughing cut of the layer removal are calculated at the first location of the workpiece (at the 9th node of the beam model). Thus the magnitudes of the FRFs at the step removal are higher due to high workpiece flexibility at the free end. In addition, the peaks of the two FRFs are at the same frequencies since the geometry of the workpiece is exactly the same.

The FRFs of the workpiece at the 1st step of the semifinishing cut of the layer removal and at the 2nd step of the step removal are given in Figure 4.35.

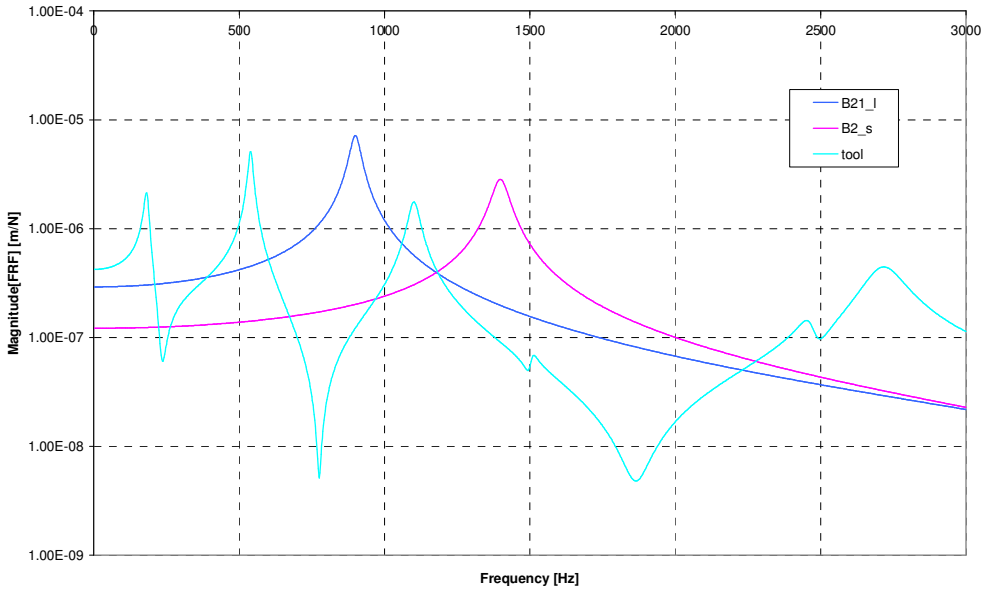

Figure 4.35 The FRFs of the workpiece at the 1st step of the semifinishing cut of the layer removal and at the 2nd step of the step removal

Since unmachined thickness of the workpiece is higher at the second step of the step removal (15 mm), the workpiece is more rigid at the step removal. As a result the workpiece at the first step of the semifinishing cut of the layer removal has the higher FRF levels and lower natural frequency due to high flexibility of the workpiece.

The FRFs of the workpiece at the 1st step of the finishing cut of the layer removal and at the 3rd step of the step removal are given in Figure 4.36.

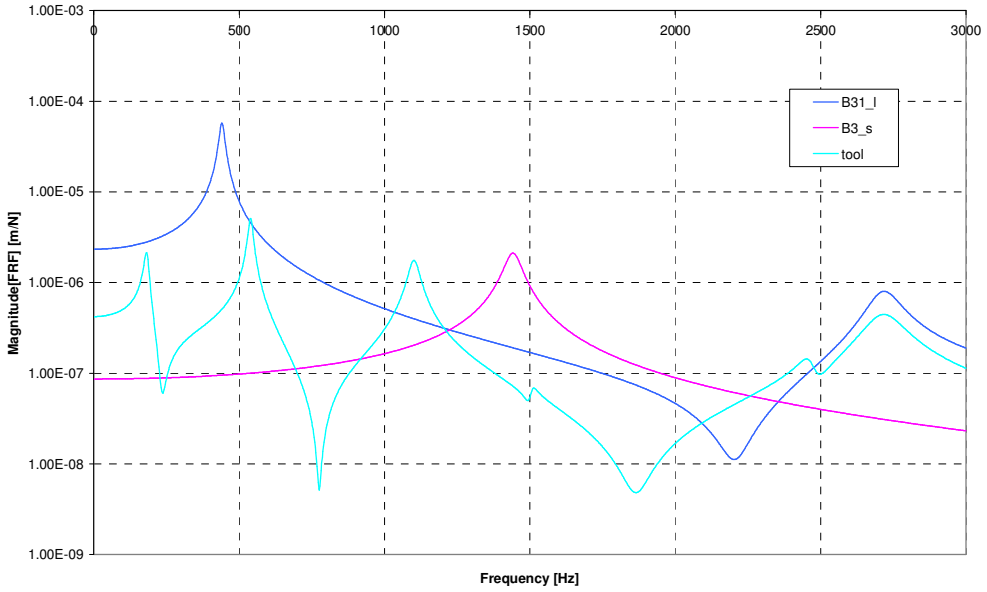

Figure 4.36 The FRFs of the workpiece at the 1st step of the finishing cut of the layer removal and at the 3rd step of the step removal

The same behaviour at the semifinishing cut of the layer removal is observed at this step. At the 3rd step of the step removal the FRFs of the workpiece is the nearly the same with the previous steps since the thickness of the unmachined region is still 15 mm and the flexibility of the workpiece does not increase significantly. However, at the first steps of the every cut of the layer removal the workpiece gets more flexible due to the layer mass removal which means that the unmachined region of the workpiece gets thinner at each cut of the layer removal.

The stability diagram including the FRFs of the workpiece at the 1st step of the roughing cut at the layer removal and at the 1st step of the step removal are given in Figure 4.37.

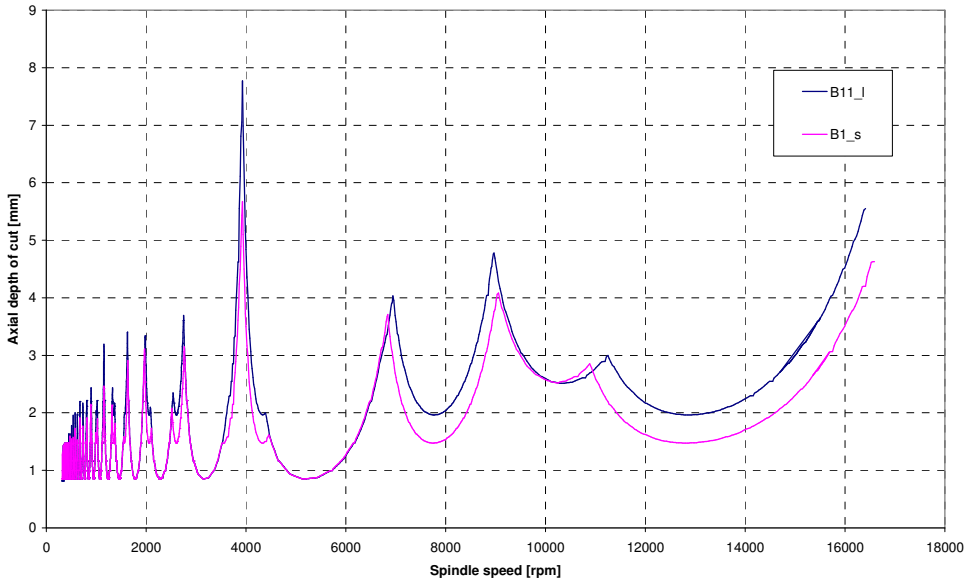

Figure 4.37 The stability diagram including the FRFs of the workpiece at the 1st step of the roughing cut of the layer removal and at the 1st step of the step removal

As shown in Figure 4.37 the stability curves of the first steps of the layer and the step removal are nearly the same as expected from the FRFs of the workpiece at these machining steps as seen in Figure 4.34. Only some peak stabilities are smaller at the 1st step of the step removal due to the higher workpiece FRFs.

The stability diagrams including the FRFs of the workpiece at the 1st step of the semifinishing cut at the layer removal and at the 2nd step of the step removal are given in Figure 4.38.

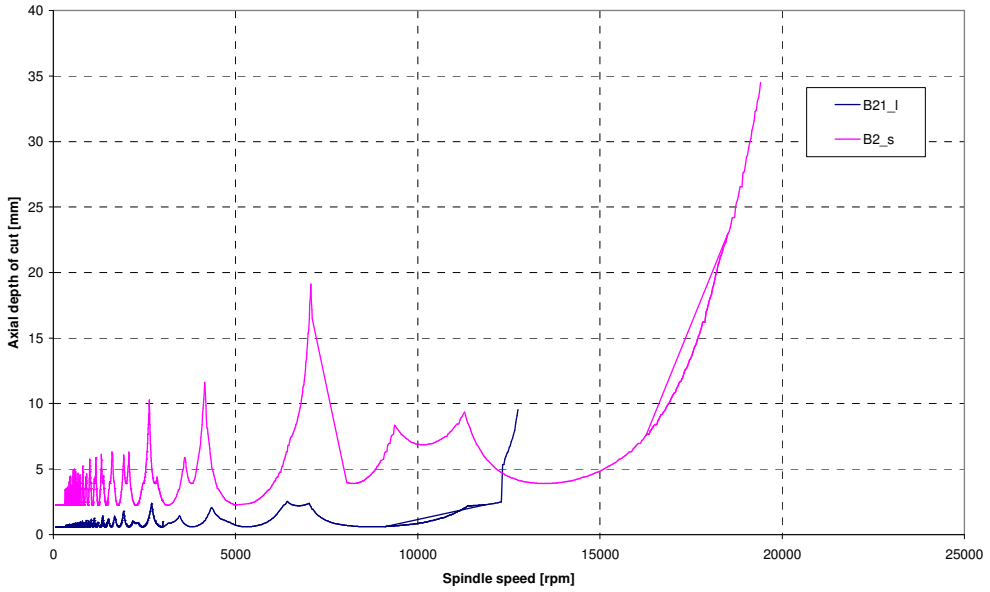

Figure 4.38 The stability diagrams including the FRFs of the workpiece at the 1st step of the semifinishing cut of the layer removal and at the 2nd step of the step removal

The stability curve including the workpiece effect at the 2nd step of the step removal is higher than that at the 1st step of the semifinishing cut of the layer removal. This is due to the fact that the workpiece is more rigid and has lower FRFs at the 2nd step of the step removal as seen in Figure 4.35.

The stability diagram including the FRFs of the workpiece at the 1st step of the finishing cut at the layer removal and at the 3rd step of the step removal are given in Figure 4.39.

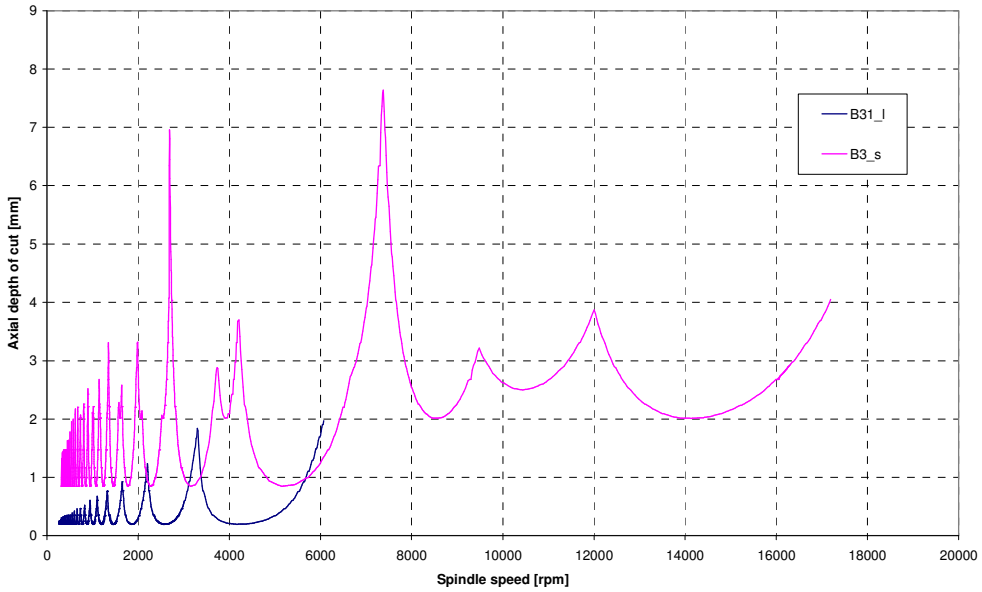

Figure 4.39 The stability diagram including the FRFs of the workpiece at the 1st step of the finishing cut of the previous and new machining process

Since only the thickness of the free end of the workpiece reduces at the step removal, as in the layer removal the whole workpiece gets thinner, the stability values at the 3rd step of the step removal are higher as shown in Figure 4.39.

From these results, it can be observed that the stability values of the step removal machining are higher due to the cutting pattern which keeps the unmachined region of the workpiece at the maximum thickness. It can be concluded that the machining time becomes shorter in the step removal process.

4.2.1.10.2 Minimum Chatter-Free Machining Time

In this section the chatter-free machining time of the step removal process is calculated using the second method mentioned in Section 4.2.1.8.

The machining times of the step removal found by using the second method are given in Table 4.13. In this table, B1_0, B1_1 and B1_2 stand for the 1st step of the roughing, semifinishing and finishing cut of the step removal, respectively.

Table 4.13 Machining time calculation parameters at the step removal process using second method

All_steps	Spindle speed(rpm)	Depth of cut(mm)	nop	Feed per tooth	Time(min)
B1_0	8745	4.46	3	0.15	0.03
B1_1	9105	3.27	4	0.1	0.05
B1_2	11160	7.49	2	0.1	0.02
B2_0	7365	6.11	2	0.15	0.02
B2_1	7643	10.93	1	0.1	0.02
B2_2	12765	15.84	1	0.1	0.01
B3_0	8363	12.76	1	0.15	0.01
B3_1	13890	9.16	2	0.1	0.02
B3_2	14115	41.68	1	0.1	0.01
B4_0	8190	22.10	1	0.15	0.01
B4_1	8190	22.07	1	0.1	0.02
B4_2	8175	64.91	1	0.1	0.02
B5_0	8205	21.27	1	0.15	0.01
B5_1	8205	21.26	1	0.1	0.02
B5_2	8250	38.72	1	0.1	0.02
B6_0	8228	19.60	1	0.15	0.01
B6_1	8228	19.60	1	0.1	0.02
B6_2	8225	52.08	1	0.1	0.02
B7_0	8235	19.45	1	0.15	0.01
B7_1	8235	19.49	1	0.1	0.02
B7_2	8220	51.65	1	0.1	0.02
B8_0	8235	19.16	1	0.15	0.01
B8_1	8228	19.16	1	0.1	0.02
B8_2	8220	51.27	1	0.1	0.02
B9_0	8235	19.11	1	0.15	0.01
B9_1	8235	19.11	1	0.1	0.02
B9_2	8228	51.03	1	0.1	0.02
B10_0	8235	19.08	1	0.15	0.01
B10_1	8235	19.08	1	0.1	0.02
B10_2	8228	50.89	1	0.1	0.02
				Total time	0.48

Full machining time of the step removal process is 0.48 minutes as seen from Table 4.13 as this value is 2.18 minutes in the layer removal process in Section 4.2.1.8. The layer removal machining takes 4.5 times longer than the step removal process and it means that to machine such a workpiece can be shortened very significantly using the step removal process. The similar cutting patterns can be developed by examining the workpiece geometry, its cutting and boundary conditions in detail and the machining time can be minimized using both maximum stability values from the stability diagrams and selecting an efficient cutting strategy.

The step removal process is also applied to the machining with different radial depth of cuts (7 mm, 4 mm, 1 mm) at the roughing, semifinishing and finishing cuts. This machining was explained in Section 4.2.1.9.1 in detail. In this section, this machining process is performed by the step removal cutting strategy and the machining times obtained are given in Table 4.14.

Table 4.14 Machining time calculation parameters at the step removal process of the machining with different radial depth of cuts using second method

All_steps	Spindle speed(rpm)	Depth of cut(mm)	nop	Feed per tooth	Time(min)
B1_0	8768	3.11	4	0.15	0.04
B1_1	9105	3.69	3	0.1	0.04
B1_2	11115	19.20	1	0.1	0.01
B2_0	11985	2.16	5	0.15	0.03
B2_1	12585	5.51	2	0.1	0.02
B2_2	12690	49.78	1	0.1	0.01
B3_0	13515	4.54	3	0.15	0.02
B3_1	14040	13.86	1	0.1	0.01
B3_2	13875	122.34	1	0.1	0.01
B4_0	8190	14.90	1	0.15	0.01
B4_1	8153	18.76	1	0.1	0.02
B4_2	8220	222.05	1	0.1	0.02
B5_0	8213	14.40	1	0.15	0.01
B5_1	8205	27.24	1	0.1	0.02
B5_2	8228	99.21	1	0.1	0.02
B6_0	8228	13.88	1	0.15	0.01
B6_1	8228	25.21	1	0.1	0.02

B6_2	8205	115.53	1	0.1	0.02
B7_0	8235	13.82	1	0.15	0.01
B7_1	8228	24.68	1	0.1	0.02
B7_2	8205	113.83	1	0.1	0.02
B8_0	8235	13.76	1	0.15	0.01
B8_1	8228	24.42	1	0.1	0.02
B8_2	8198	111.77	1	0.1	0.02
B9_0	8235	13.70	1	0.15	0.01
B9_1	8235	24.04	1	0.1	0.02
B9_2	8168	97.04	1	0.1	0.02
B10_0	8243	13.65	1	0.15	0.01
B10_1	8228	24.50	1	0.1	0.02
B10_2	8175	96.99	1	0.1	0.02
				Total time	0.48

As mentioned in Section 4.2.1.9.2, the machining time for this machining with layer removal was calculated by using the second method as 2.44 minutes. The same machining with the step removal strategy takes 0.48 minutes which is 1/5 of the machining time with layer removal.

In both examples, the machining times reduce significantly using the step removal cutting strategy. Using the appropriate cutting patterns which can be found by studying the workpiece dynamics and maximum stability values in detail, the machining time can be minimized significantly.

4.2.1.11 Summary of the Results of the Beam Model

In Section 4.2.1, in order to see the effect of the thickness change of the workpiece at the same location, the FRFs of the workpiece and the stability diagrams at different cuts (roughing, semifinishing and finishing cuts) were compared. It was observed that the magnitudes of the workpiece's FRFs take higher values as the workpiece becomes thinner and more flexible. Also the natural frequencies of the workpiece reduce with thinning workpiece due to the stiffness reduction of the

workpiece. The absolute and peak stability values decrease due to increased FRF amplitudes of the workpiece with thickness reduction. At the same time the spindle speeds corresponding to peaks of the stability curve take lower values due to reduced natural frequencies of the system.

In addition, the variation of the workpiece FRF and the stability limits due to the change on the cutting location, i.e. the location where the workpiece's FRFs are calculated, was studied. In order to see this effect the FRFs of the workpiece and the stability diagrams at different cutting steps (at different locations) were examined. It was observed that the FRFs of the workpiece take the highest values at the free end of the workpiece which is a cantilever beam, and the magnitudes of the FRFs reduce as the location of the FRFs changes from the free end to the fixed end of the workpiece. This is an expected result as the stiffness of the fixed end of the workpiece is higher than that of the free. The natural frequencies of the workpiece increase as the material is removed from the free end or near to the free end due to less stiffness reduction in removing the material from the free end. On the contrary the material removed from the fixed end results in decreasing natural frequencies due to significant stiffness loss. According to the FRF magnitudes of the workpiece relative to those of the tool, the absolute and peak stabilities become higher or lower during machining of the workpiece from the free end to the fixed end. The stability limits usually increase as machining from the free end to the middle of the workpiece, then they remain constant as machining from the middle to the fixed end since the FRFs of the workpiece become lower than those of the tool and the tool FRFs become dominant at the system FRFs. The similar change can be observed in the corresponding spindle speeds of the peaks of the stability curve. However, this may change depending on the workpiece and tool geometry and materials.

In Section 4.2.1.8, the minimum chatter-free machining time values were calculated and studied in detail. Using both one common maximum stable depth of cut for every cut and one maximum stable depth of cut for every machining step, the machining times were estimated. From the results, it was concluded that

finding the maximum stable depth of cuts at higher speeds for every machining step reduces the machining time significantly and results in higher chatter-free productivity.

The effect of using different radial depth of cuts on the stable machining was also studied. It is known that increasing the radial depth of cut results in decrease in the stable axial depth of cut. From the analysis of the stable machining times with different radial depths at different passes, it was concluded that taking higher radial depths in the first cut (roughing cut) can cause the reduction of the total machining time by decreasing the number of total machining steps. Taking lower radial depths in the final cuts (semifinishing/finishing cuts) results in the higher stable axial depth of cuts and shorter machining times.

In addition to the cutting parameters, the machining strategy may also have significant effects on the variation of the workpiece dynamics and the stable machining time. The effects of different cutting strategies on the stable machining time were analyzed using the beam model. The layer removal method which is the reduction of the workpiece's thickness at everywhere equally in each cut was compared with the step removal method which is the reduction of the thickness to its final dimension by taking the material from the same location step-by-step. It should be mentioned here that this is only feasible when all passes, i.e. roughing, semi-finishing and finishing, are done using the same tool. Otherwise, step removal method is not feasible since the tool has to be changed at every step resulting in excessive tool change time. Since the thickness of the unmachined part of the workpiece remains its initial value, the FRFs of the workpiece in the step removal process take lower values in the machining steps compared to the layer removal. Also, the natural frequencies of the workpiece become higher at the step removal. It can be said that the machined workpiece is stiffer during the step removal machining compared to the layer removal process. Then it can be concluded that lower stable machining times can be obtained by considering different cutting methods. The machining times of the layer and step removal

processes with radial depth of cuts 5 mm, 5 mm, 2 mm at steps of the roughing, semifinishing and finishing respectively can be given in Table 4.15.

Table 4.15 The machining times of the step and layer removal with the radial depth of cuts 5 mm, 5 mm, 2 mm of corresponding cuts

	Step Removal				Layer Removal		
All_steps	**Spindle speed(rpm)**	**Depth of cut(mm)**	**Time (min)**	**All steps**	**Spindle speed(rpm)**	**Depth of cut(mm)**	**Time (min)**
B1_0	8745	4.46	0.03	**B10**	8753	4.45	0.03
B1_1	9105	3.27	0.05	**B11**	8978	3.82	0.03
B1_2	11160	7.49	0.02	**B12**	9068	3.63	0.03
B2_0	7365	6.11	0.02	**B13**	7568	6.77	0.02
B2_1	7643	10.93	0.02	**B14-B19**	8213	16.10	0.04
B2_2	12765	15.84	0.01	**B20**	6240	2.01	0.10
B3_0	8363	12.76	0.01	**B21**	6675	2.02	0.09
B3_1	13890	9.16	0.02	**B22**	7508	3.00	0.07
B3_2	14115	41.68	0.01	**B23**	7868	5.13	0.03
B4_0	8190	22.10	0.01	**B24**	7965	7.59	0.03
B4_1	8190	22.07	0.02	**B25**	7830	8.25	0.03
B4_2	8175	64.91	0.02	**B26-B29**	8220	16.71	0.05
B5_0	8205	21.27	0.01	**B30**	3047	0.90	0.49
B5_1	8205	21.26	0.02	**B31**	3255	0.88	0.46
B5_2	8250	38.72	0.02	**B32**	3465	1.37	0.29
B6_0	8228	19.60	0.01	**B33**	3683	1.85	0.20
B6_1	8228	19.60	0.02	**B34**	3743	2.87	0.13
B6_2	8225	52.08	0.02	**B35**	7290	11.83	0.02
B7_0	8235	19.45	0.01	**B36**	7275	11.99	0.02
B7_1	8235	19.49	0.02	**B37-B39**	8190	44.53	0.02
B7_2	8220	51.65	0.02				
B8_0	8235	19.16	0.01				
B8_1	8228	19.16	0.02				
B8_2	8220	51.27	0.02				
B9_0	8235	19.11	0.01				
B9_1	8235	19.11	0.02				
B9_2	8228	51.03	0.02				
B10_0	8235	19.08	0.01				
B10_1	8235	19.08	0.02				
B10_2	8228	50.89	0.02				
		Total time	0.48			**Total time**	2.18

Comparing the machining times of every step is not appropriate here, since the location where the workpiece's FRFs calculated is not the same at the mutual steps of the two processes. However, by looking at all steps in Table 4.15, the maximum stable axial depth of cuts and the spindle speeds are usually higher for the step removal process. Thus, the total machining time is also shorter for the step removal than the layer removal method. The same trend can be seen for different radial depth of cuts, i.e. 7 mm, 4 mm, 1 mm. The step removal machining takes 0.48 minutes whereas with the layer removal takes 2.44 minutes. Also, it can be concluded that the radial depth of cuts of the machining are less effective at the step removal case as seen in the results of two cases.

4.2.2 Plate Model of the Workpiece

In order to obtain FRFs at different stages and locations of the workpiece during machining, secondly the workpiece is modeled as a plate in the FE program, MSC. Marc Mentat©.

The plate model is shown in Figure 4.40 where the respective sizes are given follows:

Length : 100 mm
Width : 80 mm
Thickness : 15 mm

The material of the beam is steel with Young's modulus of 200 GPa, Poisson's ratio of 0.3 and the density of 7800 kg/m^3. As mentioned in Section 3.3.1 the damping coefficients $\boldsymbol{a}$ and $\boldsymbol{b}$ are taken as 0.03 and 0.02 respectively. The boundary conditions of the plate are taken as fixed-free-free-free.

Figure 4.40 Plate model

The workpiece is modeled in MSC. Marc Mentat© with shell elements (Element type 139) as shown in Figure 4.41. Each node of the shell element has 6 degrees of freedom (displacement in x axis, displacement in y axis, displacement in z axis, rotation in x axis, rotation in y axis and rotation in z axis) and the total degree of freedom of the model is 150 with 20 elements.

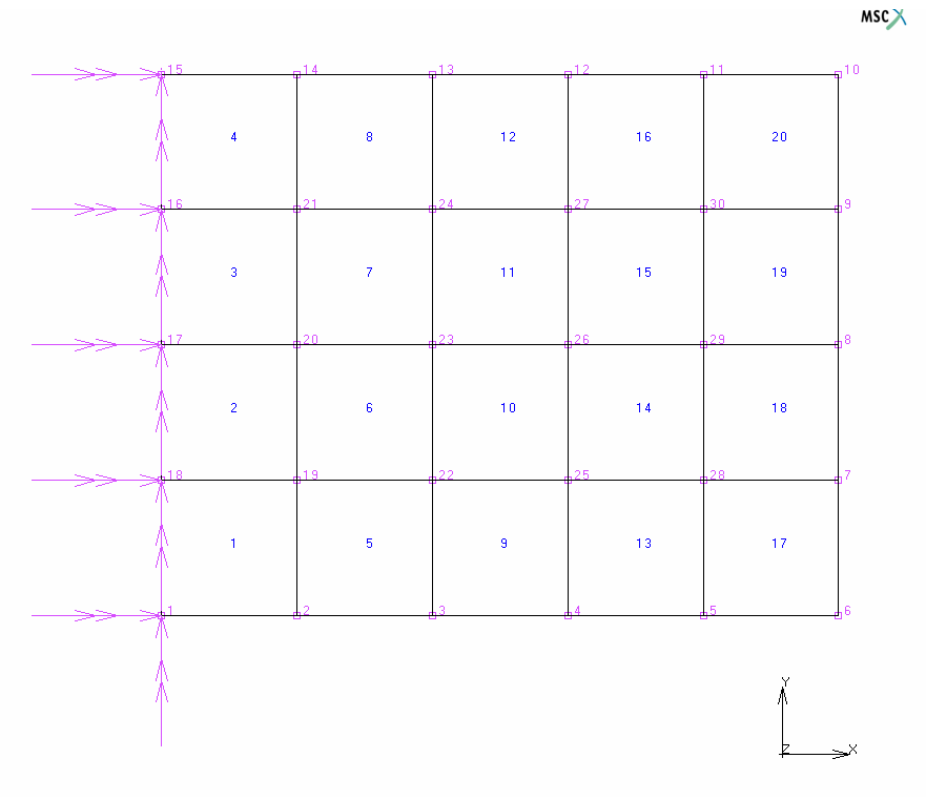

Figure 4.41 Plate model in MSC. Marc Mentat©

4.2.2.1 Tool-Holder-Spindle Model

As mentioned in Section 4.2.1.1, the same spindle-holder-tool combination and its tool point FRF is used to predict the stability diagrams of the plate model.

4.2.2.2 Machining Process and FRFs of the Workpiece

The workpiece is assumed to be machined in three main cutting cycles. These are

- ***Roughing cut*** : Thickness of the workpiece is reduced from 15 mm to 10 mm (radial depth of cut = 5 mm) completely.

- ***Semifinishing cut*** **:** Thickness of the workpiece is reduced from 10 mm to 5 mm(radial depth of cut = 5 mm) completely.

- ***Finishing cut*** : Thickness of the workpiece is reduced from 5 mm to 3 mm(radial depth of cut = 2 mm) completely.

The tangential and radial cutting force coefficients, K_t and K_r, used in order to determine the stability limits are taken as 626 MPa and 0.1597 respectively. As an initial assumption, the axial depth of cut is taken as 20 mm so that the workpiece is machined in 20 steps per cut and in a pass 4 steps are machined as shown in Figure 4.42. As mentioned in Section 4.2.1.2, a similar coding convention is used in order to name the machining steps. For example, P15 stands for 5^{th} step of the first cut (roughing cut). The machining steps of the workpiece in the roughing cut are shown in Figure 4.42. In order to see the variation of the dynamics of the plate clearly, the FRFs of the plate at the same location, but in different cuts are compared as done with the beam model. By comparing the FRFs of the workpiece in different cuts at the same location, the effects of the thickness change of the workpiece on the FRFs of the system and on the stability diagrams are studied. By comparing the FRFs of the workpiece at different locations, the effect of the location change during machining on the stability limits is also examined with case studies.

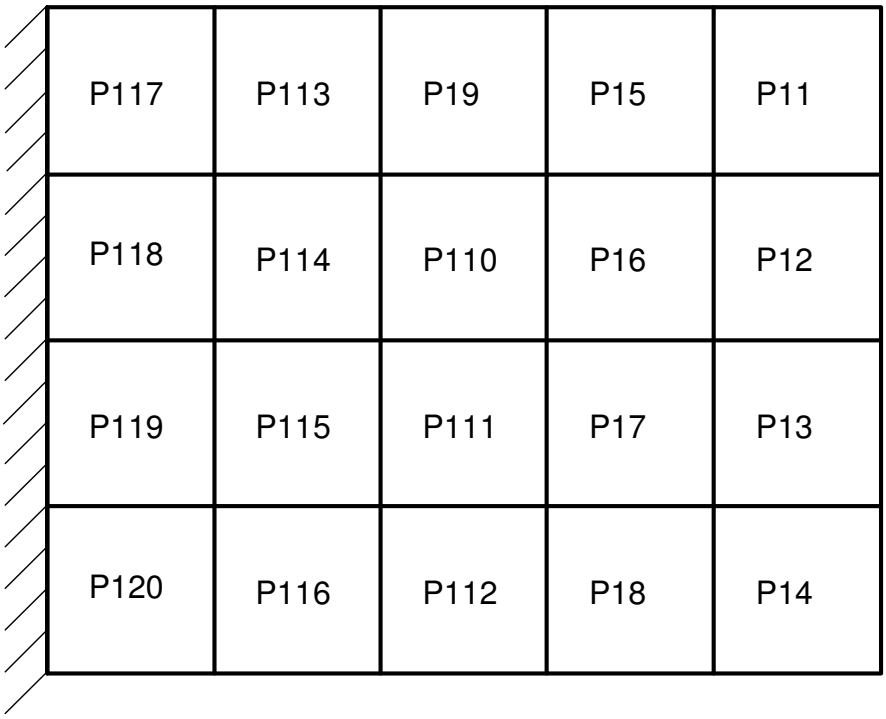

Figure 4.42 The machining steps of the plate model in the roughing cut

4.2.2.3 FRFs of the Workpiece and Stability Diagrams at the First Step of the Cut

In order to see the effect of the thickness change of the workpiece, the FRFs of the plate P11, P21 and P31 are drawn in Figure 4.43. The FRFs of the plate combined with the FRFs of the tool are given in Figure 4.44, to observe the effect of the FRFs of the workpiece on combined system FRFs.

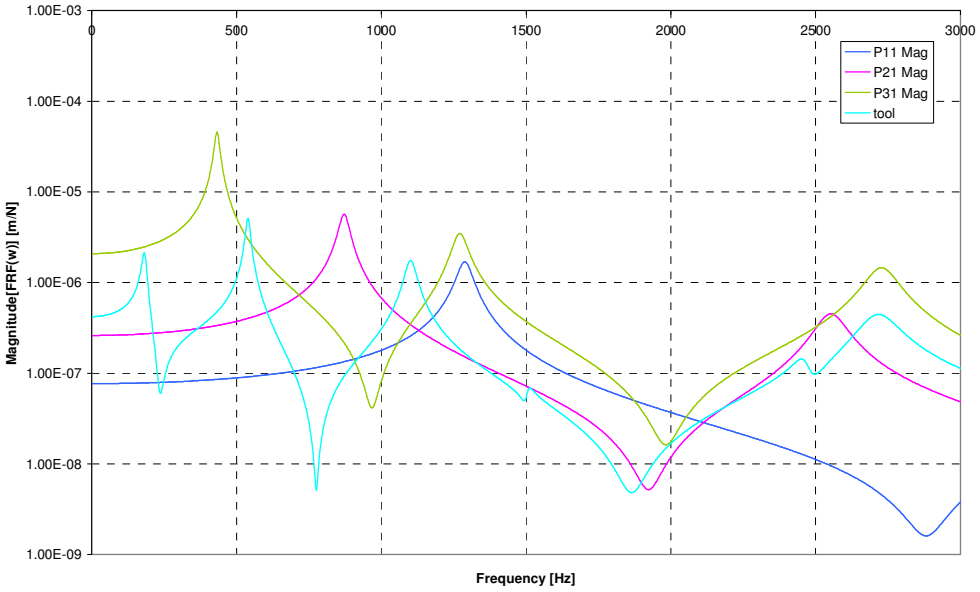

Figure 4.43 FRFs of the workpiece at the end of first step of 1st, 2nd and 3rd cut

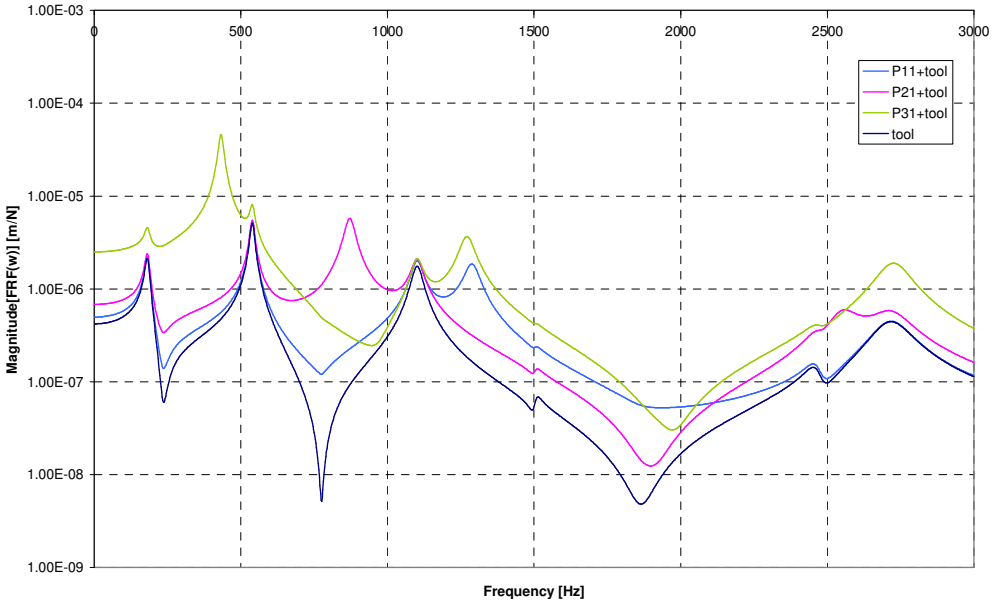

Figure 4.44 Combined FRFs of the workpiece and tool at the end of first step of 1st, 2nd and 3rd cuts

As seen from Figure 4.43 and 4.44, the magnitude of the FRFs of the workpiece increases, as the workpiece becomes thinner as observed in the beam model. The natural frequencies of the workpiece become smaller while the thickness of the workpiece decreases as shown in Figure 4.43 due to increasing flexibility of the workpiece.

The stability lobe diagrams including the changing dynamics of the workpiece at the end of the first step of the 1st, 2nd and 3rd cuts are shown in Figure 4.45.

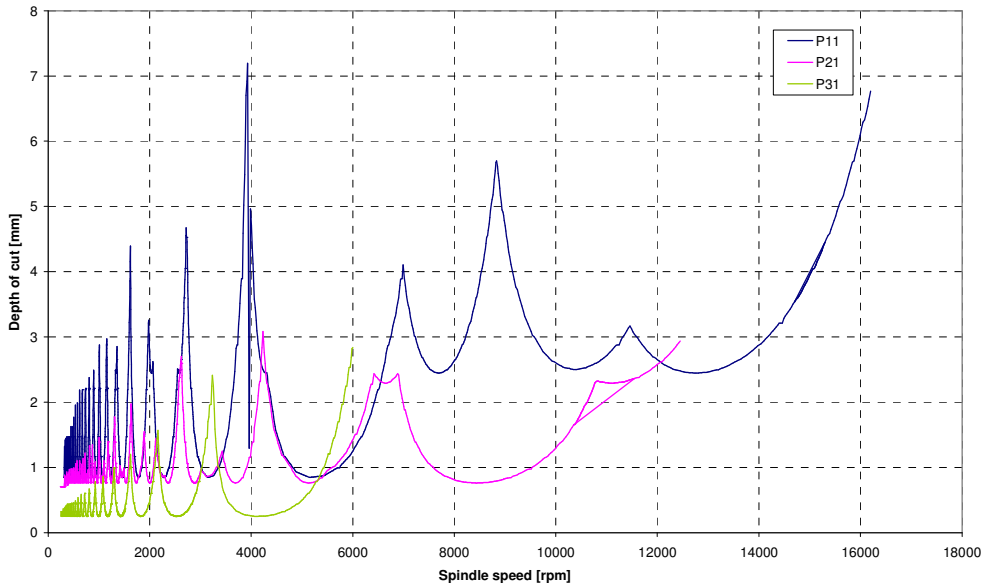

Figure 4.45 Stability lobe diagram including the FRFs of the workpiece at the end of first step of 1st, 2nd and 3rd cuts

As shown in Figure 4.45, the absolute stability limit which is the minimum value of stable depths, becomes lower, as the thickness of the workpiece is reduced. Similarly, the peak amplitudes of the stability limit curve decreases, and some lobes even disappear as the workpiece becomes thinner. The spindle speeds corresponding to the stability lobes usually move to lower speeds with increasing flexibility of the workpiece. It can be concluded that the reduction in the stiffness

of the workpiece causes a significant decrease in stable axial depths and speeds if the workpiece is much more flexible than the tool and the workpiece dynamics should include in the system FRFs used in stability calculations.

4.2.2.4 FRFs of the Workpiece and Stability Diagrams at the Second Step of the Cut

In order to see the effect of the thickness change of the workpiece, the FRFs of the plate P12, P22 and P32 are drawn in Figure 4.46. The FRFs of the plate combined with the FRFs of the tool are given in Figure 4.47 to see the variation in the combined system FRFs with changing workpiece thickness.

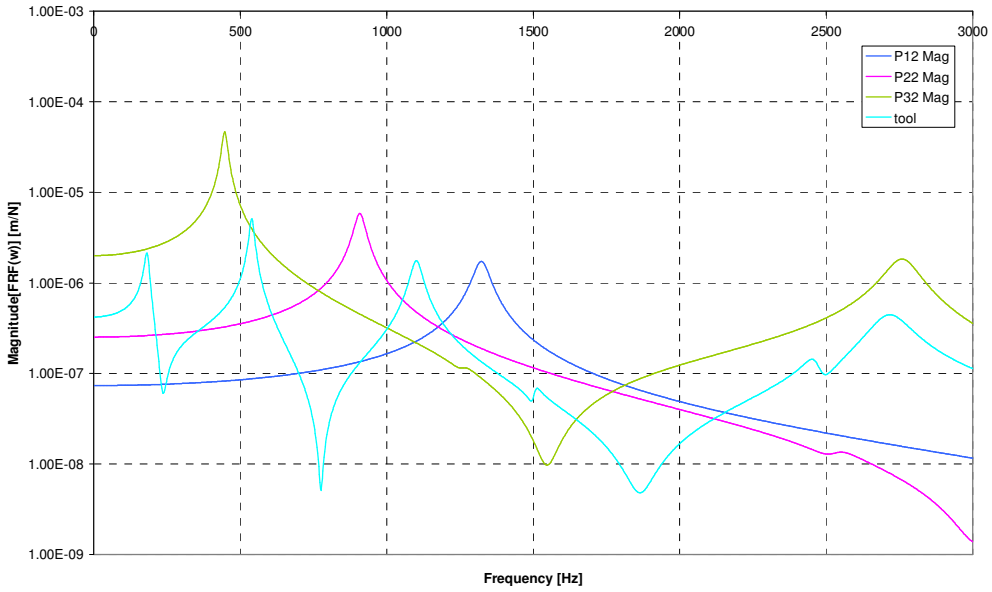

Figure 4.46 FRFs of the workpiece at the end of second step of 1st, 2nd and 3rd cuts

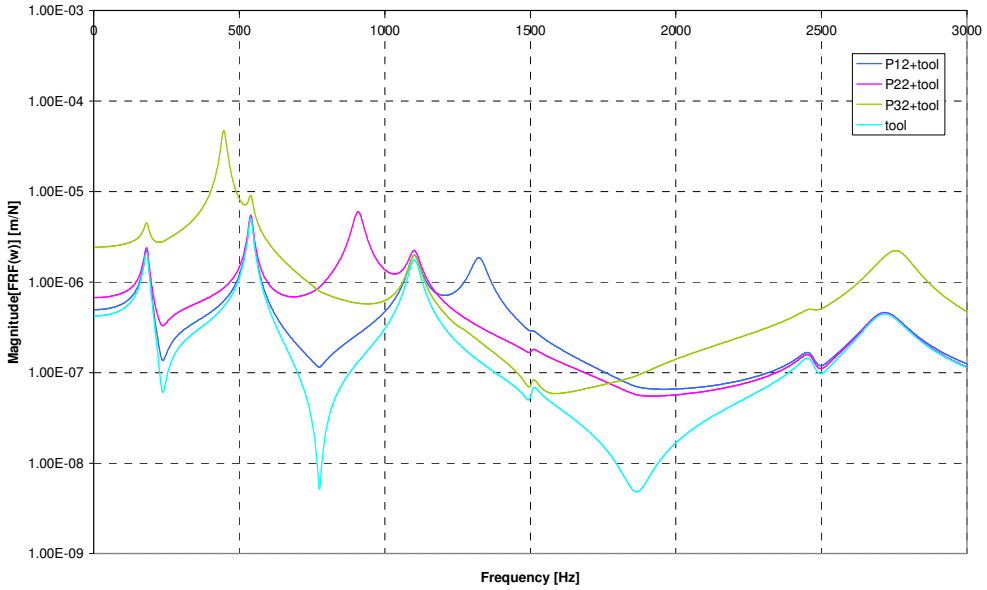

Figure 4.47 Combined FRFs of the workpiece and tool at the end of second step of 1st, 2nd and 3rd cuts

As can be seen in Figure 4.46, the peak FRFs of the workpiece are nearly the same as the peak FRFs at the 1st location of the workpiece in all cutting cycles. The only difference is the FRF magnitude of the 2nd natural frequency. Since the 2nd mode shape of the plate is the first torsional mode, the middle of the plate becomes the nodal line of the 2nd mode so that the peak of the FRF of 2nd natural frequency at second location is not seen clearly. As a result, the 2nd mode does not affect the stability at this location.

The stability lobe diagrams including the changing dynamics of the workpiece at the end of the second step of 1st, 2nd and 3rd cuts are shown in Figure 4.48.

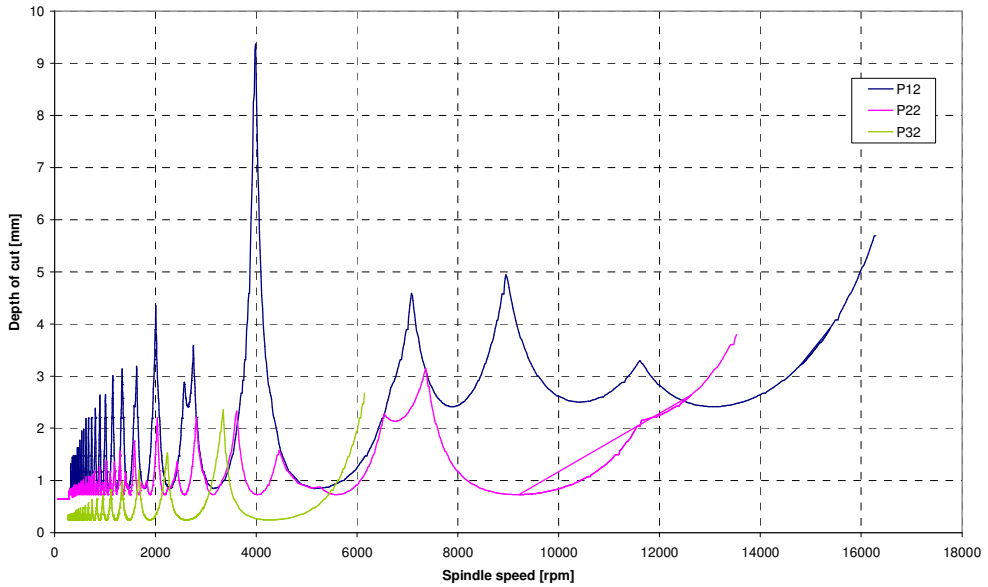

Figure 4.48 Stability lobe diagram including the FRFs of the workpiece at the end of second step of 1st, 2nd and 3rd cuts

As shown in Figure 4.48, the stability curves at the second location are not very different than the first location, only the peak amplitudes of the stability curve are lower than those of the first location due to the reduction in the workpiece's thickness.

4.2.2.5 FRFs of the Workpiece and Stability Diagrams at the Ninth Step of the Cut

In order to see the effect of the thickness change of the workpiece, the FRFs of the plate P19, P29 and P39 are drawn in Figure 4.49. The FRFs of the plate combined with the FRFs of the tool are given in Figure 4.50 to see the variation in the combined system FRFs with changing workpiece thickness.

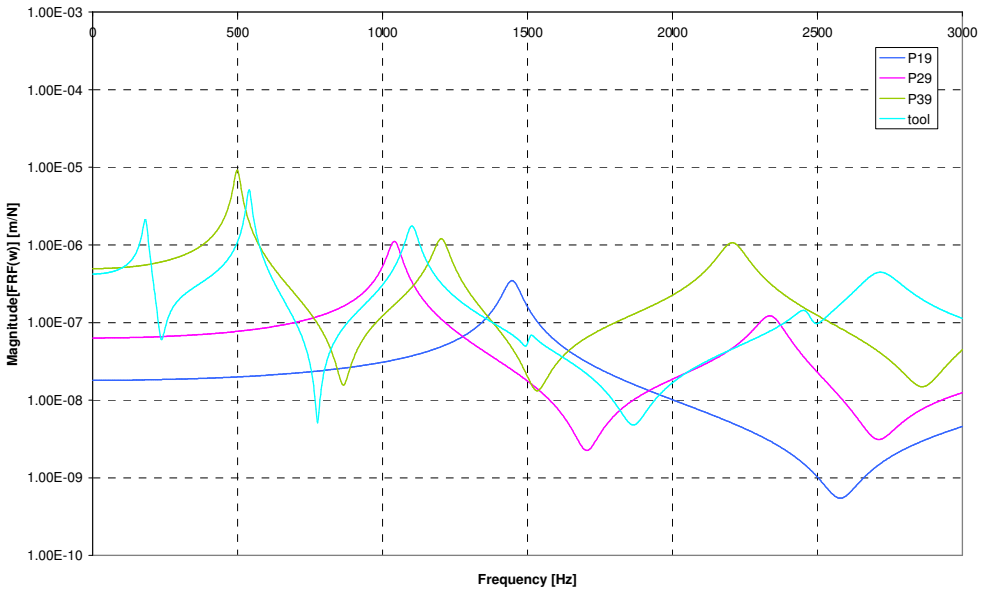

Figure 4.49 FRFs of the workpiece at the end of ninth step of 1st, 2nd and 3rd cuts

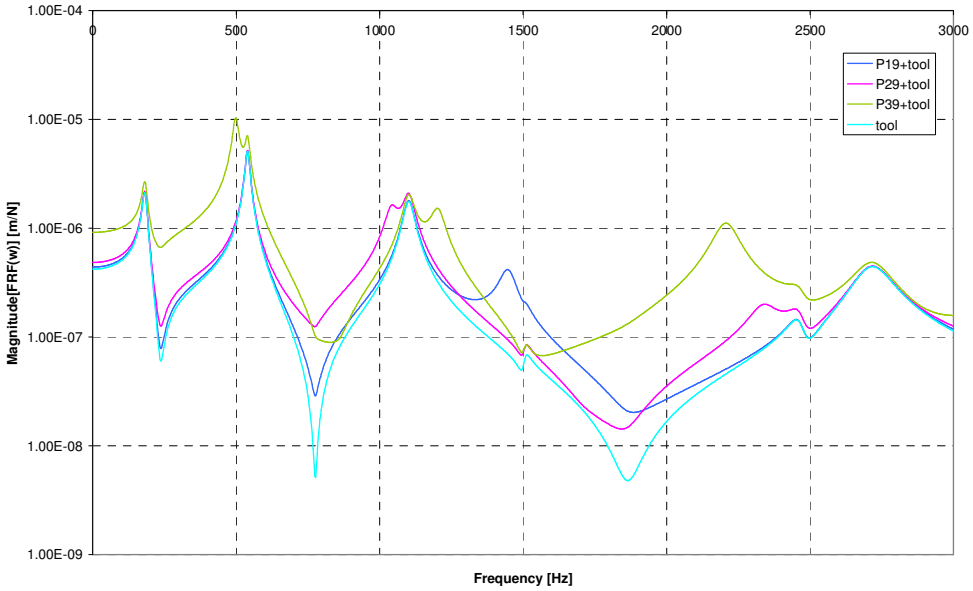

Figure 4.50 Combined FRFs of the workpiece and tool at the end of ninth step of 1st, 2nd and 3rd cuts

As shown in Figure 4.49, the peak FRFs of the workpiece are less than the peak FRFs at the free end (at the 1st and 2nd location) of the workpiece in all cutting cycles due to the boundary conditions as mentioned in Section 4.2.1.4. Since the workpiece is stiffer at the middle, its FRFs become lower than those at the free end of the workpiece although the workpiece gets thinner. Similarly it can be observed that the first natural frequencies of the plate at three cuts increase due to the same phenomenon.

The stability lobe diagrams including the changing dynamics of the workpiece at the end of the ninth step of 1st, 2nd and 3rd cuts are shown in Figure 4.51.

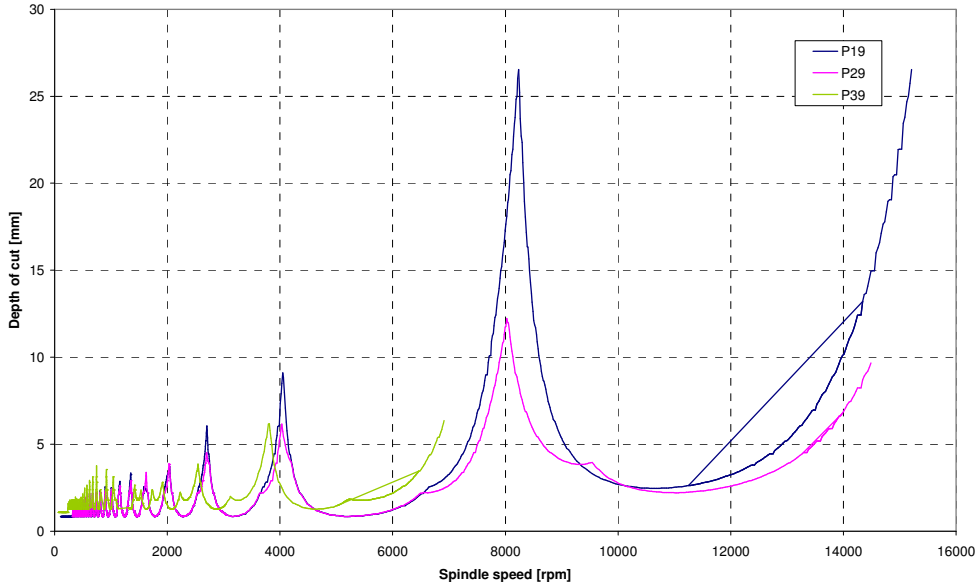

Figure 4.51 Stability lobe diagrams including the FRFs of the workpiece at the end of ninth step of 1st, 2nd and 3rd cuts

As can be seen from Figure 4.51, since the FRFs of the workpiece at the first and second cuts are lower than the FRFs of the tool, the flexibility of the tool becomes dominant and absolute stability levels at these stages are the same. The higher

peaks of the stability curve of the second cut take lower depths of cut values than the first cut as the workpiece becomes thinner. At the third cut, however, the workpiece becomes as flexible as the tool. The absolute stability level of the workpiece at the third cut is higher than those of the first and second stages as seen in Figure 4.51, due to small radial depth of cut at the third cut.

4.2.2.6 FRFs of the Workpiece and Stability Diagrams at the Tenth Step of the Cut

In order to see the effect of the thickness change of the workpiece at this location, the FRFs of the plate P110, P210 and P310 are given in Figure 4.52. The FRFs of the plate combined with the FRFs of the tool are given in Figure 4.53 to see the variation in the combined system FRFs with changing workpiece thickness.

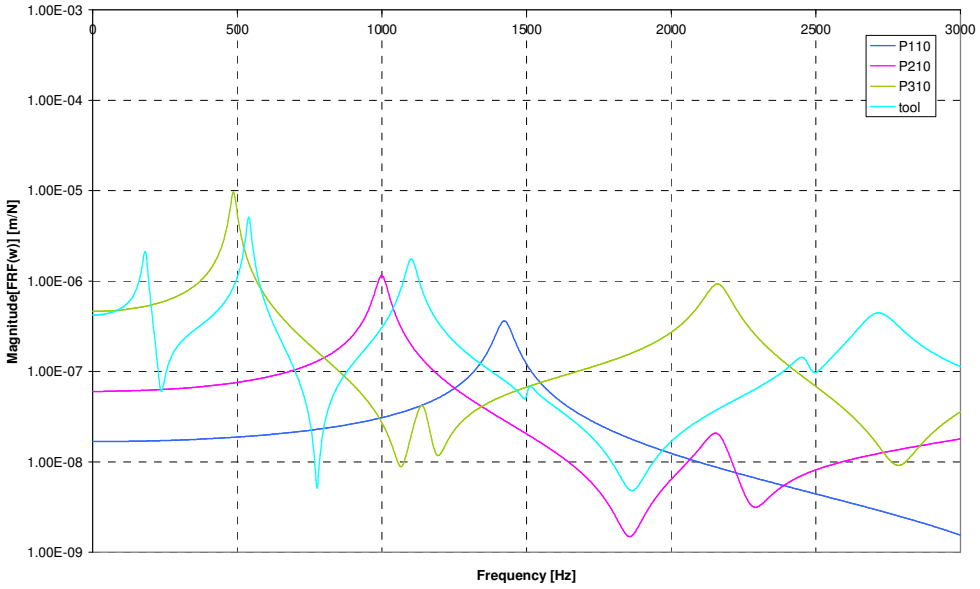

Figure 4.52 FRFs of the workpiece at the end of tenth step of 1st, 2nd and 3rd cuts

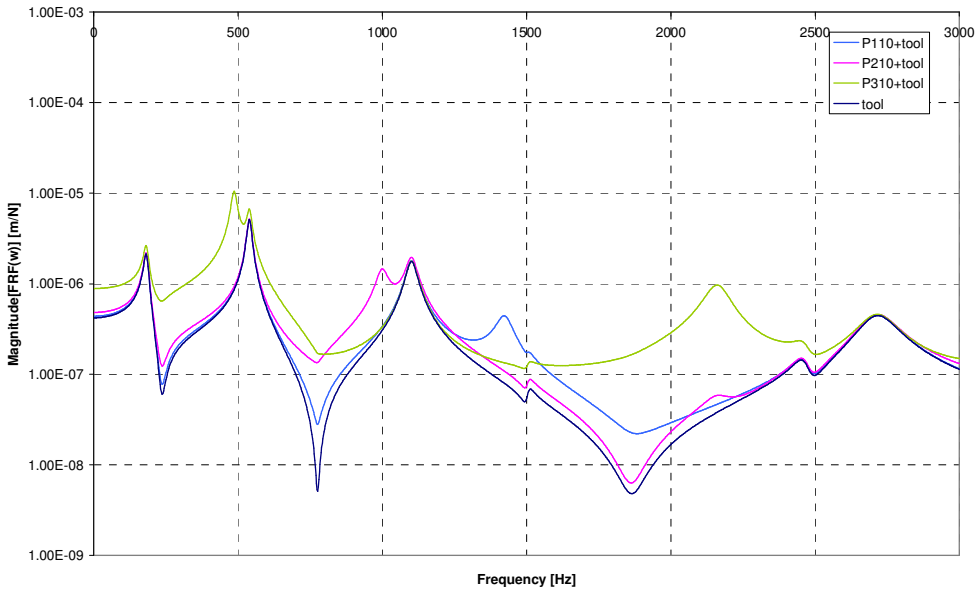

Figure 4.53 Combined FRFs of the workpiece and tool at the end of tenth step of 1st, 2nd and 3rd cuts

The FRF levels of the workpiece at the tenth step of all the cuts are nearly the same with those of the ninth step as shown in Figure 4.52. The FRF magnitudes of the second natural frequency of the workpiece get very low since this location coincides with the nodal line of the second mode (first torsional mode) of the workpiece. The FRFs of the workpiece at tenth step become lower than those of the free end as explained in previous section.

The stability lobe diagrams including the changing dynamics of the workpiece at the end of the tenth step of the 1st, 2nd and the 3rd cuts are shown in Figure 4.54.

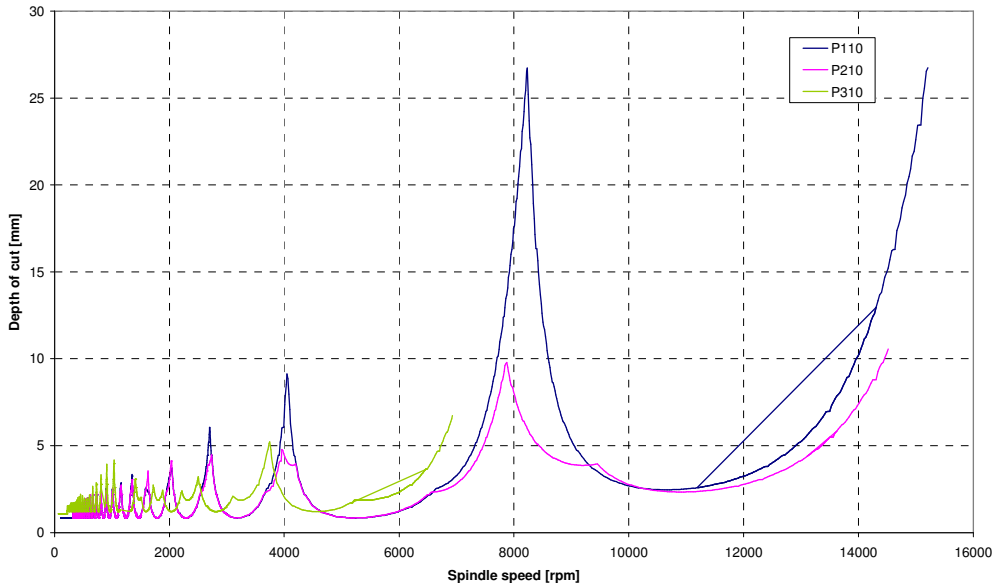

Figure 4.54 Stability lobe diagrams including the FRFs of the workpiece at the end of tenth step of 1st, 2nd and 3rd cuts

Like at the ninth step, at the 1st and 2nd cuts the absolute stabilities are the same except some peak stability values. As mentioned at the previous section, the absolute stability of the system at the third cut is higher than the other two cuts because of small radial depth. Since both the tool and the workpiece have the comparable FRFs, both of their effect should be included in the stability diagrams.

4.2.2.7 FRFs of the Workpiece and Stability Diagrams at the Seventeenth step of the Cut

In order to see the effect of the thickness change of the workpiece at this location, the FRFs of the plate P117, P217 and P317 are given in Figure 4.55. The FRFs of the plate combined with the FRFs of the tool are given in Figure 4.56 to see the variation in the combined system FRFs with changing workpiece thickness.

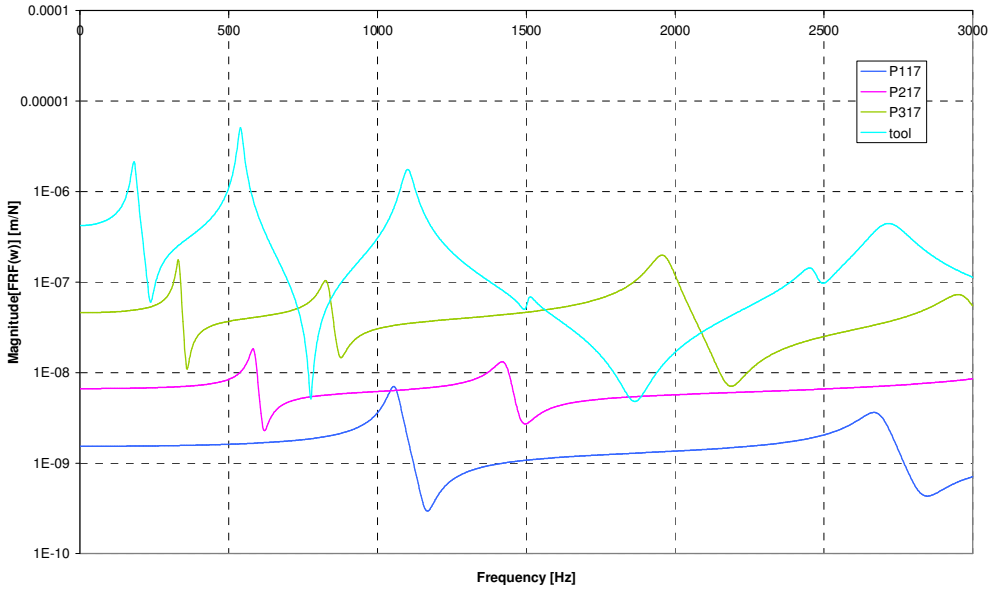

Figure 4.55 FRFs of the workpiece at the end of seventeenth step of 1st, 2nd and 3rd cuts

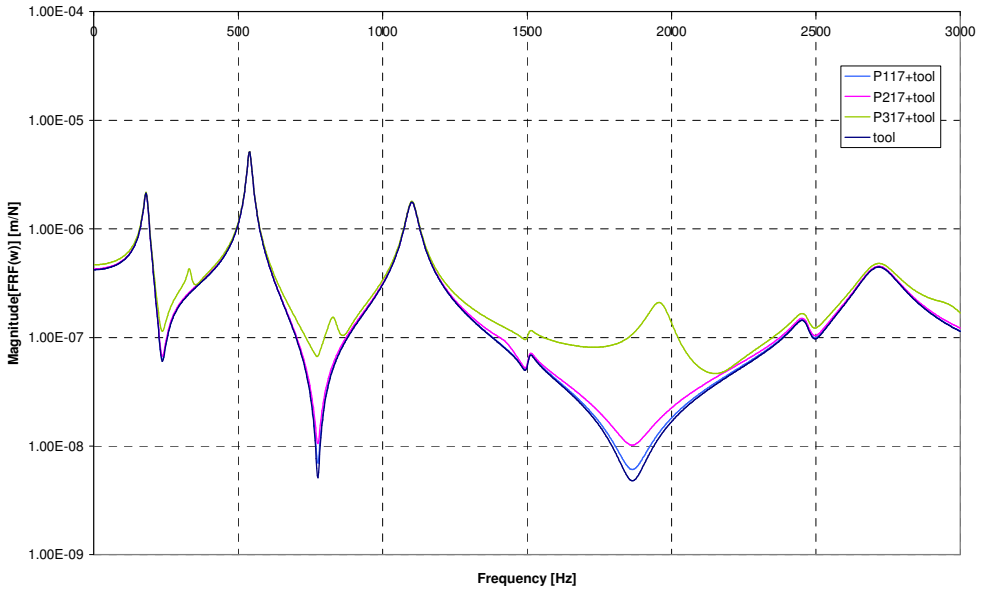

Figure 4.56 Combined FRFs of the workpiece and tool at the end of seventeenth step of 1st, 2nd and 3rd cuts

As mentioned before, the FRFs of the workpiece near to the fixed end have very low values compared to the other locations due to increase in the stiffness of the workpiece. Since the FRFs of the workpiece are very low compared to those of the tool, total FRFs of the system and the tool are nearly the same except in the third cut as seen in Figure 4.56. In such a case, only the FRF of the tool can be used to predict the stability diagrams accurately.

The stability lobe diagrams including the changing dynamics of the workpiece at the end of the tenth step of the 1st, 2nd and 3rd cuts are shown in Figure 4.57. Since the stability diagrams of P117 and P217 are the same, they seem as one curve in Figure 4.57.

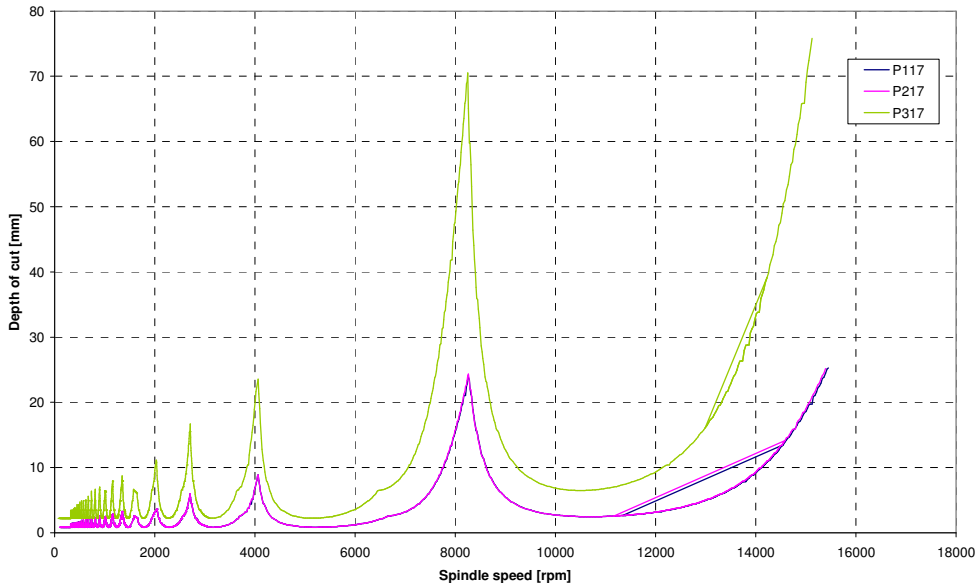

Figure 4.57 Stability lobe diagrams including the FRFs of the workpiece at the end of seventeenth step of 1st, 2nd and 3rd cuts

The FRFs of the system is nearly the same at all the cuts since the system dynamics is mainly governed by the tool FRF at this location. Therefore, the

stability curves are the same for all cuts at this location except the finishing cut where the radial depth of cut is different than the previous two cuts. As a result, it can be concluded that the workpiece dynamics can be neglected when the tool is much more flexible than the workpiece since the variation of the workpiece dynamics does not affect the stability limits.

4.2.2.8 FRFs of the Workpiece and Stability Diagrams at the Eighteenth step of the Cut

In order to see the effect of the thickness change of the workpiece at this location, the FRFs of the plate P118, P218 and P318 are given in Figure 4.58. The FRFs of the plate combined with the FRFs of the tool are given in Figure 4.59 to see the variation in the combined system FRFs with changing workpiece thickness.

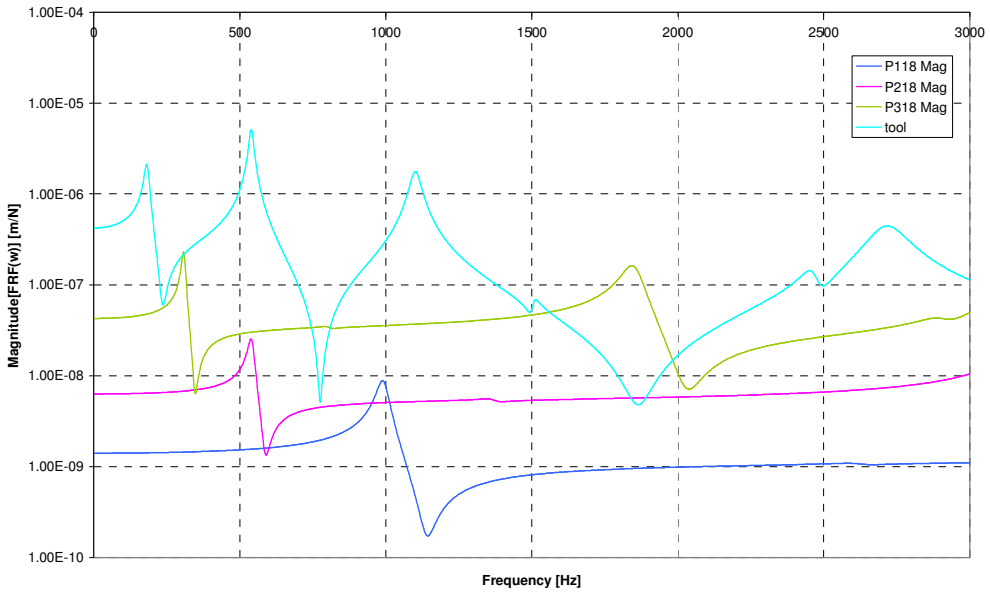

Figure 4.58 FRFs of the workpiece at the end of eighteenth step of 1st, 2nd and 3rd cuts

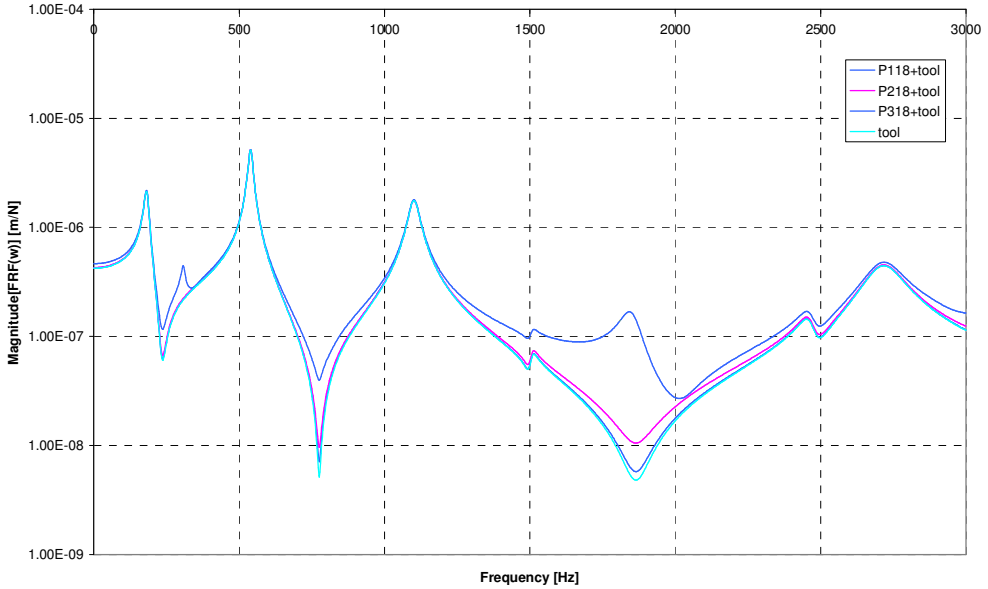

Figure 4.59 Combined FRFs of the workpiece and tool at the end of eighteenth step of 1st, 2nd and 3rd cuts

As like at the seventeenth step, the FRFs of the workpiece have the lowest values according to the other locations. As shown in Figure 4.58, again the peaks of the second natural frequencies disappear due to coinciding with the nodal line of the first torsional mode. Total FRF of the system is given by the FRF of the tool since the FRF of the workpiece is very low compared to that of the tool as shown in Figure 4.59. Only the FRF of the tool can be used to predict the stability diagrams accurately in such cases.

The stability lobe diagrams including the changing dynamics of the workpiece at the end of the tenth step of the 1st, 2nd and 3rd cuts are shown in Figure 4.60. Since the stability diagrams of P118 and P218 are the same, they seem as one curve in Figure 4.60.

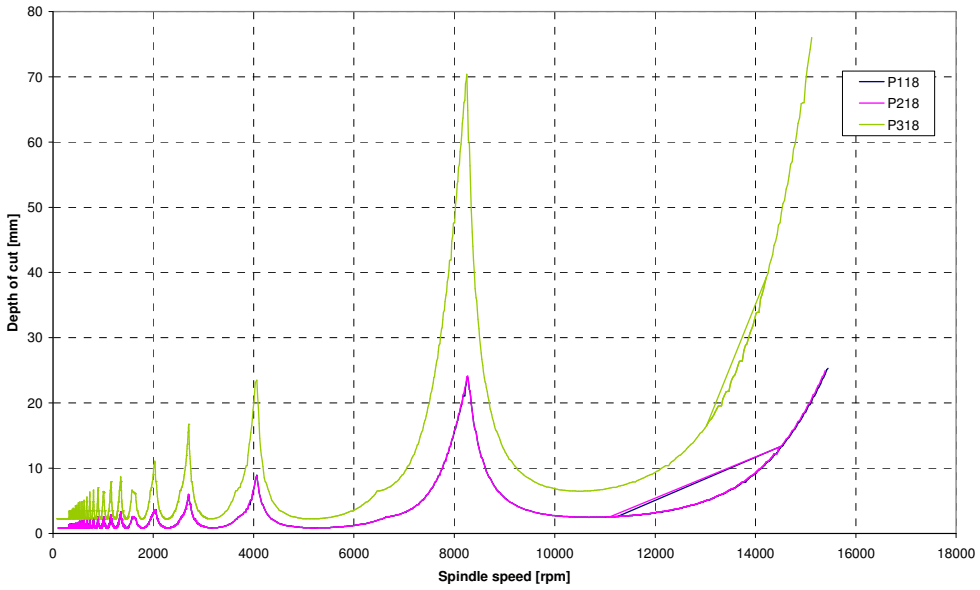

Figure 4.60 Stability lobe diagrams including the FRFs of the workpiece at the end of eighteenth step of 1st, 2nd and 3rd cuts

The FRFs of the system are the same at all the cuts as it was the case at the seventeenth step due to dominance of the tool FRFs on the system dynamics at this location. Except the finishing cut which has smaller radial depth of cut, the stability curves are the same at this location. As a result, in such a case the FRFs of the workpiece can be neglected when finding stability diagrams.

4.2.2.9 Variation of the Workpiece Dynamics

In this section, the variation of the workpiece dynamics as a result of mass removal is analyzed in terms of peak FRF values and natural frequencies. Every step in the machining cycle is numbered according to the machining order (sequence). The changes in the 1st, 2nd and 3rd natural frequencies of the workpiece are given in

Figure 4.61. In addition, the variations in the peak FRF amplitudes of the workpiece for the first three natural frequencies are shown in Figure 4.62.

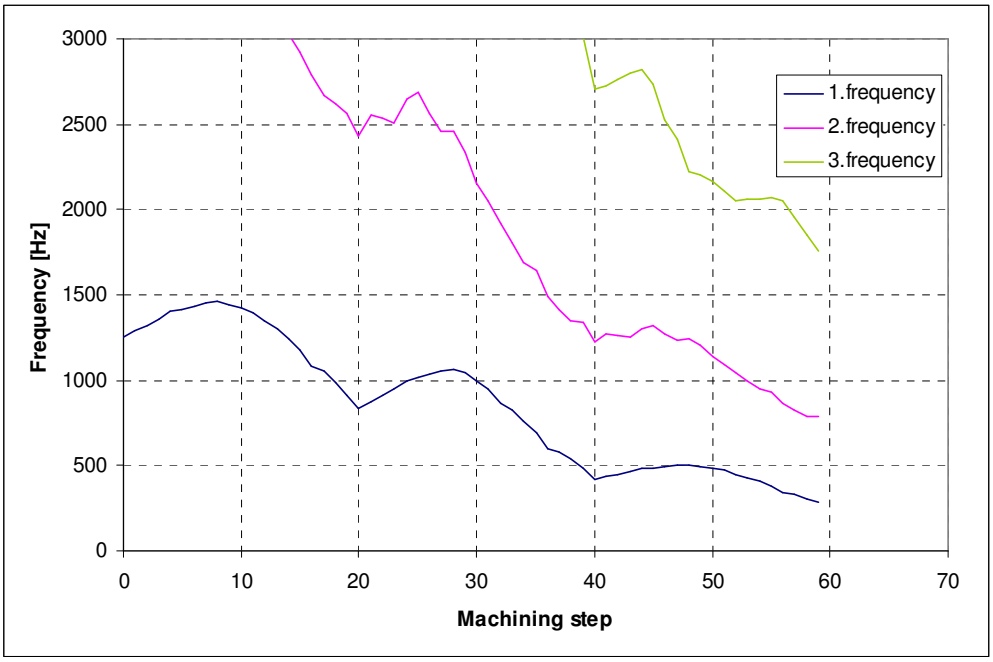

Figure 4.61 Variation in the 1st, 2nd and 3rd natural frequencies of the workpiece during machining.

As seen in the beam model of the workpiece, the variation in the natural frequencies of the workpiece shows a similar trend at every cut. The natural frequency of the workpiece increases until the workpiece is machined from the free end to the middle of the workpiece. Then, the frequency decreases while machining from the middle to the fixed end of the workpiece. This behaviour was explained in Section 4.2.2.6 by considering the respective stiffnesses of the workpiece at the free and fixed ends. The material removed from the free end does not affect the stiffness of the plate significantly so that the removed mass from the free end results in increased natural frequencies. The situation is just the opposite

for the fixed end where the removed material results in significant loss of stiffness and the mass removal from the fixed end results in reduced natural frequencies.

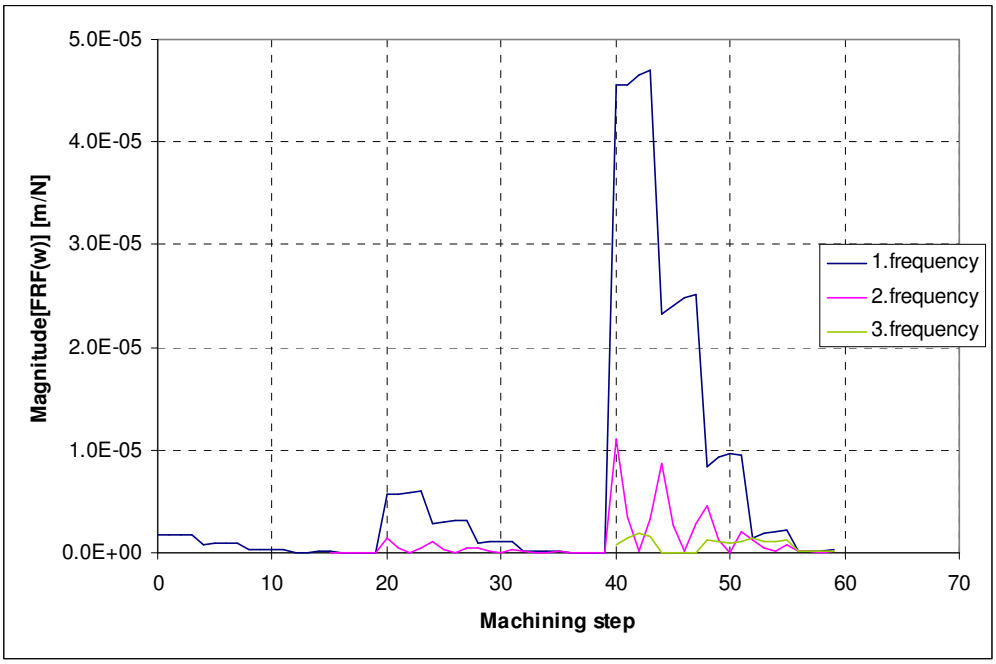

Figure 4.62 Variation of the peak FRF amplitudes of the workpiece at the 1st, 2nd and 3rd natural modes

Change in the magnitudes of the FRFs of the workpiece show an expected behaviour as mentioned earlier in Section 4.2.2.5. The FRF values of the workpiece decrease as the location is varied from the free end to the fixed end of the workpiece due to the respective stiffnesses of the workpiece at different locations. As the workpiece becomes more flexible at each cut compared to the previous cut, the amplitudes of the peak FRFs at the free end of the workpiece (at the 1st, 20th and 40th steps) become higher and higher as shown in Figure 4.62.

4.2.2.10 Variation of the Stable Spindle Speeds and Depth of Cuts

In this section, the effect of the variation of the workpiece dynamics as a result of the mass removal on stability is analyzed in terms of stable depth of cut values and corresponding spindle speeds. The variation in maximum stable depth of cut and spindle speeds for the 1st and 2nd lobes of the stability diagram are given in Figure 4.63 and 4.64 for different machining steps.

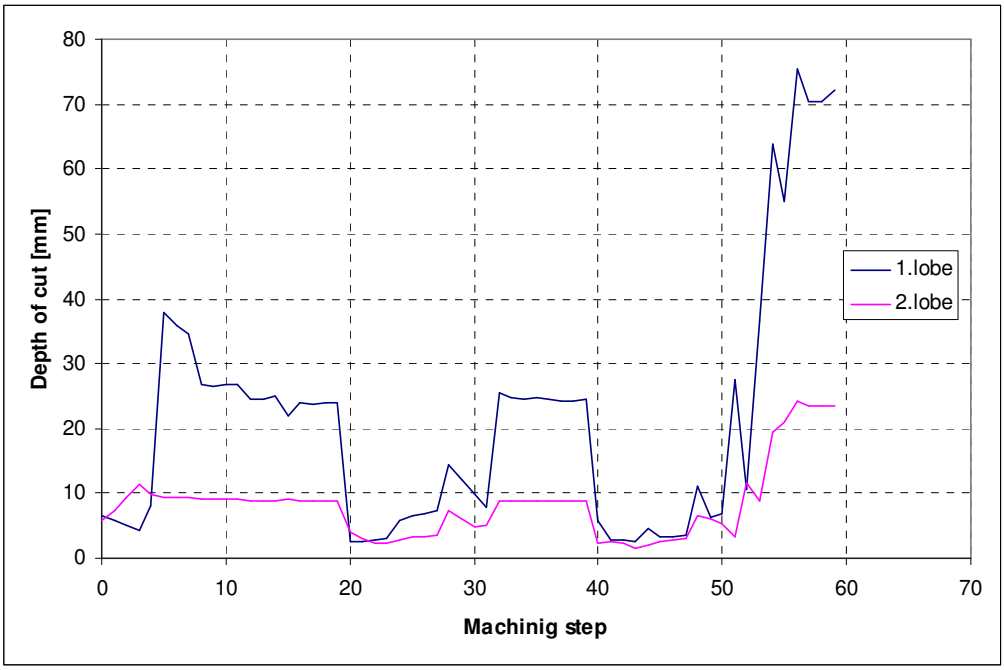

Figure 4.63 Variation of the stable depth of cuts for the 1st and the 2nd stability lobes during machining of the workpiece.

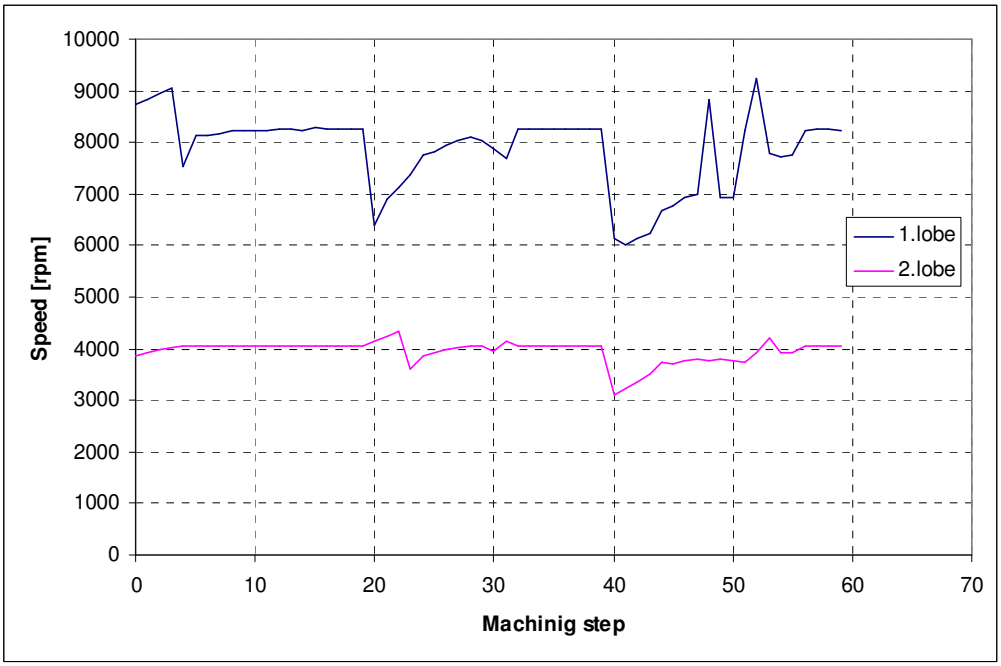

Figure 4.64 Variation of the spindle speeds corresponding to the 1st and the 2nd lobes during machining of the workpiece.

The variation patterns for the stable spindle speeds and depth of cuts in the first and the second lobes can be explained by examining the FRF variations during machining as presented in the previous sections. For instance, in the roughing cut from 1st step to 8th step, since the FRFs of the workpiece are higher than the FRFs of the tool at these locations, the workpiece dynamics become dominant in the FRFs of the system and the first steps of the cut take the lowest stable depth values. However, the amplitudes of the workpiece's FRFs reduce due to the movement of the locations where the FRFs are calculated, from free end to the middle of the workpiece and the stable depth of cuts in the 1st and 2nd lobes take higher values. After the 8th step, the FRFs of the tool become more flexible than the workpiece and the variation in the stable depth of cuts and speeds nearly remains constant. The similar trend can be observed in the semifinishing cut; however the stable depth of cut values remain constant after 12th step of the semifinishing cut due to increasing flexibility of the workpiece. In the finishing

cut, the workpiece becomes very flexible and the increase in the stable depth of cuts continues until the last step, because the workpiece FRFs are still dominant according to those of the tool.

If the stable depth of cuts at the same locations but different cutting cycles are compared, from the roughing cut to the finishing cut stable depths become smaller between 1^{st} - 8^{th} step locations due to increase in the flexibility of the workpiece. In the roughing and the semifinishing cut the stable depth of cuts take almost the same values at the constant regions, since only the tool dynamics affect the stability. In the finishing cut until the last step, the workpiece dynamics dominate the stability curve and stable axial depth of cuts get higher values compared to the other two cuts.

The spindle speeds corresponding stable depth of cuts nearly remain constant at the roughing and the semifinishing cuts; only at the 1^{st} steps of these cuts a decrease is observed. The first location is the most effective region of the FRFs of the workpiece on stability, and the flexibility of the workpiece causes sudden drops in speeds at the 20^{th} and 40^{th} steps in Figure 4.64. The speed values remain constant when the tool FRFs become dominant on the system FRFs. In the finishing cut the lowest region of the spindle speeds of the lobes corresponds to the machining from the 1^{st} step to 7^{th} step. Since the workpiece becomes significantly flexible at these steps of the machining, the decrease is observed in a wider region of the machining process compared to the other two cuts. Another observation from Figures 4.63 and 4.64 is that the machining steps in which the stable depth of cuts show a fall in value are the same as the steps in which the spindle speeds decrease.

In conclusion, the variation in chatter-free depth of cuts and spindle speeds is consistent with the variation in the workpiece dynamics, and the influence of the workpiece flexibility on the chatter stability can be observed easily when the workpiece is as flexible as the tool. The stable depth of cuts attain low values at the first cutting steps of every cut due to low FRFs of the workpiece at the free end.

They take higher values while machining from the middle to the head of the workpiece, as it is the case in the FRFs of the workpiece.

4.2.2.11 Minimum Chatter-Free Machining Time

As mentioned in Section 4.2.1.8, stability analysis in order to predict chatter-free depth of cuts at the high spindle speeds becomes an important necessity to increase the stable mass removal rate. This will lead to minimized machining time. In this study, two methods used in the beam model of the workpiece are used in order to determine the possible minimum chatter-free machining time of the workpiece.

In the first method, one common maximum chatter-free depth of cut and the corresponding spindle speed values are identified for every cut, and used for the whole cut as explained in Section 4.2.1.8.

In the second method, for every 4 steps of a cut (because the depth of cut and the spindle speed are not changed until the tool leaves the workpiece) , the possible maximum depth of cut and the corresponding spindle speed are identified and used for that specific pass.

Machining time in a milling process is given as by combining Equation 4.1 and 4.2,

$$t_m = nop.\frac{l_w}{V_f} = nop.\frac{l_w}{N.f_t.n_t} \tag{4.8}$$

where t_m is machining time,

nop is number of pass (step),

l_w is cutting length at one pass (step),

V_f is feed rate,

N is the number of teeth (flutes) of the cutter,

f_t is feed per tooth (in mm/rev per tooth),

n_t is rotational frequency of the cutter (in rpm).

In machining time calculations, f_t is taken as 0.15 for roughing cut and 0.10 for semifinishing and finishing cuts. These values are used for all cases as the effect of the feed on the stability is minimal. N is taken as 4 assuming a 4 fluted milling cutter, and l_w is 80 mm in the plate model. ***nop*** is determined by dividing the length of the workpiece (100 mm in the plate model) to the maximum axial depth of cut and n_t is taken maximum spindle speed corresponding to maximum axial depth of cut. Then, the optimum depth of cut and spindle speed values are determined as explained in Section 4.2.1.8 in detail.

By applying the procedure of the first method to determine one common depth of cut and spindle speed at every cut, the machining time values are found as shown in Table 4.16.

Table 4.16 Machining time calculation parameters at every cut using first method

	Spindle speed(rpm)	Depth of cut(mm)	nop	Feed per tooth	Time(min)
Roughing cut	9090	3.3	30	0.15	0.44
Semi-finishing cut	11490	1.3	75	0.1	1.31
Finishing cut	5918	1.0	96	0.1	3.24
				Total time	4.99

If maximum chatter-free depth of cut and spindle speed are found for every 4 step (pass) in one cut using the second method, the results are found as shown in Table 4.17 - 4.19. If the maximum stable depth of cuts and the speeds are the same as the other steps, the total machining time will be as shown in the same row of the table.

Table 4.17 Machining time calculation parameters at the roughing cut

Roughing cut	Spindle speed(rpm)	Depth of cut(mm)	nop	Feed per tooth	Time(min)
P10-P13	8723	3.3	6	0.15	0.09
P14-P17	8183	18.6	2	0.15	0.03
P18-P119	8220	15.5	4	0.15	0.06
				Total time	0.18

Table 4.18 Machining time calculation parameters at the semi-finishing cut

Semi-finishing cut	Spindle speed(rpm)	Depth of cut(mm)	nop	Feed per tooth	Time(min)
P20-P23	6608	1.9	11	0.1	0.33
P24-P27	7793	4.6	5	0.1	0.13
P28-P211	7755	6.3	4	0.1	0.10
P212-P219	8205	16.9	3	0.1	0.07
				Total time	0.63

Table 4.19 Machining time calculation parameters at the finishing cut

Finishing cut	Spindle speed(rpm)	Depth of cut(mm)	nop	Feed per tooth	Time(min)
P30-P33	6000	1.1	19	0.1	0.63
P34-P37	6780	2.6	8	0.1	0.24
P38-P311	6635	4.4	8	0.1	0.15
P312-P315	8303	7.4	3	0.1	0.07
P316-P319	8175	49.3	1	0.1	0.02
				Total time	1.11

Full machining time can be found in the second method as,

$$\text{Full machining time} = 0.18 + 0.63 + 1.11 = \boldsymbol{1.92\ min = 115.2\ s} \qquad (4.9)$$

As shown in Table 4.16, full machining time is found as 4.99 minutes (299.4 s) if the first method is used. As a result, taking maximum depth of cuts and spindle speeds at every 4 steps of the process reduce the machining time to 2/5 of the time required when one common depth of cut and spindle speed are used for every cutting cycle. Using the stability lobe diagrams found by combining the FRFs of

the tool and the workpiece, the maximum chatter-free values can be calculated at the intermediate stages of the process, and the machining time can be shortened significantly.

4.2.2.12 Summary of the Results of the Plate Model

The FRFs of the workpiece and the corresponding stability diagrams of the plate model are similar to those of the beam model at almost the same locations. The FRFs of the plate increase as the workpiece becomes thinner during the machining as it is the case in the beam model. Similarly, the natural frequencies of the workpiece reduce with decreasing thickness of the workpiece. The stability limits also reduce due to the increased FRFs. In machining from the free end to the fixed end, the same trend in the FRFs of the beam model can be also observed in the plate model. The FRFs of the workpiece reduce while the workpiece is machined from the free end to the fixed end due to higher stiffness at the fixed end. The natural frequencies increase as machining to the middle of the plate, and then the frequencies decrease while machining from the middle to the fixed end. This is due to the difference in the stiffnesses of the fixed and the free end of a cantilever workpiece as it is in the beam model. The stability limits take higher values as machining towards the fixed end until the FRFs of the tool becomes dominant, and then the stability limits remain constant. However, this behavior may change depending on the workpiece and tool geometry and materials.

In the plate model the second mode of the workpiece is different from the second mode of the beam model. It is the first torsional mode of the plate whereas in the beam model it is the second bending mode. The nodal line of the first torsional mode passes from the middle of the plate (parallel to the x axis). Therefore, in the FRFs at the middle of the plate, the peak of the second mode is not seen clearly. Thus the second mode does not affect the stability at these locations.

The minimum chatter-free machining time was studied for the plate model as well. As in the beam model, using both methods, the machining times were estimated and it was observed that using the maximum stable depth of cuts at higher speeds for every machining step reduces the machining time significantly.

CHAPTER 5

SUMMARY AND CONCLUSION

In this thesis, the effect of workpiece dynamics on the prediction of the stability diagrams in order to avoid self-excited chatter vibrations is studied in detail. In order to predict chatter-free depth of cuts at high speeds analytically, the frequency response functions (FRFs) of the system which consists of a tool-holder-spindle combination must be known. In the case of high workpiece flexibility, the workpiece dynamics should also be included into the overall system dynamics, and the changing dynamics of the workpiece must be considered in the stability calculations.

In order to determine the changing dynamics of the workpiece during the machining process an exact structural modification method, Matrix Inversion [43] was used. The FRFs of the unmodified workpiece and the modification parameters used in the structural modification method were found by using finite element (FE) models. The FRFs of the unmodified workpiece were calculated by using the modal parameters (eigenfrequencies and eigenvectors) obtained from the modal analysis of the FE model. The modification stiffness and mass matrices were also taken from the finite element program by using the FE model of the modifying elements. In order to read the modal parameters from the output file of the MSC. Marc© finite element program and write in a matrix form, a computer program was written in Visual C++ 6.0©. The structural modification method was also programmed in Matlab© in order to perform the structural modification by using the FRFs of unmodified workpiece and modification matrices. The verification of the program was made by comparing the FRFs of the modified workpiece obtained

from the computer program developed in this thesis with those obtained from the MSC. Marc©.

By obtaining the FRFs of the workpiece at the intermediate stages of the machining, first, the effect of the variation of the workpiece dynamics on the system FRFs which are found by the summation of the FRFs of the workpiece and tool-holder-spindle combination at the tip of the tool was studied. Secondly the effect of the changing workpiece dynamics on chatter stability was examined by using an analytical stability diagram generation method [16, 17]. Summary of important conclusions are given below.

In order to make an initial judgment about the effect of the workpiece flexibility and to decide whether it should be included in the analysis the workpiece FRF at the end of the machining and at the most flexible location must be compared with the tool point FRF. If the FRF of the workpiece is similar to or higher than the tool point FRF, the workpiece's FRF must be taken into account while determining the stability diagrams..

5.1 Effect of Part Dynamics on FRFs

By considering the machining steps of a workpiece, the effect of the change in the workpiece dynamics on FRFs of the workpiece and the system was studied in detail in this thesis. By modeling the workpiece first as a beam and then as a plate in a FE program, the workpiece dynamics' effects on the FRFs were investigated with various case studies.

It is observed that mainly two important parameters affect the FRFs of the workpiece. The first is the location where the FRFs of the workpiece are calculated (cutting location). Depending on the boundary conditions of the workpiece, the

location of the cutting affects the magnitudes of the FRFs calculated at this location. Due to the nature of the machining process, the point of contact of the tool with the workpiece changes continuously. Thus, the location of the FRFs also changes at every machining step due to changing point of contact. The case studies performed in this study showed that the FRFs of the workpiece at the free end take the highest value compared to the other locations. It means that the flexibility of the workpiece is the highest at the free end as expected. Moving from the free end to the fixed end of a cantilever workpiece, the magnitudes of the FRFs of the workpiece become smaller. If the FRFs of the workpiece at this region are comparable or higher than those of the tool, the machining of this region becomes more critical.

The second parameter is the change in the thickness of the machined workpiece. It is observed that the thickness change of the workpiece due to machining affects the FRFs of the workpiece. As the workpiece gets thinner during the machining, the magnitudes of the FRFs of the workpiece become higher since the workpiece becomes more flexible. Also, the frequencies of the peak FRFs (which are the natural frequencies of the workpiece) become lower with decreasing thickness, and it changes the total system FRF significantly, especially when the peak frequencies of the workpiece coincide with those of the tool.

In a machining operation, both the thickness of the workpiece is reduced and the location of the point where FRFs are calculated for the stability calculations change, and thus both parameters affect the FRFs of the workpiece significantly. The FRFs of the workpiece during the machining or before the machining may become comparable to the tool point FRFs. Since the system FRFs found by adding the FRFs of the workpiece and tool are used in the analytical generation of the stability diagrams, the workpiece dynamics can effect the stability only if the FRFs of the workpiece are in the same order of magnitude with the tool point FRFs. By examining the variation of the workpiece dynamics during machining, it can be decided when to include workpiece dynamics in the stability calculations.

Also cutting patterns or some parameters can be changed in order to perform stable and high performance machining by observing the changing workpiece dynamics.

In order to observe the effect of different radial depth of cuts in machining, the variation of the workpiece FRF was examined by performing several case studies. It is observed that taking more mass from the workpiece at the initial cut can be advantageous in order to decrease the machining steps and minimizing the machining time, since the workpiece FRF changes less at the initial cut where the thickness of the workpiece is maximum during machining.

Also different cutting patterns were compared in this study. It is observed that with different cutting strategies, the stability limits in the machining can be increased so that the machining time can be minimized in order to maximize the productivity by avoiding chatter.

5.2 Effect of Part Dynamics on Chatter Stability

In this study the chatter stability prediction was carried out by using the stability lobe diagrams generated by using the analytical formulations given in [16, 17]. In order to obtain the stability curves, the system FRFs must be known. The FRFs of the system can be found by combining the FRFs of the tool assembly and the workpiece. When the FRFs of the workpiece are comparable (or become comparable at any stages of the machining) to the tool point FRFs, the effects of the workpiece dynamics on the process dynamics and the stability must be taken into account. As the stability limit is inversely proportional to the real part of the FRF of the system, the stability limit decreases if the system FRF increases. It may be the case when the flexibility of the workpiece becomes higher during the machining.

In this thesis, it is observed that while machining the regions of the workpiece where the FRF of the workpiece is at similar or higher levels compared to the tool point FRF, the stability limits of the system decrease significantly. Especially while machining the free end of a cantilever workpiece, the stability curve takes the lowest values. Then the peaks of the lobes in the stability diagrams take smaller values, which means that the maximum stable depth of cut values becomes smaller. Furthermore, the spindle speeds corresponding to maximum stable depths also lower when machining highly flexible regions of the workpiece.

The effect of the radial depth of cut on stability diagrams was also studied in this thesis. The radial depth of cut can also be used to generate the stability diagrams instead of the axial depth of cut. Usually the stable axial depth of cut is inversely proportional to the stable radial depth of cuts [48]. Thus taking higher radial depth of cut in machining causes reduction in the stable axial depth of cut values and makes the machining time longer.

In this thesis, the effect of the different machining strategies on the stability and the machining time is also studied in detail. It is observed that by using a cutting pattern which is selected by considering the geometry, boundary and the cutting conditions of the workpiece, the stability limits of the system can be increased and the machining time can be reduced significantly.

5.3 Suggestion for Future Work

In this study, the structural modification method without adding new degrees of freedom is used in order to find the FRFs of the modified workpiece during the machining process. The workpiece is modeled as a beam and as a plate by using finite elements, and then modifications are made by changing the thickness of the workpiece without adding extra degrees of freedom in the finite element program.

As a future work, this study can be enhanced to 3-D finite element models and structural modification methods with additional degrees of freedom can be used. Thus a variety of different and large workpiece models can be studied and their effects on the chatter stability can be observed.

REFERENCES

[1] S.A. Tobias, W. Fishwick, The chatter of lathe tools under orthogonal cutting conditions, Transactions of ASME 80, 1079 - 1088 (1958).

[2] F. Koenisberger, J. Tlusty, Machine Tool Structures – vol. I: Stability Against Chatter, Pergamon Press, Englewood Cliffs, NJ (1967).

[3] F.W. Taylor, On the Art of Cutting Metals, ASME Trans 28, 31-350 (1907).

[4] S.A. Tobias, Machine Tool Vibration, Blackie and Sons Ltd, 1965.

[5] J. Tlusty, M. Polacek, The stability of machine tools against self excited vibrations in machining, International Research in Production Engineering, ASME, 465-474 (1963).

[6] H. Merrit, Theory of self-excited machine tool chatter, Transactions of ASME Journal of Engineering for Industry 87, 447-454 (1965).

[7] H. Opitz, Chatter behavior of heavy machine tools. Quarterly Technical Report No. 2 AF61 (052)-916. Research and Technology Division, Wright-Patterson Air Force Base, OH (1968).

[8] H. Opitz, F. Bernardi, Investigation and calculation of the chatter behavior of lathes and milling machines. Annals of the CIRP. 18: 335-343(1970).

[9] J. Tlusty, F. Ismail, Basic nonlinearity in machining chatter, Annals of the CIRP 30, 21-25 (1981).

[10] J. Tlusty, Dynamics of high-speed milling, Transactions of ASME Journal of Engineering for Industry 108 (2), 59-67(1986).

[11] S. Smith, J. Tlusty, Efficient simulation programs for chatter in milling, Annals of the CIRP 42 (1) 463-466 (1993).

[12] R. Sridhar, R.E. Hohn, G.W. Long, General formulation of the milling process equation, ASME Journal of Engineering for Industry. 317-324 (1968a).

[13] R. Sridhar, R.E. Hohn, G.W. Long, A stability algorithm for the general milling process, ASME Journal of Engineering for Industry, 330-334(1968b).

[14] I. Minis, T. Yanushevsky, R. Tembo, R. Hocken, Analysis of linear and nonlinear chatter in milling, Annals of the CIRP 39, 459-462 (1990).

[15] I. Minis, T. Yanushevsky, A new theoretical approach for prediction of machine tool chatter in milling, ASME Journal of Engineering for Industry, 115, 1-8(1993).

[16] Y. Altintas, E. Budak, Analytical prediction of stability lobes in milling, Annals of the CIRP 44, 357-362 (1995).

[17] E. Budak, Y. Altintas, Analytical prediction of chatter stability in milling – part I: general formulation; part II: application to common milling systems, Transactions of ASME, Journal of Dynamic Systems, Measurement, and Control, 120, 22-36(1998).

[18] Y. Altintas, Manufacturing Automation, Cambridge University Press, Cambridge (2000).

[19] T.L. Schmitz, Predicting high speed machining dynamics by substructure analysis, Annals of the CIRP 49 (1), 303–308 (2000).

[20] T.L. Schmitz, M.A. Davies, M.D. Kennedy, Tool point frequency response prediction for high speed machining by RCSA, Transactions of ASME, Journal of Manufacturing Science and Engineering 123, 700–707 (2001).

[21] A. Ertürk, H.N. Özgüven, E. Budak, Analytical modeling of spindle-tool dynamics on machine tools using Timoshenko beam model and receptance coupling for the prediction of tool point FRF, International Journal of Machine Tools and Manufacture, 46, 1901-1912 (2006).

[22] E. Budak, A. Ertürk, H.N. Özgüven, A modeling approach for analysis and improvement of spindle-holder-tool assembly dynamics, Annals of the CIRP 55, 369-372 (2006).

[23] A. Ertürk, H.N. Özgüven, E. Budak, Effect analysis of bearing and interface dynamics on tool point FRF for chatter stability in machine tools by using a new analytical model for spindle-tool assemblies, International Journal of Machine Tools and Manufacture, 47(1), 23-32 (2007).

[24] A. Ertürk, E. Budak, H.N. Özgüven, Selection of design and operational parameters in spindle-holder-tool assemblies for maximum chatter stability by using a new analytical model, International Journal of Machine Tools and Manufacture, 47, 1401-1409 (2007).

[25] W.C. Hurty, Dynamic analysis of structural systems using component modes, AIAA Journal, 3, 678-685 (1965).

[26] R.R. Craig, A review of time-domain and frequency- domain component mode synthesis method, Combined Experimental Analytical Modeling of Dynamic Structural Systems AMD, 67, 1-30 (1985).

[27] J.S. Arora, Survey of structural reanalysis techniques, Journal of the Structural Division ASCE, 102, 783-801 (1976).

[28] B.P. Wang, W.D. Pilkey, A.B. Palazzolo, State-of-the-Art Surveys on Finite Element Technology, Chap. 8, Newyork: ASME (1983).

[29] V.W. Synder, Structural modification and modal analysis-a survey, International Journal of Analytical and Experimental Modal Analysis, 1 ,45-52 (1985).

[30] J.T. Weissenburger, Effects of local modifications on the vibration characteristics of linear systems, Journal of Applied Mechanics, 90, 327-332 (1968).

[31] R.J. Pomazal, V.W. Snyder, Local modifications of damped linear systems, AIAA Journal, 9, 2216-2221 (1971).

[32] J.O. Hallquist, V.W. Snyder, Synthesis of two discrete vibratory systems using eigenvalue modifications, AIAA Journal, 11, 247-249 (1973).

[33] J.C. O'Callahan, C.M. Chou, Structural dynamics modification using generalized beam mass and stiffness matrices, Proceedings of the Third International Modal Analysis Conference, Vol. 1, 477-482 (1985).

[34] Y.W. Luk, System modeling and modifications via modal analysis, Ph.D. Dissertation, Virginia Polytechnic and State University, Blacksburg, VA. (1981).

[35] Y.W. Luk, L. D. Mitchell, Implementation of the dual modal space structural modification method, Proceedings of the Second International Modal Analysis Conference, Vol. 2, 930-936 (1984).

[36] Y.W. Luk, Reanalysis of modal data using dual modal space structural modification method, Reanalysis of Structural Dynamic Models, AMD 76, 45-56 (1986).

[37] K.B. Elliot, L.D. Mitchell, Realistic structural modifications: Part 1 Theoretical development, Proceedings of the Third International Modal Analysis Conference, Vol. 1, 471-476 (1985).

[38] K.B. Elliot, L.D. Mitchell, Structural modification utilizing beam elements, Proceedings of the Fifth International Modal Analysis Conference, Vol. 2, 956-965 (1987).

[39] S. Braun, Y.M. Ram, On structural modification in truncated systems, Proceedings of the Fifth International Modal Analysis Conference, Vol. 2, 1550-1556 (1987).

[40] K.B. Elliott, L.D. Mitchell, The effect of modal truncation on modal modification, Proceedings of the Fifth International Modal Analysis Conference, Vol. 1, 72-78 (1987).

[41] D.J. Ewins, M.G. Sainsbury, Mobility measurements for the vibration analysis of connected structures, Shock and Vibration Bulletin, 42, 105-122 (1972).

[42] C.H. Chou, J. O'Callahan, P. Avitabile, Improved modal data for generalized beam structural modifications, Reanalysis of Structural Dynamic Models, AMD 76, 35-34 (1986).

[43] H.N. Özgüven, Determination of receptances of locally damped structures, Proceedings of the Second International Conference on Recent Advances in Structural Dynamics, Vol. 2, 887-892 (1984).

[44] H.N. Özgüven, A new method for harmonic response of non-proportionally damped structures using undamped modal data, Journal of Sound and Vibration, 117, 313-328 (1987).

[45] H.N. Özgüven, Structural modifications using frequency response functions, Mechanical Systems and Signal Processing, Vol. 4, n.1, 53-63 (1990).

[46] J. Tlusty, Manufacturing Processes and Equipment, Prentice Hall, Upper Saddle River, NJ, 2000.

[47] E. Budak, Y. Altintas, E.J.A. Armarego, Prediction of Milling Force Coefficients From Orthogonal Cutting Data, Trans. ASME Journal of Manufacturing Science and Engineering, 118, 216-224 (1996).

[48] E. Budak, Analytical models for high performance milling. Part II: Process dynamics and stability, International Journal of Machine Tools & Manufacture 46, 1489–1499 (2006).

[49] E. Budak, The mechanics and dynamics of milling thin-walled structures, Ph.D. Dissertation, University of British Columbia (1994).

[50] W. Magnus, S. Winkler, Hill's Equation, Wiley, N.Y. (1966).

APPENDIX A

OUTPUT FILE FORMAT OF MSC. MARC MENTAT©

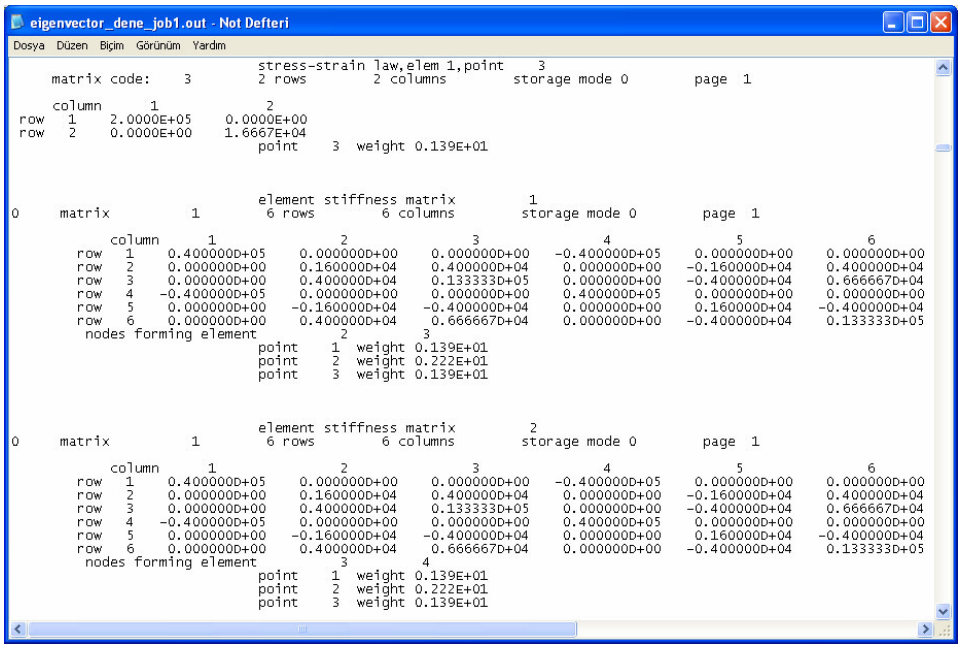


```
                              stress-strain law,elem 1,point     3
     matrix code:    3        2 rows        2 columns        storage mode 0        page  1

     column      1             2
 row   1    2.0000E+05    0.0000E+00
 row   2    0.0000E+00    1.6667E+04
                              point    3  weight 0.139E+01



                              element stiffness matrix         1
0     matrix          1        6 rows        6 columns        storage mode 0        page  1

           column      1             2             3             4             5             6
        row   1    0.400000D+05    0.000000D+00    0.000000D+00   -0.400000D+05    0.000000D+00    0.000000D+00
        row   2    0.000000D+00    0.160000D+04    0.400000D+04    0.000000D+00   -0.160000D+04    0.400000D+04
        row   3    0.000000D+00    0.400000D+04    0.133333D+05    0.000000D+00   -0.400000D+04    0.666667D+04
        row   4   -0.400000D+05    0.000000D+00    0.000000D+00    0.400000D+05    0.000000D+00    0.000000D+00
        row   5    0.000000D+00   -0.160000D+04   -0.400000D+04    0.000000D+00    0.160000D+04   -0.400000D+04
        row   6    0.000000D+00    0.400000D+04    0.666667D+04    0.000000D+00   -0.400000D+04    0.133333D+05
         nodes forming element          2             3
                              point    1  weight 0.139E+01
                              point    2  weight 0.222E+01
                              point    3  weight 0.139E+01



                              element stiffness matrix         2
0     matrix          1        6 rows        6 columns        storage mode 0        page  1

           column      1             2             3             4             5             6
        row   1    0.400000D+05    0.000000D+00    0.000000D+00   -0.400000D+05    0.000000D+00    0.000000D+00
        row   2    0.000000D+00    0.160000D+04    0.400000D+04    0.000000D+00   -0.160000D+04    0.400000D+04
        row   3    0.000000D+00    0.400000D+04    0.133333D+05    0.000000D+00   -0.400000D+04    0.666667D+04
        row   4   -0.400000D+05    0.000000D+00    0.000000D+00    0.400000D+05    0.000000D+00    0.000000D+00
        row   5    0.000000D+00   -0.160000D+04   -0.400000D+04    0.000000D+00    0.160000D+04   -0.400000D+04
        row   6    0.000000D+00    0.400000D+04    0.666667D+04    0.000000D+00   -0.400000D+04    0.133333D+05
         nodes forming element          3             4
                              point    1  weight 0.139E+01
                              point    2  weight 0.222E+01
                              point    3  weight 0.139E+01
```

Figure A.1 The element stiffness matrix format given in the output file of MSC. Marc Mentat©

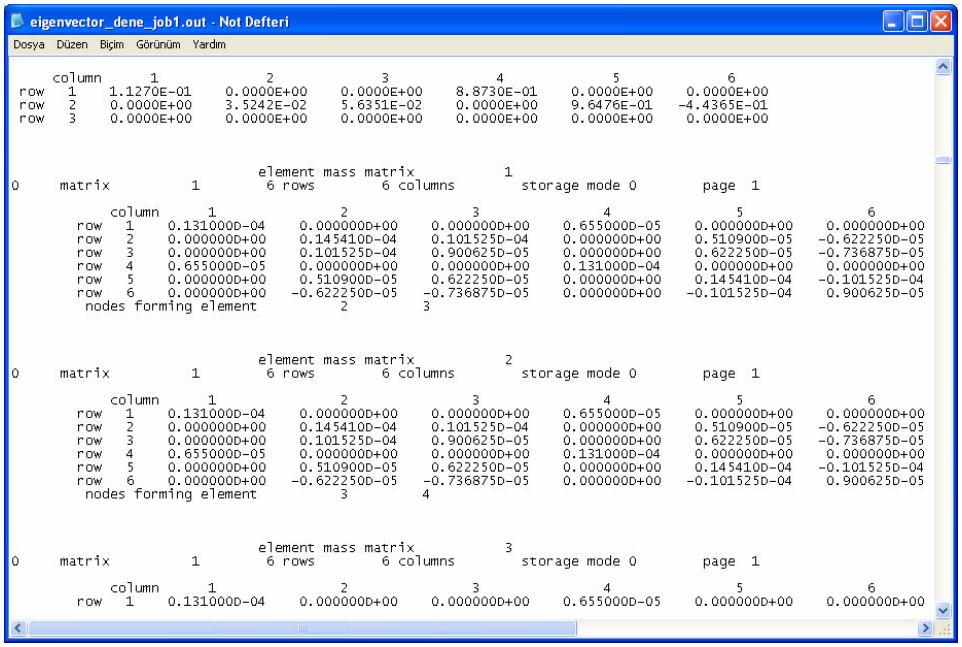

Figure A.2 The element mass matrix format given in the output file of MSC. Marc Mentat©

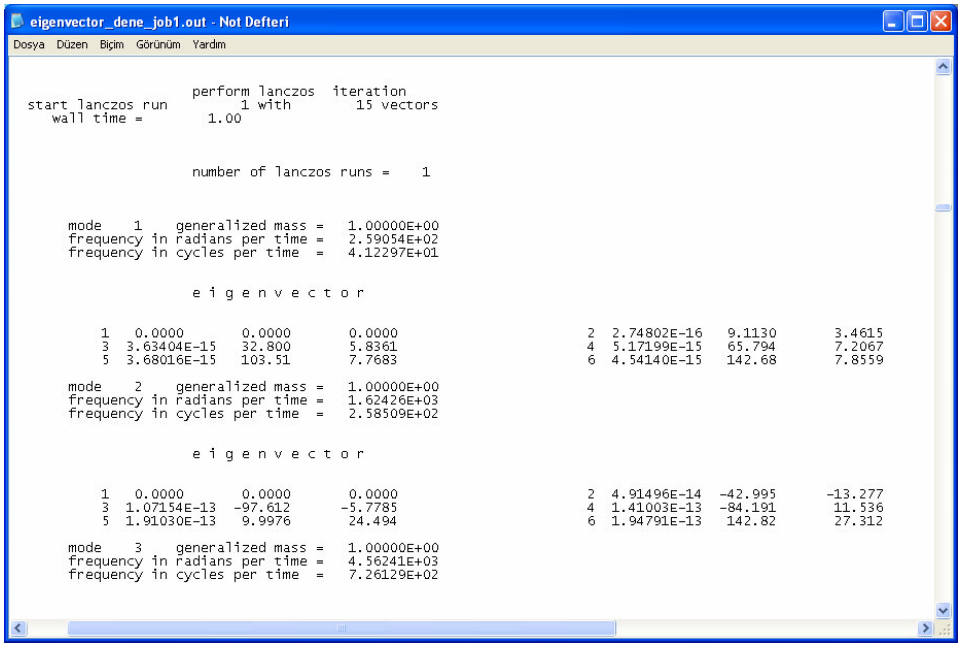

Figure A.3 Eigenfrequency and eigenvector format given in the output file of MSC. Marc Mentat©